FEDERAL UNIVERSITY OF SANTA CANTARINA
DEPARMENT OF CHEMICAL ENGINEERING AND FOOD ENGINEERING
GRADUATE PROGRAM IN CHEMICAL ENGINEERING

SERGIO NICOLAS BUITRAGO SANCHEZ

Preparation, characterization and application of graphene oxide-based materials from Brazilian mineral coals

FLORIANÓPOLIS
2023

Sergio Nicolas Buitrago Sanchez

Preparation, characterization and application of graphene oxide-based materials from Brazilian mineral coals

Master thesis submitted to the Graduate Program in Chemical Engineering of the Federal University of Santa Catarina to obtain the Degree of Master in Chemical Engineering
Advisor: Prof. Dr. Regina de Fátima Peralta Muniz Moreira
Co-advisor: Prof. Dr. Elaine Virmond

Florianópolis
2023

Buitrago Sanchez, Sergio Nicolas
Preparation, characterization and application of graphene oxide-based materials from Brazilian mineral coals / Sergio Nicolas Buitrago Sanchez ; orientadora, Regina de Fátima Peralta Muniz Moreira, coorientadora, Elaine Virmond, 2023.
132 p.

Dissertação (mestrado) - Universidade Federal de Santa Catarina, Centro Tecnológico, Programa de Pós-Graduação em Engenharia Química, Florianópolis, 2023.

Inclui referências.

1. Engenharia Química. 2. Adsorção. 3. Antibiotiótico. 4. Esfoliação. 5. Óxido de grafeno – geopolímero. I. Moreira, Regina de Fátima Peralta Muniz. II. Virmond, Elaine. III. Universidade Federal de Santa Catarina. Programa de Pós-Graduação em Engenharia Química. IV. Título.

Sergio Nicolas Buitrago Sanchez

Preparation, characterization and application of graphene oxide-based materials from Brazilian mineral coals

The present work at Master's level was evaluated and approved, on 18 of September of 2023, by the examining board composed of the following members:

Prof. Melissa Gurgel Adeodato Vieira, Dr.
State University of Campinas

Prof. Cintia Marangoni, Dr.
Federal University of Santa Catarina

We certify that this is the original and final version of the final work that was judged suitable for obtaining the degree of Master in Chemical Engineering.

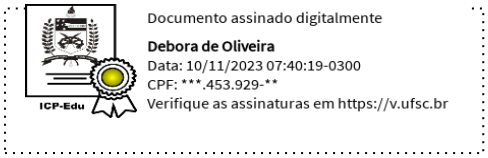

Prof. Débora de Oliveira, Dr.
Course Coordinator

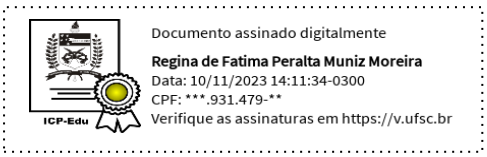

Prof. Regina de Fátima Peralta Muniz Moreira, Dr.
Advisor

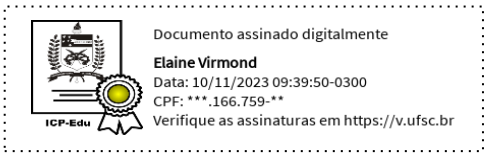

Prof. Elaine Virmond, Dr.
Co-Advisor

Florianópolis, 2023

Dedicated:

To my parents and my grandmother,

Monica, Javier and Graciela, to whom I owe everything I am today.

ACKNOWLEDGMENTS

I would like to begin by thanking God for giving me the wisdom and patience to carry out all the required activities, as well as for taking care of me during all this time.

I am very grateful to my guidance counselor, Prof. Dr. Regina de Fátima Peralta Muniz Moreira, for the knowledge imparted, for the professional example and for all the help and all the time dedicated during the completion of the master's degree.

To my parents Monica and Javier, as well as my grandmother Graciela, who have given all of themselves to be the people I am and always had a word of encouragement to achieve this great achievement in my professional life.

To my colleagues in the LEMA laboratory, Julia, Daniella, Fernanda, Alisson, Laura, for their friendship, help, support and for always having words of encouragement in difficult moments.

To Professor Dr. Elaine Virmond for her knowledge and for including me in the project in which I developed my master's degree.

To Professor Dr. Melissa Gurgel and the LEA-LEPA laboratory group at UNICAMP, for welcoming me for 22 days in the best way, and for helping me in the realization of my experiments in their laboratory.

To the analysis center of the Chemical Engineering Department at the Federal University of Santa Catarina for the FTIR analysis.

To the LINDEN laboratory at the Federal University of Santa Catarina for the zeta potential analysis, particle size determination and X-ray diffraction.

To the Graduate Program in Chemical Engineering of the Federal University of Santa Catarina for the opportunity to complete my master's degree.

To Capes for the scholarship.

To the Foundation for the Support of the Scientific and Technological Research of Santa Catarina State, Brazil (FAPESC 2021TR2151) and FEESC (202200081) for financially supporting this research.

"The cosmos is within us. We are made of star-stuff. We are a way for the universe to know itself."

(Carl Sagan)

RESUMO

A queima de combustíveis fósseis, incluindo o carvão, contribui significativamente para as mudanças climáticas, pois leva à emissão de CO_2 na atmosfera. Isso é particularmente importante para a sustentabilidade e conservação ambiental, pois o carvão é um recurso natural prontamente disponível e uma fonte de energia econômica no Estado de Santa Catarina (Brasil). Além disso, também se está testemunhando um aumento alarmante no uso de antibióticos em humanos e animais, o que representa outro desafio significativo. Os antibióticos não podem ser totalmente metabolizados no sistema digestivo, o que leva à sua liberação em águas naturais por meio de fezes e urina de humanos e animais. Portanto, é fundamental abordar essas questões ambientais. Este estudo teve como objetivo explorar a síntese de óxido de grafeno (GO) a partir de carvão mineral e coque, bem como um composto de óxido de grafeno-geopolímero para a produção de adsorventes usados na remoção de Ciprofloxacino (CIP) de soluções aquosas. O carvão e o coque foram submetidos a tratamento térmico, esfoliação com ultrassom e oxidação com ozônio na superfície sólida. Os materiais sintetizados foram caracterizados por Análise Termogravimétrica (TGA), Potencial Zeta (ZP), Distribuição de Tamanho de Partícula (PSD), Difração de Raios X (XRD), Espectroscopia de Infravermelho com Transformada de Fourier (FTIR), Microscopia Eletrônica de Varredura com Pistola de Emissão de Campo (FEG, EDS), Microscopia Eletrônica de Transmissão (TEM) e Espectroscopia RAMAN. Além disso, foram realizados testes de adsorção com os materiais sintetizados. Os resultados confirmaram a desmineralização do carvão e do coque e a introdução de grupos funcionais de oxigênio na superfície sólida. Foi observado GO com várias camadas. O polímero composto criado pelo uso de resíduos de fosfato e GO (22% em massa) apresentou a maior capacidade de adsorção. O estudo cinético indicou que o tempo de equilíbrio para concentrações de CIP entre 0,05 mmol L^{-1} e 0,2 mmol L^{-1} pode variar entre 100 min e 120 min. O modelo de pseudo-primeira ordem foi o que melhor se ajustou à concentração de 0,05 mmol L^{-1}, enquanto o modelo de pseudo-segunda ordem foi o que melhor se ajustou às concentrações de 0,1 mmol L^{-1} e 0,2 mmol L^{-1}. A modelagem molecular indicou que a molécula de CIP é estável. Além disso, as interações entre o polímero e esse composto são dependentes do pH para o adsorvente. Essa nova metodologia provou ser uma rota de síntese rápida, econômica e ecologicamente correta, agregando valor ao carvão mineral brasileiro. Por fim, o composto de OG e geopolímero é aplicável a processos de adsorção de antibióticos em meio aquoso.

Keywords: Adsorção; Antibiótico; Esfoliação; Óxido de grafeno – geopolímero.

RESUMO EXPANDIDO

Introdução

A água é um recurso natural e essencial para a manutenção da vida humana (CUERDA-CORREA; ALEXANDRE-FRANCO; FERNÁNDEZ-GONZÁLEZ, 2019). Nos últimos anos, vários poluentes "emergentes" foram encontrados nos recursos hídricos. Esses contaminantes incluem os antibióticos, cujo uso crescente tem causado preocupação (DUTTA; MALA, 2020; FRANCOEUR et al., 2023). Os antibióticos desempenham um papel crucial no tratamento de infecções em humanos e animais (WISE, 2002), mas sua metabolização incompleta leva à sua liberação em águas naturais por meio da excreção de resíduos animais e humanos (FU et al., 2017). Apesar das novas tecnologias, as estações de tratamento de águas residuais não são capazes de degradar totalmente esse tipo de composto medicinal (BHAGAT et al., 2020; EL-SHAFEY; AL-LAWATI; AL-SUMRI, 2012). O Ciprofloxacino (CIP), um membro da família das fluoroquinolonas, se destaca como o quarto antibiótico mais procurado na Europa (SALMA et al., 2016). Devido ao seu uso generalizado, esse composto está entre os antibióticos mais comumente encontrados em ambientes aquáticos (SPAOLONZI et al., 2022). Por esse motivo, é essencial desenvolver técnicas para lidar com essa contaminação em meios aquosos. Para isso, muitas técnicas foram desenvolvidas, como a separação por membrana (CHEN et al., 2023), a ozonização (ABDULLAH et al., 2023) e a adsorção (WU; YU; ZHANG, 2012). A adsorção é uma técnica fácil de projetar e econômica que surgiu como uma das tecnologias mais eficazes para a remoção de contaminantes da água (BAT) (SHAHID et al., 2021). Os adsorventes à base de carbono têm demonstrado excelente desempenho na remoção de micro poluentes da água (SINGH et al., 2023; SONTAKKE; TIWARI; PURKAIT, 2023). O óxido de grafeno (GO) é um material com uma estrutura de átomo único com hibridização sp^2. O GO difere do grafeno em termos de estabilidade termodinâmica devido aos grupos funcionais na interface da partícula (IGWEGBE et al., 2021). Sua estrutura de plano XY se traduz em mecanismos de adsorção ligados à atração, ligação de hidrogênio e empilhamento π-π (CHEN et al., 2023). Além disso, verificou-se que o GO possui tamanho de partícula pequeno, o que justifica sua implementação em compósitos de geopolímeros (GONÇALVES et al., 2014). Os geopolímeros, materiais tridimensionais amorfos, são sintetizados pela ativação alcalina de alumino silicatos e podem ser derivados de vários resíduos contendo sílica ou alumínio, como alumino silicatos e cinzas volantes.

Esses compostos apresentam propriedades mecânicas notáveis, durabilidade e podem desenvolver estrutura mesoporosa, dependendo do método de síntese (SANGUANPAK et al., 2022). Por outro lado, o GO foi incorporado aos geopolímeros devido à sua dispersão eficaz em soluções alcalinas, o que melhora a microestrutura e a resistência à flexão dos compósitos de geopolímero (HUANG; SUN, 2021). Nesse contexto, o objetivo deste trabalho foi sintetizar adsorventes à base de GO para a remoção de CIP.

Objetivos

Os principais objetivos deste trabalho foram sintetizar e caracterizar adsorventes para remoção de Ciprofloxacino à base de óxido de grafeno a partir de carvão mineral e coque para o desenvolvimento de um geopolimero com óxido de grafeno.

Metodologia

Amostras de carvão e coque foram fornecidas por uma empresa brasileira do estado de Santa Catarina. Foram realizados quatro processos diferentes de síntese de óxido de grafeno. No primeiro, vários tratamentos foram realizados nas amostras de carvão e coque, como segue: 500 mL de ácido clorídrico a 20% (HCl, PA, Exôdo Cientifica) foram adicionados a 10 g de carvão sólido em um frasco e agitados magneticamente por 24 h. A suspensão foi filtrada sob vácuo e lavada com água deionizada até se atingir o pH neutro. Em seguida, foi seca em um forno a 45 °C por 48 h. Um tratamento químico foi realizado com a adição de 10 mL de ácido sulfúrico (H_2SO_4, PA,98%, Vetec) e deixado em repouso por 24 h em temperatura ambiente. A esfoliação térmica foi então realizada em um reator de pirólise a 950 °C por 30 min sob atmosfera de nitrogênio, com o forno pré-aquecido a 20 °C min^{-1}. Para o tratamento oxidativo, o pó resultante foi tratado com ozônio por 18 h a uma taxa de fluxo de 1 L min^{-1}, seguindo para um banho ultrassônico de 60 min a 25 kHz. O GO foi separado da suspensão por filtração a vácuo usando membranas com poros de 0,55 µm e 0,22 µm (Millipore, Brasil) e seco em um forno a 45 °C durante a noite. O segundo processo foi realizado da mesma forma que o primeiro, mas a etapa de tratamento do carvão e do coque com HCl foi eliminada. O terceiro procedimento consistiu em produzir GO desmineralizado adicionando-se 100 mL de ácido fluorídrico (HF, PA, 48%, Vetec) a 5 g de material e agitando magneticamente por 24 h. Depois disso, a mistura

resultante foi filtrada usando-se uma membrana de PVDF (Difluoreto de Polivinilideno, 0,22 µm, Millipore, Brasil) sob vácuo para se atingir pH neutro usando água deionizada. Um tratamento químico subsequente consistiu em introduzir 10 mL de ácido sulfúrico (H_2SO_4) no sólido e deixá-lo em repouso à temperatura ambiente por 24 h. Para a oxidação térmica, o sólido foi exposto a uma temperatura de 950 °C dentro de um reator de pirólise tubular em um forno (Universal Dist) por 30 min sob atmosfera de nitrogênio, aumentando-se a temperatura a uma taxa de 20 °C min^{-1}. No tratamento oxidativo, o pó resultante foi misturado com água a uma concentração de 0,015 g mL^{-1} e submetido ao tratamento com ozônio por 18 h a uma taxa de fluxo de 1 L min^{-1}. Posteriormente, a solução foi sonicada por 10 min em um ultrassom (Hielscher, UP400St) com uma amplitude de 60% e uma temperatura controlada de 45 °C usando-se uma unidade de resfriamento (Marconi, MA083). O quarto processo foi realizado da mesma forma que o terceiro processo, mas a desmineralização por HF foi eliminada. Após a síntese do GO, foi feito o geopolímero. Para isso, a síntese de geopolímeros com óxido de grafeno (G_OG_CR) seguiu um procedimento descrito em um estudo anterior (FREIRE et al., 2020). Inicialmente, o metacaulim foi obtido pelo aquecimento do caulim em uma mufla (F2-DM) a 900 °C por 60 min, com aumento gradual da temperatura (5 °C min^{-1}). O metacaulim e os resíduos de fosfato foram então misturados por agitação magnética a 500 rpm por 10 min. O ativador alcalino foi preparado pela agitação de uma mistura de NaOH e silicato de sódio a 500 rpm por 10 min. Da mesma forma, os materiais sólidos foram combinados com o ativador alcalino usando agitação magnética a 2000 rpm por 20 min. A pasta resultante foi misturada com uma solução de 1% de OGCR usando agitação magnética por 2 min. Em seguida, a mistura G_OG_C foi moldada em cilindros, curada em forno (equipamento MS) a 65 °C por 48 h, desmoldada e imersa em água em temperatura ambiente por 28 dias. O material resultante foi triturado para uso em testes de adsorção. Os materiais foram caracterizados por Análise Termogravimétrica (TGA), Potencial Zeta (ZP), Determinação do Tamanho das Partículas (PSD), Difração de Raios X (XRD), Espectroscopia de Infravermelho com Transformada de Fourier (FTIR), Microscopia Eletrônica de Varredura com Pistola de Emissão de Campo (FEG/EDS) e Espectroscopia RAMAN. Para o processo de adsorção, o melhor material foi definido por meio de testes de afinidade. Nesses testes, foram preparadas cinco soluções diferentes, cada uma contendo CIP como adsorbato em uma concentração de 0,1 mmol L^{-1}, juntamente com um adsorvente padrão (1,5 g L^{-1}).

Essas soluções foram agitadas a 25 °C e 200 rpm por 24 h usando um agitador rotativo (Lab Companion SE-600R). Após a agitação, as soluções foram filtradas por um filtro de seringa PVDF hidrofílico de 0,22 μm. A concentração restante das soluções foi determinada por espectros de UV-Vis (Shimadzu/UVmini-1240) em λ = 276 nm. Por fim, foram realizados estudos cinéticos com o material selecionado. Nesses estudos, três concentrações diferentes de solução de CIP (C_0 = 0,05 mmol L^{-1}, 0,1 mmol L^{-1} e 0,2 mmol L^{-1}) foram examinadas usando óxido de grafeno-geopolímero como adsorvente. Cada Becker continha 60 mL de solução CIP e 0,09 g (1,5 g L^{-1}) do adsorvente. As soluções foram submetidas à agitação magnética (CMAG HS7/IKA) por 250 min em temperatura ambiente. As amostras foram coletadas em intervalos específicos e filtradas em um filtro de seringa PVDF hidrofílico (0,22 μm). A concentração residual do contaminante foi avaliada por espectroscopia UV-Vis em um comprimento de onda de 276 nm. Por fim, os modelos de pseudo-primeira ordem, pseudo-segunda ordem e intrapartícula foram aplicados para analisar os resultados obtidos. O software Marvin Sketch foi usado para projetar a estrutura molecular do CIP e o software Avogadro foi usado para seu projeto de estrutura tridimensional (3D). Foram calculados a energia do orbital molecular mais alto ocupado (HOMO, E_H), a energia do orbital molecular mais baixo desocupado (LUMO, E_L), o *gap* (ΔH_{H-L}), o potencial químico eletrônico (μ), a dureza química geral (η) e o índice de eletrofilicidade total (ω), através da Teoria do Funcional da Densidade (DFT) usando o *software* Gaussian 09.

Resultados e discussão

O GO multicamada foi sintetizado usando carvão e coque como materiais precursores, com oxidação eficaz por ozônio. A desmineralização foi mais eficaz com HF do que com HCl, alcançando uma redução de 82,3% das cinzas. A caracterização desses materiais demonstrou a incorporação de grupos OH em camadas de GO por meio de análise FTIR e ligações Si-O-Si no geopolímero. Os espectros FEG/EDS e RAMAN destacaram a transformação do carbono e do coque em substâncias amorfas de múltiplas camadas, enquanto o geopolímero apresentou uniformidade de partículas. Os dados de potencial zeta revelaram maior estabilidade da água para os materiais sintetizados em comparação com suas formas brutas. A difração de raios X indicou esfoliação de carbono e coque nas amostras de GO, enquanto o geopolímero apresentou composição de sílica-alumina e faujasita. O composto de GO e

geopolímero apresentou uma remoção significativa de CIP (~55%). A cinética atingiu o equilíbrio em 120 min, mais rápido do que os valores registrados na literatura (200 min e 40 h). Os modelos cinéticos, especificamente PFO para concentrações mais baixas e PSO para concentrações mais altas, foram os que melhor se ajustaram aos dados. Essa distinção sugere que a quimissorção influencia o processo em concentrações mais baixas, fazendo a transição para a fisissorção em concentrações mais altas. A modelagem molecular da CIP apoiou os resultados obtidos, revelando a estabilidade da molécula e a alta densidade de átomos de oxigênio e nitrogênio. Essa percepção esclareceu que as interações eletrostáticas e as ligações covalentes são mecanismos de reação em potencial.

Considerações Finais

As descobertas reveladas por este estudo destacam a produção bem-sucedida de óxidos de grafeno (OG) multicamadas derivadas de coque e carvão. Além disso, foi demonstrado que a integração do GO na matriz de um geopolímero produz uma nova gama de materiais com potencial substancial. Essas substâncias derivadas sinteticamente são uma promessa significativa no campo da mitigação de contaminantes farmacêuticos presentes em ambientes aquosos. Dessa forma, é altamente recomendável intensificar-se as pesquisas direcionadas à incorporação de GO na composição de geopolímeros. As investigações cinéticas e de equilíbrio relacionadas a um espectro mais amplo de antibióticos podem ser fundamentais para se desvendar a intrincada dinâmica da adsorção. Por meio dessas investigações futuras, será possível se obter uma compreensão mais profunda da relação entre as concentrações de GO e a eficácia da adsorção, orientando o refinamento de uma composição ideal para aumentar o desempenho da remoção de contaminantes farmacêuticos.

Palavras-chave: Adsorção; Antibiótico; Esfoliação; Oxido de grafeno – geopolímero.

ABSTRACT

We are currently facing a concerning environmental crisis. The burning of fossil fuels, including coal, is a significant contributor to the issue as it leads to the emission of CO_2 into the atmosphere. This is particularly problematic as coal is a readily available natural resource and a cost-effective energy source. In addition, we are also witnessing an alarming rise in the use of antibiotics in both humans and animals, which poses another significant challenge. Antibiotics cannot be fully metabolized in the digestive system, leading to their release into natural waters through human and animal feces and urine. Therefore, it is crucial to address these environmental issues. The aim of this study was to explore the synthesis of graphene oxide (GO) from coal and coke as well as a graphene oxide-geopolymer composite for producing adsorbents used in removing Ciprofloxacin (CIP) from aqueous solutions. The coal and coke were submitted to heat treatment, exfoliation using ultrasound, and oxidation with ozone on the solid surface. The synthesized materials were characterized by Thermogravimetric Analysis (TGA), Zeta Potential (ZP), Particle Size Distribution (PSD), X-Ray Diffraction (XRD), Fourier Transform Infrared Spectroscopy (FTIR), Field Emission Gun Scanning Electron Microscopy (FEG, EDS), Transmission Electron Microscopy (TEM) and RAMAN spectroscopy. In addition, adsorption tests with the synthesized materials were performed. Results confirmed the demineralization of coal and coke and the introduction of oxygen functional groups on the solid surface. Also, multi-layered GO was observed. The composite polymer created by using phosphate residues and graphene oxide (22 wt%) displayed the greatest adsorption capacity. The kinetic study indicated that the equilibrium time for concentrations of CIP between 0.05 and 0.2 mmol L^{-1} can vary between 100 min and 120 min. Furthermore, the pseudo-first order model best fitted the concentration of 0.05 mmol L^{-1}, while the pseudo-second order model best fitted the concentrations of 0.1 mmol L^{-1} and 0.2 mmol L^{-1}. Molecular modeling indicates that Cip is a stable molecule. Additionally, the interactions between the polymer and CIP compound are pH-dependent for the adsorbate. This novel methodology proved to be a rapid, cost-effective, and eco-friendly synthesis route, adding value to Brazilian mineral coal. Moreover, it demonstrated that the GO-geopolymer composite is applicable to antibiotic adsorption processes in aqueous media.

Keywords: Adsorption; Antibiotic; Exfoliation; Graphene Oxide – geopolymer.

LIST OF FIGURES

LIST OF TABLES

LIST OF ABBREVATIONS AND ACRONYMS

Abbreviation	Definition
AFM	Atomic Force Microscopy
Al	Aluminum
BET	Braeuer Emmett Teller
C	Carbon
CB	Mineral Coal B
CB_HCl_OG	Graphene Oxide from Mineral Coal B with HCl treatment
CB_OG	Graphene Oxide from Mineral Coal B
CIP	Ciprofloxacin
CO_2	Carbon Dioxide
Cq	Coke
Cq	Mineral Coke
Cq_HCl_OG	Graphene Oxide from Coke with HCl treatment
Cq_OG	Graphene Oxide from Coke
CR	Bituminous Coal
CS	Mineral Coal S
CS_HCl_OG	Graphene oxide from Mineral Coal B with HCl treatment
CS_OG	Graphene oxide from Mineral Coal S
CZ	Ash
CZ'	Ash without moisture
DFT	Density Functional Theory
DLS	Dynamic Light Scattering
ELS	Electrophoretic Light Scattering
F	Fluorine
FC	Fixed Carbon
FC	Fixed Carbon without moisture
FEG/EDS	Field Emission Gun Scanning Electron Microscopy
FeS_2	Pyrite
FTIR	Fourier Transform Infrared Spectroscopy
G_OG_C	Geopolymer with Graphene Oxide from Coal
GO	Graphene Oxide
H	Hydrogen
H_2SO_4	Sulfuric Acid
HF	Hydrofluoric Acid
HNO_3	Nitric Acid
HOMO	Occupied Molecular Orbital Energy
I_D/I_G	Intensity of the D peak to the intensity of the G peak
IPD	Intra-particle diffusion
K_2SiO_3	Potassium Silicate
$KClO_3$	Potassium Chlorate
$KMnO_4$	Potassium Permanganate
KOH	Potassium Hydroxide
La	Crystallite Size
LUMO	Lowest Unoccupied Molecular Orbital Energy
MnO_4^-	Permanganate Ion
N_2	Nitrogen
N_2O_4	Nitrogen Tetroxide
Na_2SiO_3	Sodium Silicate

$NaNO_3$	Sodium Nitrate
NaOH	Sodium Hydroxide
NO_2	Nitrogen Dioxide
O	Oxygen
O_3	Ozone
OG_D_Cq	Graphene Oxide demineralized from mineral Coke
OG_D_CR	Graphene Oxide demineralized from Bituminous Coal
OGCq	Graphene Oxide from mineral Coke
OGCR	Graphene Oxide from Bituminous Coal
PDI	Polydispersity Index
PFO	Pseudo-first Order
PSD	Particle Size Distribution
PSDP	Particle Size Determination
PSO	Pseudo-second Order
PVDF	Polyvinylidene Fluoride or Polyvinylidene Difluoride
SATC	Coal Workers Assistance Society
Si	Silicon
TEM	Transmission Electron Microscopy
TGA	Thermogravimetric analysis
U	Moisture
UV	Ultra visible
VM	Volatile Material
VM	Volatile Material without moisture
W	Watts
XRD	X-ray diffraction
XRD	X-ray Diffraction
ZP	Zeta Potential

LIST OF SYMBOLS

Symbol	Meaning	Unit
°C	Celsius Grades	-
A	Ampere	-
C	Constant related to diffusion resistance	mmol g^{-1}
C_0	Initial Concentration	-
cm	Centimeter	-
C_t	Final Concentration	-
k_1	velocity constant	min^{-1}
k_2	second order rate constant	min^{-1}
Kg	Kilograms	-
k_i	Intraparticle diffusion coefficient	mmol g^{-1} $min^{0.5}$
m	meter	-
ms	milliseconds	-
nm	nanometers	-
π	Pi interactions	-
q_e	Equilibrium adsorption	mg g^{-1}
q_t	Amount of solute adsorbed	mmol g^{-1}
S	Siemens	-
T	Time	-
Tpa	Tera Pascal	-
V	Volume	L
ΔH_{H-L}	Energy gap	-
η	Overall chemical hardness	-
μ	Electronic chemical potential	-
ω	Total electrophilicity index	-

SUMMARY

1 CHAPTER 1

1.1 INTRODUCTION

The combustion of fossil fuels, such as coal, are significant contributors to global warming and climate change due to their primary role in emitting carbon dioxide into the atmosphere (MAGAZZINO; MELE; SCHNEIDER, 2021). Coal, being a natural resource, is both widely available and economically accessible, making it one of the world's most crucial energy sources. However, it is anticipated that in nations like China, it will continue to be significant for progress in the upcoming 30 years (LI et al., 2022). In Brazil, coal production for 2021 was 7,347 million tons of coal (STATISTA, 2021). While consumption was 22 million tons of coal (STATISTA, 2021). Therefore, of the amount produced in 2021, only a low percentage of it is used in the country. So, Brazil has a large amount of coal reserves that are available for a more environmentally friendly use. Following the sustainability agreements give one. The twelfth ONU sustainability goal is responsible consumption and production. And following this goal, the replacement of fossil fuels by renewable ones is environmentally favored, while these natural resources could be used as raw materials to synthesize carbon-based adsorbents, such as activated carbon, carbon nanotubes or graphene-based materials. Carbon-based adsorbents have usually high adsorptive capacity to remove pollutants from gas and liquid phases.

Another environmental problem is the pollution of water resources. Water, as a natural resource, is an essential element whose availability is limited and whose importance for sustaining human life is indispensable. It is also an essential resource for the balance and functioning of various ecosystems. In recent years, there has been a remarkable increase in the identification of various pollutants present in natural water discharges. Among the wide range of "emerging" pollutants, the presence of antibiotics deserves special attention (CUERDA-CORREA; ALEXANDRE-FRANCO; FERNÁNDEZ-GONZÁLEZ, 2019). These affect the quality of water resources by spreading antibiotic resistance and are toxic to some aquatic organisms (QALYOUBI; AL-OTHMAN; AL-ASHEH, 2022).

Antibiotics play an extremely important role in the treatment of microbial infections in humans and animals. The annual production of these compounds can reach up to 200 thousand tons per year (WISE, 2002). Ciprofloxacin is a second-

generation fluoroquinolone antibiotic. It is the fourth most sold antibiotic, accounting for 73% of total antibiotic consumption in Europe (SALMA et al., 2016). This antibiotic is commonly used to treat urinary tract infections, sexually transmitted diseases and lung diseases (SHEHU IMAM; ADNAN; MOHD KAUS, 2018). The main source of release of this drug into waterways is attributed to incomplete metabolism of the drug in humans and inadequate disposal of such compounds in wastewater. In addition, Ciprofloxacin is only partially removed in wastewater treatment plants (EL-SHAFEY; AL-LAWATI; AL-SUMRI, 2012). Several technologies have been proposed to remove the presence of Ciprofloxacin. These alternatives include advanced oxidation (CUERDA-CORREA; ALEXANDRE-FRANCO; FERNÁNDEZ-GONZÁLEZ, 2019), ozonation (REKHATE; SRIVASTAVA, 2020), and adsorption processes (DĄBROWSKI, 2001). In particular, adsorption is emerging as a highly attractive process due to its remarkable efficiency and reduced cost. A wide variety of adsorbents have been proposed, ranging from carbonaceous materials to geopolymers and clays, among others (IGWEGBE et al., 2021).

Graphene is an sp^2 hybrid structure with two carbon atoms per unit cell. This material has been the subject of much research in recent years due to its large specific surface area, high electron mobility, improved thermal conductivity and mechanical strength (IGWEGBE et al., 2021). The oxidation of graphene produces graphene oxide (GO), which has large amounts of oxygen atoms on its surface. The epoxy, hydroxyl and carboxyl groups make graphene oxide more thermodynamically stable (SONTAKKE; TIWARI; PURKAIT, 2023). Likewise, GO has an XY plane that reaches several micrometers. This lattice-like structure makes its potential for removing contaminants from water highly attractive. It has also been shown that the mechanisms controlling antibiotic adsorption with GO are electrostatic attraction, hydrogen bonding, and π-π stacking (CHEN; GAO; LI, 2015). Nevertheless, GO-based adsorbents are generally produced in a very small particle size and the application in large scale could be limited.

Thus, the difficulty of applying these types of materials in fixed bed adsorption columns could be facilitated using GO in a suitable solid matrix. For this purpose, the incorporation of GO onto geopolymer has been proposed. Geopolymers are materials formed by a reaction between an alkaline activator and solid aluminosilicate precursors (LUUKKONEN et al., 2017). They have also recently been investigated as an effective alternative for adsorption of contaminants in wastewater (KARA; YILMAZER; AKAR,

2017). These polymeric composites have high mechanical strength, durability, mesoporous structure and ion exchange capacity (SANGUANPAK et al., 2022). On the other hand, graphene oxide-geopolymer composites have also been investigated. GO shows good dispersion in alkaline solution, which is a basic requirement for geopolymer synthesis (YAN et al., 2015).

In this study, the synthesis of GO produced from coal and coke, and incorporated to produce a composite with a phosphate residue-based geopolymer, was carried out. The synthesized materials underwent thorough characterization through zeta potential analysis, particle size distribution assessment, RAMAN spectra analysis, as well as FEG/EDS imaging, FTIR spectroscopy, and TGA analysis. The synthesized materials were employed for the adsorption of Ciprofloxacin. In order to scrutinize the attributes of the adsorption procedure, a kinetic investigation was conducted. Furthermore, quantum chemical descriptors including electronic chemical potential (μ), total chemical hardness (η), and total electrophilicity index (ω) of Ciprofloxacin were computed via molecular modeling, utilizing density functional theory (DFT).

1.2 OBJECTIVES

1.2.1 GENERAL OBJECTIVE

The overall objective of this study is to synthesize, characterize graphene oxide produced from Brazilian coal and coke, and evaluate its adsorption capacity as a graphene-geopolymer composite for antibiotic Ciprofloxacin in aqueous media.

1.2.2 SPECIFIC OBJECTIVES

The specific objectives were presented below according to each chapter of this thesis:

Chapter 3

- To develop and characterize multi-layer graphene oxide from coal and coke using heat treatment, ultrasonic exfoliation, and ozone oxidation.

Chapter 4

- To develop and characterize a graphene oxide-based polymeric composite for adsorption of Ciprofloxacin in aqueous media.
- To investigate the adsorption kinetics with three different concentrations.
- To investigate the possible mechanisms of adsorption between graphene oxide-geopolymer and Ciprofloxacin.

2 CHAPTER 2

This chapter provides a bibliographic review and theoretical background for the thesis, focusing on the main theoretical aspects related to carbon, graphene oxide, geopolymers, and the adsorption of pharmaceutical compounds. The understanding of these concepts, advantages and limitations presents new possibilities for the use of charcoal and the development of new adsorbent materials.

2.1 LITERATURE REVIEW

2.1.1 Coal

Coal is a sedimentary rock of vegetable origin that is easily combustible. It has a black appearance and is composed of carbon, hydrogen, oxygen, nitrogen, sulfur and some inorganic elements (BRITANNICA, 2023). Its composition, more than 50% by weight and more than 70% by volume is carbonaceous material. It is formed from plant remains that have been compacted, hardened, and chemically altered by heat and pressure over time (USGS, 2017). The process for this coal formation must go through its various types, lignite, sub-bituminous, high, medium and low volatile bituminous, semi-anthracite and anthracite. This process is slow and natural and is known as coalification, where the vegetable matter undergoes modifications for a denser, drier, richer and harder material (THIESSEN, 1947).

2.1.1.1 Classification of coals

The most widely accepted classification today is that of the American Society for Testing and Materials (ASTMD-388-799), which divides coal into anthracite, bituminous, subbituminous, and lignite. The types of coal with their main characteristics are listed in Table 2.1.

Table 2.1 - Coal classification

COAL TYPES				
	LIGNITE	SUB-BITUMINOUS	BITUMINOUS	ANTHRACITE
CARBON COMPOSITION (%)	25 % - 35%	34%-45%	45-86%	86-97%
AGE	Relative young	100 million years old	100-300 million years old	299-359 million years old
VOLATIL MATERIAL (%)	96	50	32	1
HUMIDITY (%)	>30	20-30	15-20	<15
APPLICATION	Electric power generation	Steam-electric power generation, Cement manufacturing and Chemical synthesis industry	Steam-electric power generation, steel production, manufacturing of iron and steel	Domestic fuel for space heating

Source: Modified from UPME (2005).

2.1.1.2 Global Coal Reserves

By the end of 2021, world coal reserves (Figure 2.1) were approximately 1161 billion short tons. These reserves are 75% concentrated in five countries: the United States with 22%, Russia with 15%, Australia with 14%, China with 14%, and India with 11% (EIA, 2022). These reserves are 70% anthracite/bituminous and 30% lignite/bituminous (EI, 2023).

Figure 2.1 - Global Coal Stocks

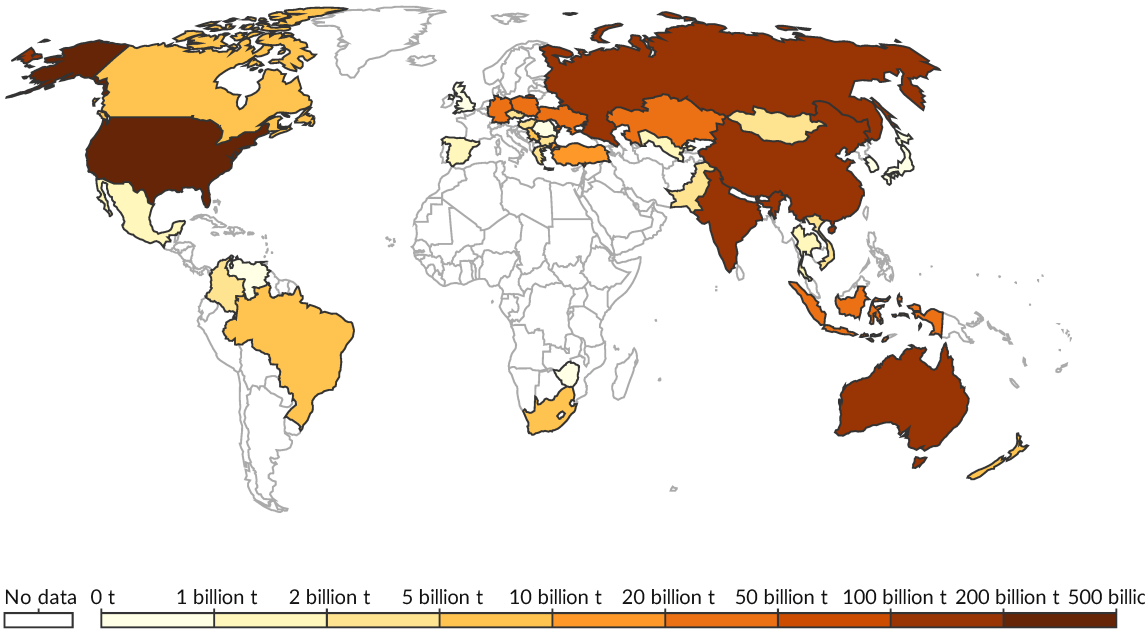

Source: EI (2023).

2.1.1.3 Coal reserves in Brazil

Brazil has the second largest coal reserves in Latin America. In 2020 there was a reserve of 600,000 million tons of coal (OXFORD, 2020). This coal has disadvantages such as high content of ash, sulfur and alkalis, which limits its industrial application. Currently, the most common use of coal is combustion and power generation (TEIXEIRA, 2018). Due to the low quality of the coal, Brazil still imports 50% of the coal used in the country (MASSA, 2022). In the Figure 2.2, the coal map of the southern region of Brazil is observed.

Figure 2.2 - Carboniferous map of the southern region of Brazil

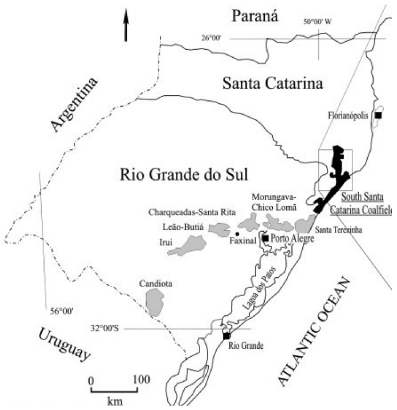

Source: KALKREUTH et al. (2010).

In this part, the state of Santa Catarina is located, which is the largest coal producer in Brazil (ANM, 2018). In addition, this state also has the best quality coal (PETRY; PHILIPP; GONZATTI, 2018). The coal produced in Santa Catarina is divided into white mantle, nice mantle and Irapuá mantle. X-ray diffraction studies showed that the Santa Catarina coal is dominated by quartz and kaolinite, and gypsum, gibbsite, jarosite and calcite are also present in small amounts. The quality of the coal is measured according to the International Classification of Coals, which places this material in the coking coal range, with an average ash content of 54.9% (KALKREUTH et al., 2010).

2.1.1.3.1 Carboniferous Belluno Ltda.

Carboniferous Belluno Ltda. has two main mines in the State of Santa Catarina. The "Cantão Norte" mine, located in the city of Treviso, started operations in 2012 and can produce 50 thousand tons of Barro Branco coal per month. The "Lauro Muller" mine, located in the city of Lauro Muller, has been in operation since 2009 and has a production capacity of 100 thousand tons of Rio Bonito coal per month (BELLUNO, 2020).

2.1.1.3.2 Rio Deserto Coal Industry Ltda.

Rio Deserto Coal Industry Ltda. it is located in the State of Santa Catarina. It has two mining units in operation, the "Cruz de Malta" mine and the "101" mine. These have an installed capacity of 300 t/h and 200 t/h, respectively. In 2021, this mine reached a production of 1 million tons of coal (RIO DESERTO, 2022).

2.1.1.4 Demineralization of Coals

Coal has two types of mineral matter. The first type is chemically bound to the organic material and the second type is found as a separate material. To remove such mineral material there are physical and chemical methods. The physical methods include gravity separation (PHENGSAART et al., 2023), froth flotation (SHEAN; CILLIERS, 2011), oil agglomeration (ÖZER; BASHA; MORSI, 2017), magnetic

separation (SHOUMKOVA, 2011), electrostatic separation (MASUDA et al., 1983), microwave processing (GASNER; DENLOYE; REGAN, 1986) and dry fluidization (LUO et al., 2022). Chemical methods include acid leaching (WU; YU; ZHANG, 2012), alkaline leaching (SHOPPERT et al., 2020) and alkali followed by acid leaching (NABEEL; KHAN; SHARMA, 2009).

To obtain ultra-clean coal, it must be left with an ash content in the range of 0.15 to 0.6%. In this case, it has been shown that the most effective chemical treatment for treating bituminous coal is hydrofluoric acid (HF) treatment, followed by HNO_3 (RAHMAN; PUDASAINEE; GUPTA, 2017). HF plays a very important role by removing the ash content of coal, and its performance is much more effective when the particle size of coal is less than 75 μm (JORJANI; CHAPI; KHORAMI, 2011). HF treatment can produce compounds such as $NaAlF_4$, CaF_2 and MgF_2. The reaction mechanism occurs when HF reacts readily with kaolinite ($Al_2Si_2O_5(OH)_4$) and quartz (SiO_2) to form Al and Si species with fluoride. In this case, a reduction of 3.5 to 0.1% in quartz and 2.2 to 0.3% in kaolinite is achieved. One of the problems with this technique is that HF cannot react with pyrite (FeS_2), so its ash content can only be reduced to a value close to 2% by weight (STEEL; PATRICK, 2001).

2.1.1.5 Coal Based Materials

There is currently a direct correlation between the three countries with the highest coal consumption and the three countries with the highest CO_2 emissions. In 2017, coal accounted for more than 70% of electricity generation in the United States (IEA, 2019). As well as China and India, which have increased their industrial energy demand in recent years due to high economic growth in these countries (ZHANG; BROADSTOCK, 2016). As a result, these countries are among the most coal consuming countries in the world. Therefore, these three countries are expected to be the largest contributors of greenhouse gas emissions to the Earth's atmosphere (COWAN et al., 2014).

Therefore, and because of current concerns about the greenhouse effect, various uses of the extracted carbon have been investigated. Carbon-based materials (Figure 2.3) have been of great interest due to their functionalities (LI et al., 2022). These materials include porous carbons (PRIYA; KENNEDY; ANAND, 2023; YAN et al., 2023; ZHAO et al., 2023), fullerenes (DOS SANTOS et al., 2023; GILL et al., 2023;

SAIKIA et al., 2023), carbon nanotubes (NAIEF et al., 2023; YESUDHAS JAYAKUMARI; NATTANMAI SWAMINATHAN; PARTHEEBAN, 2023; ZHANG et al., 2023a), carbon spheres (CAO et al., 2023; LAN et al., 2023; ZHANG et al., 2023b), carbon fibers (ASHRAF; IDREES; AKBAR, 2023; CHEN et al., 2023; LIU et al., 2023a), graphene (BI et al., 2023; LIU et al., 2023b; SHU et al., 2023) and graphene oxide (DEHGHANI; OSTOVARI; SHARIFI, 2023; JOY et al., 2023; LIU et al., 2023c).

Figure 2.3 - Coal based materials.

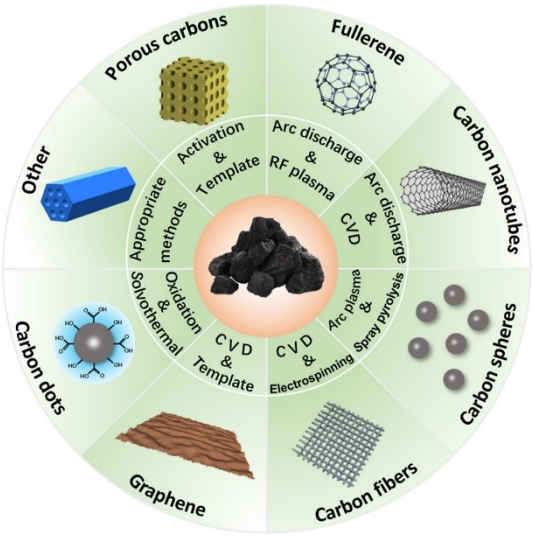

Source: LI et al. (2022).

2.1.2 Graphene and graphene oxide

Graphene (first synthesized by scientist Benjamin C. Brodie in 1859) is a layer of carbon atoms arranged in a 2D honeycomb lattice one atom thick by means of sp^2 hybridized C-C bonds between two adjacent carbon atoms (ZHU et al., 2018). In addition, graphene is made of carbon atoms in the shape of a honeycomb and is considered to be composed of benzene rings (CASTRO NETO et al., 2009). Graphene can have monolayers and bilayers, which are known as single and double layers of graphite. Graphene is considered multilayer graphene when the material has between five and thirty layers.

Due to the inconsistency between the graphene sheets, it was not possible to identify the applications of this material. Therefore, it was not until 2004 that the synthesis of graphene through the exfoliation process was revealed (IKRAM; JAN;

AHMAD, 2020). This carbon alloy has been extensively studied in recent years. Equally important, graphene can function as a planar macromolecule, which gives it unique physical and chemical properties (ZHANG et al., 2017).

Graphene oxide (GO) is the oxidized equivalent of graphene. It is a single layer of carbon atoms of a graphene lattice that has formed C-O bonds and has a heterogeneous electronic structure in Figure 2.4, one can see the differences between graphene and graphene oxide. GO is a non-stoichiometric and amorphous material, resulting in a complicated structure to study. This material can take the structure of Hofmann, Scholz-Boehm, Ruess, Lerf-Klinowski and other models (RASHI, 2023). Unlike graphene, GO is highly endowed with hydroxyl, carboxyl and epoxy functional groups, which improve its stability and dispersibility in water. Similarly, these functional groups enhance the combination of GO with ceramic or polymeric matrices (KHAN et al., 2016).

Figure 2.4 – (a) Graphene, (b) Graphene and (c) Graphene Oxide Structures

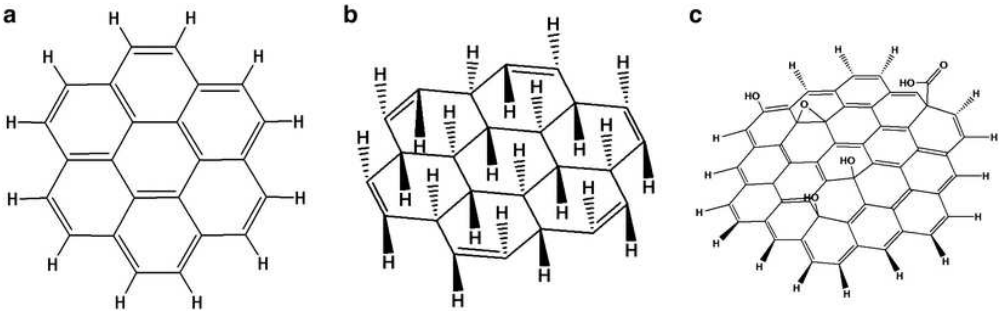

Source: Hernández Rosas et al. (2011).

2.1.2.1 Graphene Properties

Graphene has a layer thickness of 0.33 nm and the distance between the carbon-carbon bond σ is 0.142 nm or 1.42 A (ASHOK KUMAR et al., 2022). This demonstrates the structural flexibility of graphene, just as the σ band represents the robustness of the lattice structure in allotropes. Other electrical properties to be observed are its low-energy excitations, which in the case of monolayer graphene have a band structure containing massless chiral Dirac fermions (PAPAGEORGIOU; KINLOCH; YOUNG, 2017). When these are filled with energy levels up to the band

crossover point, they give graphene its semi-metallic behavior (PRAMANIK et al., 2022; ROBERTS; WISEMAN, 2022).

Based on the key properties of graphene (Table 2.2), graphene has several advantages over other carbon allotropes in various applications. Graphene is also 200 times stronger than steel (LEE et al., 2019).

Table 2.2 - Coal classification

Properties	Value
Surface Area (m^2g)	2600
Mobility	15000
Means free path (nm)	300 - 500
Fermi velocity (ms^{-1})	1 000 000
Electron effective mass (kg)	0,06
Hole effective mass (kg)	0,03
young modulus (TPa)	1,0
Opacity (%)	2,3
Optical Transparency (%)	97,7

Source: Modified from HU; WANG; HU (2010).

The properties of graphene are due to the sp^2 orbitals. These orbitals form the π-state bands that are shifted in the carbon sheet. As a result, graphene is recognized as a material that is extremely stiff, has very high thermal conductivity, zero effective mass, is impermeable to gases, has high charge carrier mobility, and has very high charge carrier mobility (PAPAGEORGIOU; KINLOCH; YOUNG, 2017). On the other hand, graphene has very good thermal properties. The conductivity of graphene is 4500 - 5200 W m^{-1} K^{-1}, while the electrical conductivity is 104 S cm^{-1}. The specific heat of graphene is still uncertain because it has not been measured directly. In this case, the specific heat is stored by the free electrons (POP; VARSHNEY; ROY, 2012). A final interesting property of graphene is its impermeability. This is because its π orbitals create a dense cloud that blocks the gap within its aromatic rings. In addition to its ease of electron passage and ability to prevent the diffusion of molecules and gases. This makes graphene a very interesting material because of its high impermeability. Graphene has the ability to withstand pressure differences (6 atm), resulting in a material with high resistance to heat (BERRY, 2013).

2.1.2.2 Graphene Oxide Properties

Understanding the properties of GO is important because of the structural changes it makes to graphene. These changes give it different electrical, mechanical and thermal properties. These properties make it an easily producible material on a large scale and can be used as composites, electronics, biomedicine and biosensors (AJALA et al., 2022).

GO has low electrical conductivity and low thermal stability. It has also been shown to have photoluminescence that can range from the UV to the near infrared (LOH et al., 2010). Also, unlike graphene, GO exhibits a strong polar character (HERNÁNDEZ ROSAS et al., 2011). These electrical properties are due to the incorporation of hydroxyl and carboxyl groups in GO. On the other hand, it has been shown that the electrical properties of GO can be controlled by the selection of radicals adsorbed on its surface. In this case, the loss of carboxyl groups would lead to a semimetal-semiconductor transformation (HERNÁNDEZ ROSAS et al., 2011). In the same way, having a low oxidation level makes GO become an insulating or electrically resistive material ($1{,}64 \times 10^4$ S m^{-1}) (KASHIF et al., 2021).

Mechanical properties are characteristics such as intrinsic strength, plasticity, toughness, hardness, brittleness, stiffness, etc. that graphene oxide has. For GO, due to the sp^2 carbon cleavage and the increase of oxide agents, it has a lower intrinsic strength and Young's modulus (0.207 TPa) than pristine Graphene (AJALA et al., 2022; SUK et al., 2010). Similarly, the increase of -O and -OH groups convert brittle graphene into ductile GO. Likewise, the elastic constants of GO are also reduced (KHOEI; KHORRAMI, 2016).

For the thermal properties of GO, its thermal conductivity must be studied. For this case, GO also has a low thermal conductivity (0.5 - 1 W m^{-1} K^{-1}) as well as electrical conductivity, unlike its precursor pristine graphene (YILDIZ; BOLTON-WARBERG; AWAJA, 2021). In this case, to improve the planar thermal conductivity of GO, this material can be reduced to a reduced graphene oxide, achieving a conductivity of 61 W m^{-1} K^{-1} (SMITH et al., 2019).

2.1.2.3 Graphene and Graphene Oxide synthesis methods

The most common precursors for the synthesis of graphene and graphene oxide include graphite and carbon. Due to the similarity of the polyatomic structure to the sp^2 bond of graphene and GO synthesis from carbon is economical and scalable (LEE et al., 2019). In recent years, graphene has been synthesized in a 2D heterostructure and graphene has also been synthesized in a 3D nanostructure. This 3D material has taken the form of nano-layers, hydrogels, graphene foams and encapsulates. (IKRAM; JAN; AHMAD, 2020).

In general, graphene and GO has been produced by two different synthetic routes, the top-down and bottom-up approaches. Top-down approaches involve the cleavage of carbon precursors, while the bottom-up approach involves the accumulation of carbon-derived materials (KUNDU; SADHUKHAN; SARKAR, 2022) The most commonly used routes for these syntheses are Mechanical Exfoliation (CHEN; DUAN; CHEN, 2012; SHARMA; MORISADA; FUJII, 2022; ZHANG et al., 2023c), Arc-Discharge (KIM et al., 2023; NIKOLAY; VICTOR, 2023; VERMA et al., 2022), Oxidative Exfoliation (ABDELKADER et al., 2015; AN; JEON; JEONG, 2012; LIU; XUE, 2015), Liquid-phase Exfoliation (CIESIELSKI; SAMORÌ, 2014; COLEMAN, 2009; HAAR et al., 2015), Chemical Exfoliation (CITAR), Chemical Vapour deposition (LEE et al., 2013; LUPINA et al., 2015; SONG et al., 2021), and chemical synthesis.

2.1.2.3.1 Chemical Synthesis (Oxidation)

Chemical synthesis is one of the most traditional ways to produce graphene and graphene oxide in large quantities. Currently, three different routes have been reported for this synthesis. The Brodie method, the Staudenmair method and the best known of all, the Hummers method. In general, this method is characterized by oxidation using strong acids (ADETAYO; RUNSEWE, 2019). Brodie first reported a new carbon structure by treating graphite with potassium chlorate ($KClO_3$) and nitric acid (HNO_3) (BRODIE, 1859). In 1898, Staudenmair slowly added chlorate in the presence of sulfuric acid (H_2SO_4) and nitric acid (HNO_3). Finally, Hummer in 1958, developed a mixture of potassium permanganate ($KMnO_4$), sodium nitrate ($NaNO_3$) in H_2SO_4 (FARJADIAN et al., 2020). This method is better for the preparation of Graphene Although the Hummers method is the most used for this type of synthesis,

but of the same is a process that leaves a lot of pollution by nitrogen dioxide (NO_2), nitrogen tetroxide (N_2O_4) and heavy metals. There is also a high risk of explosion because the oxidants ($NaNO_3$/$KMnO_4$) are oxidants against H_2SO_4. Difficult removal of Na^+ and $NO3^-$ ions is another disadvantage of this method (FARJADIAN et al., 2020).

Sometime later, a new method developed by Marcano appeared in which he synthesized graphene oxide with phosphoric acid, less corrosive compounds (WANG et al., 2022). Compared to the Hummers method, this method does not release toxic gases and does not have exothermic processes, and the final material has a higher degree of oxidation. The problems of the method proposed by Marcano is the treatment of waste liquids, because it requires a large amount of potassium permanganate and concentrated H_2SO_4 To better understand this oxidation process, it is necessary to study the reaction mechanism proposed by Marcano. In general, it has been said that the mechanism of the modified Hummers method is given by the oxidation of graphite with MnO_3^+. Recent studies have shown that the process is a hidden oxidation, where the permanganate ion (MnO_4^-) produces GO with different degrees of oxidation (KANG et al., 2016).

$$\text{STEP I } 2KMnO_4 + 2H_2SO_4 \rightarrow Mn_2O_7 + 2H_2O + KHSO_4 \quad (1)$$

$$\text{STEP II } Mn_2O_7 + 2H_2SO_4 \rightarrow 2MnO_3+ + 2HSO_4^- + H_2O \quad (2)$$

$$Mn_2O_7 + 3H_2O \rightarrow 2MnO_4^- + 2H_3O^+ \quad (3)$$

$$MnO_3^+ + 3H_2O \rightarrow MnO_4^- + 2H_3O^+ \quad (4)$$

In the first step, graphite is oxidized with H_2SO_4 and the reaction is completed with water. At this point, the MnO_3^+ oxidants in Step I are converted to MnO_4^- in Step II. The GO produced in step I is a material with different types of epoxy, hydroxyl, carboxyl, and carbonyl functional groups due to the high wettability of graphite with MnO_3 (PARK et al., 2018). In step II, the sp^2 hybridization of the graphene layers is destroyed to produce carbonyl or carboxyl groups (KIM et al., 2012). Finally, it should be emphasized that since the reactions are endothermic, any change in time, reaction temperature, and oxidant concentration will affect the GO properties (ZHANG et al., 2009).

2.1.2.3.2 Ozone Oxidation

Ozone is an advanced oxidation process based on hydroxyl materials. It is an oxidant commonly used in the treatment of contaminants in water. Advanced oxidation processes (AOPs) are chemical treatments that have the ability to remove organic materials from wastewater through oxidation reactions with a selective hydroxyl radical (REKHATE; SRIVASTAVA, 2020). This radical is capable of oxidizing organic contaminants. Ozone has been the subject of significant research in recent years due to its low production cost and advantages over other oxidants (HUANG et al., 2016). Corona discharge is the process available for ozone generation, in which a high-voltage discharge is applied to a cooled, dry gas phase containing oxygen. Equations 5 and 6 represent the reaction of the discharge gas (HOIGNÉ; BADER, 1983).

$$O_2 + \text{electric spark} \rightarrow 2O^{\cdot} \quad (5)$$

$$O_2 + 2O^{\cdot} \rightarrow O_3 \quad (6)$$

On the other hand, previous studies have reported that ozone is the oxidant to treat carbon-based materials (DIMIEV et al., 2012; EIGLER et al., 2013). Most of the ozone reactions towards carbon-based materials have been carried out in gaseous form, so the ozone generation has to be done *in situ* (SI; SAMULSKI, 2008; SUN et al., 2014). In this case, carbon surfaces can act as an initiator for ozone decomposition. It has been studied that in activated carbon, O_3 decomposes on the surface of activated carbons and is capable of forming -OH (MORCOMBE; ZILM, 2003). Similarly, the O_3 that decomposes on the base of activated carbon forms active oxygen species -O and -OH (MORCOMBE; ZILM, 2003). On the other hand, ozone has never been associated with GO synthesis, and it is now known that O_3 production is achieved in the reaction of $KMnO_4$ and H_2SO_4 of the Hummers method (CHEN et al., 2016). Likewise, it has been shown that in this method, the oxidation of graphite occurs through the production of ozone in the chemical reaction involved (CHEN et al., 2016). In this reaction, ozone is able to form atomic oxygen and hydroxyl radicals, which leads to the oxidation of graphite (GROVEMAN et al., 2017). In this reaction, ozone is able to form atomic oxygen and hydroxyl radicals, which leads to the oxidation of graphite (GROVEMAN et al., 2017). (GROVEMAN et al., 2017) showed that GO can undergo reoxidation by ozonation. The oxygen percentage could be increased from 27.55% to 36.05 after 8 h

of *in situ* ozonation. In addition, they studied the addition of hydrogen peroxide (H_2O_2) and found that the reaction mechanism with this compound is different from the mechanism without the addition of H_2O_2. This compound has the function of being the initiator of the reaction with O_3 to generate -OH radicals, which makes this reaction (Equation 7) faster in the oxidation of GO.

$$2O_3 + H_2O_2 \rightarrow 2OH + 3O_2 \quad (7)$$

Finally, there are still insufficient studies to fully explain the reaction mechanisms of *in situ* ozonation for graphene oxide production, but there is evidence that this process promotes the oxidation of GO.

2.1.2.3.3 Exfoliation

The exfoliation process is the individual separation of carbon sheets. Mechanical exfoliation occurs by applying pressure to multilayer graphene by ball milling or adhesive tapes. This cleavage is due to the breakdown of weak van der Waals interactions (ADETAYO; RUNSEWE, 2019). The adhesive tape technique implements an external force capable of cleaving the monolayer graphene from graphite. The quality of the materials obtained by this method is not good due to graphene fragmentation (SINGH et al., 2023).

Chemical exfoliation requires alkali metals to disrupt van der Waals interactions between graphene layers (RAO; SOOD, 2013). Although this process is more scalable than mechanical exfoliation, monolayer graphene oxide tends to revert to its initial graphite state (ADETAYO; RUNSEWE, 2019).

Similarly, techniques such as thermal peeling can result in monolayer materials. In this case, the time required for thermal peeling is much shorter than for mechanical or chemical peeling (SCHNIEPP et al., 2006). In this process, the vapors of the decomposing substances create pressure between the graphite layers. Exfoliation occurs when this pressure overcomes the van der Waals attractions of the interlayer (MCALLISTER et al., 2007). This method only works if the starting materials have functional groups between their layers. This exfoliation can occur in two ways, at high and low temperatures. An alternative synthesis route to traditional exfoliation is the exfoliation of chemically wet graphite layers to separate individual graphene sheets

(CAI et al., 2012). For high temperature thermal exfoliation, it has been shown that the best conditions are at 1050 °C and 30 s, emphasizing the need to preheat the furnace (MCALLISTER et al., 2007). It has also been found that the smaller the lateral size and crystallinity of the graphite, the better the deposition process. For high temperatures, methods such as microwave irradiation and arc discharge have also been tested. For low temperature exfoliation, it can be performed at conditions between 250 and 400 °C in air for 5 minutes (MARINOIU et al., 2015).

2.1.2.4 Applications

Graphene and graphene oxide will have different applications due to the different properties explored in sections 3.2.1 and 3.2.2. (UMAR et al., 2023).

2.1.2.4.1 Graphene Applications

The excellent properties of 3D graphene have led to its implementation in applications in bioengineering, electrical engineering, energy storage, and environmental remediation. Due to its high electrical conductivity, large surface area and high electron hopping rate, graphene has been studied as an electrode in lithium-ion batteries (KIM et al., 2013). Graphene has also been mixed with cathode electrode materials to improve the performance of the electrode material (YUAN et al., 2018). Similarly, it has been used as a conductive additive to increase the rate of electron transfer and improve the conductivity of the electrode (UMAR et al., 2023; ZHAO et al., 2010). This material has also been studied for the food industry. Therefore, studies have been carried out because graphene has the ability to change the charge density, which provides a change in electronic properties. Therefore, graphene has an excellent potential for the fabrication of sensitive biosensors (JOSHI et al., 2023). Finally, graphene has also been applied to displays for mobile devices (JI et al., 2020), ultracapacitors (STOLLER et al., 2008), water desalination (SURWADE et al., 2015), transistors (SCHWIERZ, 2010) and corrosion-resistant coatings (BHARECH; KUMAR, 2015; OLLIK; LIEDER, 2020).

2.1.2.4.2 Graphene Oxide Applications

The range of applications of GO is very wide and may depend on its oxidation level, number of layers, and other properties. Due to the oxygen functional groups of GO, this material can be used as a raw material for the synthesis of graphene derivatives such as fluorographene, bromo graphene, graphene, and others (JIŘÍČKOVÁ et al., 2022). Similarly, the functional groups that make up GO nanosheets make it a promising material for adsorption of gas molecules. This is due to the fact that the electrical properties of GO change when exposed to certain gases (TODA; FURUE; HAYAMI, 2015). Likewise, thanks to the excellent physical properties of GO, such as its conductivity, fluorescence, flexibility, among others, numerous devices based on this material have been created. These materials range from transparent conductors (ZHENG et al., 2014), electrical sensors (GUO et al., 2011), photovoltaic cells (KYMAKIS et al., 2013), and many more (HUANG et al., 2020). This material can also be applied to drug delivery, high-temperature materials, and construction materials(TODA; FURUE; HAYAMI, 2015).

One of the most studied applications in this work is the adsorption of antibiotics in aqueous media. In this case, due to the functional groups on the surface of GO, it is a very hydrophilic material, providing the ability to apply GO in aqueous and biological media (BARROSO-BUJANS et al., 2010). The aromatic compounds of drugs can be easily adsorbed on GO, thanks to the π- π stacking (GAO et al., 2012), as well as the cation-π bonding, which can be part of the reaction mechanisms of antibiotic adsorption. (AI et al., 2019) showed that π-π interaction and hydrogen bonding play an important role in the adsorption of tetracycline. C-H-π interactions may also play a minor role in the mechanism. Another study by (CHEN; GAO; LI, 2015), shows that the adsorption mechanism of Ciprofloxacin may be given by electrostatic attraction, hydrogen bonding and π-π stacking.

2.1.3 Geopolymers

Geopolymers, known as alkali activated, are inorganic polymeric materials. They can have a source of aluminosilicates, fly ash or metakaolin with alkaline solutions (ASHRAF; IDREES; AKBAR, 2023). They have an amorphous, semi-crystalline structure. In this reaction, dehydroxylation occurs where the aluminum

changes from octahedral to tetrahedral coordination. To obtain lattice stability, positive ions (Na^+, Ca_2^+, Ba_2^+, NH_4^+, H_3O^+, K^+) must be added to the presence of Al^{3+} in tetrahedral coordination (DAVIDOVITS, 2005). On the other hand, three different polymeric forms can be obtained as polysialate (-Si-O-Al-O-O-), polysialate-siloxo (-Si-O-Al-Al-O-Si-O-) and polysialate-disiloxo (-Si-O-Al-O-Si-O-Si-O-), depending on the amount of SIO_2 monomer added (KOMNITSAS; ZAHARAKI, 2007).

The geopolymerization process takes place in three stages: destruction, polymerization and stabilization (YAO et al., 2009). The first stage is the dissolution of the aluminosilicate source by the alkaline activator. The Si-O-Si bonds are the first to dissolve due to the electronic instability created by the alkali metals. External factors such as temperature, particle size, reactivity of the material and concentration of the alkaline solution can modify the concentration of aluminosilicates (SHI; JIMÉNEZ; PALOMO, 2011). In the second part of the reaction, the formation of aluminosilicate oligomers produces an increasing concentration. The structural orientations depend on the Si/Al concentration (ZHOU et al., 2016). The third step is polymerization, which is favored with increasing aluminosilicates (FREIRE, 2022).

2.1.3.1 Precursor materials

The materials used for the synthesis of geopolymers are generally a source of aluminosilicates and an alkaline activator. The most commonly used alkaline activators include sodium hydroxide (NaOH), potassium hydroxide (KOH), sodium silicate (Na_2SiO_3), and potassium silicate (K_2SiO_3) (Assi et al., 2020; Pacheco-Torgal et al., 2008). Other materials have been used for the synthesis of geopolymers, including kaolin, phosphate residues, fly ash, and red mud (FREIRE, 2022).

Fly ash is an industrial byproduct of burning coal. Different types of coal produce different types of ash. Bituminous coal produces ash with low CaO content (CONG; CHENG, 2021). Lignite and sub-bituminous coals produce ash with high calcium content (GUO; SHI; WEI, 2017). Metakaolin is a clay composed of anhydrous aluminum silicate. This clay is produced by dehydrating kaolin at a temperature between 600 and 900 °C. This type of clay is able to impart properties to the geopolymer such as high compressive strength and bond strength (CONG; CHENG, 2021; PRUD'HOMME et al., 2011).

2.1.4 Adsorption

Ancient civilizations used adsorption as a separation technology for water purification (DĄBROWSKI, 2001). Nowadays, adsorption has been widely used in wastewater treatment due to its simple design and easy operation (MANCHISI et al., 2020).

Adsorption is a surface process defined as an increase in the concentration of a pollutant at the surface or at the interface between two phases (FAUST; OSMAN, 2013). It can also be defined as a mass transfer process in which solutes are transported from a liquid phase to a solid surface (MANCHISI et al., 2020). The adsorbate is the contaminant that adheres to the surface or interface, which is called the adsorbent (ALI; GUPTA, 2006).

There are three steps involved in the adsorption process: (I) external mass transfer, (II) intraparticle transport within the particle, and (III) reaction kinetics at phase boundaries (QIU et al., 2009). The first step occurs between the outer surface of the adsorbent particles and the surrounding liquid phase. The second can be limited by pore and solid diffusion. For the latter, the adsorption rate is controlled by the kinetics of bond formation (FAUST; OSMAN, 2013). Similarly, it is crucial to understand the difference between physical and chemical adsorption (Figure 2.5). Physical adsorption involves only weak intermolecular forces, whereas chemisorption involves the formation of a chemical bond between the adsorbate and the adsorbent surface (FAUST; OSMAN, 2013). Similarly, adsorption processes can be modified by the properties of the adsorbates and adsorbents, interactions between them, and factors such as pH and temperature (MANCHISI et al., 2020).

Figure 2.5 - Schematic process of chemical and physical adsorption

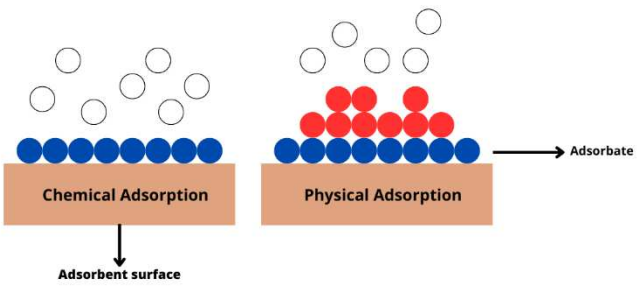

Source: Adapted from: LYUBCHIK et al. (2011).

2.1.4.1 Adsorption Kinetics

Kinetics provides information on the adsorption rate, performance of the adsorbent used and mass transfer mechanisms. In addition to this, kinetics is of vital importance for the design of adsorption systems (WANG; GUO, 2020).

One of the main parameters obtained from the kinetic study is the time required for the system to reach equilibrium, which is generally not instantaneous because of the resistance to mass transfer from the solution to the particle pores. The kinetics of the process is generally faster at the beginning, as the process occurs on the outer surface of the adsorbent, and slower as it reaches the inner surface of the adsorbent (GREEN; PERRY, 1934).

The study of the kinetics of static systems without significant volume variation is performed by applying kinetic models to the experimental data, and the amount of solute adsorbed at each instant (qt, mmol g^{-1}) is calculated by equation 8.

$$q_t = \frac{V}{m}(C_0 - C_t) \quad (8)$$

Where C_0 is the initial concentration of the adsorbate solution (mmol L^{-1}); C_t is the concentration of the adsorbate solution at time t (mmol L^{-1}); V is the volume of the solution (L); and m is the mass of adsorbent (g).

In this work, the pseudo-first order (PSO), pseudo-second order (PFO), and intraparticle diffusion models were studied.

2.1.4.1.1 Model of pseudo-first order (PSO)

Lagergren in 1898 presented a first order velocity equation. With this equation he succeeded in describing the liquid-solid phase adsorption model (QIU et al., 2009).

$$q_t = q_e(1 - e^{-k_1 t}) \quad (9)$$

Where q_e and q_t (mg g^{-1}) are the equilibrium adsorption capacities and time t (min), respectively. And k_1 (min^{-1}) is the velocity constant.

2.1.4.1.2 Model of pseudo-second order (PSO)

This equation was presented in 1995 by Ho and McKay. For this they described a process of adsorption of divalent metal (HO; MCKAY, 1999).

$$q_t = \frac{q_e^2 k_2 t}{1+q_e k_2 t} \quad (10)$$

Where q_e and q_t (mg g^{-1}) are the equilibrium adsorption capacities and time t (min). And k_2 (min^{-1}) is the second order rate constant.

2.1.4.1.3 Intraparticle Diffusion Model

Since the PPO and PSO models are based on the adsorption capacity of the solid phase, the Weber and Morris (1963) model, described by Equation 6, was developed to fill the gap in these models when intraparticle diffusion is the rate-determining factor (WEBER; MORRIS, 1963)

$$q_t = k_i t^{0.5} + C \quad (11)$$

Where k_i is the intraparticle diffusion coefficient (mmol g^{-1} $min^{0.5}$); and C is the constant related to diffusion resistance (mmol g^{-1}).

Since the constant I is related to the thickness of the boundary layer, the greater its value, the greater the interference of this layer in the process. If the plot of q_t vs $t^{0.5}$ is linear and passes through the point 0, we have that intraparticle diffusion is the predominant step in mass transfer and therefore the value of I is zero. It is possible for multilinearity to occur in three distinct steps if other processes are occurring. The first step is characterized by external mass transfer, the second step is characterized by intraparticle diffusion that occurs with gradual adsorption, and the third step is the final equilibrium phase where there is a decrease in intraparticle diffusion (WEBER; MORRIS, 1963).

2.2 STATE OF THE ART

2.2.1 Coal as a precursor of graphene and graphene oxide

Currently, there has been an increase in studies related to carbon as the main material for the preparation of various carbon nanomaterials. Similarly, since 2012, there has been an increase in the synthesis of carbon nanomaterials such as graphene and graphene oxide. This has happened because traditional methods use graphite as a raw material. Although this is a natural resource, it is also a limited resource that is only found in a few countries (SIERRA et al., 2016). Therefore, in Table 2.3, it can be found the works that have been carried out for the synthesis of graphene and graphene oxide from different types of mineral coal. From this study, it can be seen that both bituminous and anthracite coal are used for this type of synthesis. Coal residues can also be used as raw material. Much more information about graphene synthesis methods than graphene oxide synthesis methods can be found in the literature. This may be due to the complexity of some oxidation processes to achieve a quality GO. The Hummers method is still widely used for this type of synthesis, which leads us to confirm that it has not yet been possible to find an alternative process that is environmentally friendly for the synthesis of these materials. Finally, it should be noted that there is no pattern in the characterizations. Likewise, when these characterizations are analyzed in detail, there is also some disparity in the results, to the point of contradicting each other.

Table 2.3 - Overview of coal as precursor of graphene and graphene oxide

Raw Material	Synthesis Method	Product	Characterizations	Applications	Reference
Anthracite coal	Graphitization of coal, chemical oxidation and dielectric barrier discharge (DBD) plasma	Graphene Sheets	XRD, SEM, FTIR, XPS	Various applications	ZHOU et al. (2012).
Bituminous coal	Electric arc discharge with annealed coal electrode as anode and graphite electrode as cathode in H_2 and Ar mixture atmosphere	Graphene nanosheets	TEM, Raman spectrum, FTIR		AWASTHI et al. (2015).
Coal tar pitch	Pyrolysis with the presence of aluminum and HCl pickling treatment	Graphene nanosheets with crystalline structure	FESEM, XRD, TEM, Raman spectrum, XPS		XU et al. (2014).
Subbituminous Coal	Chemical vapor deposition (CVD)	Large area few layer graphene films	AFM	Electronics and energy storage	VIJAPUR et al. (2017).; VIJAPUR; WANG; BOTTE (2013).
Bituminous coal	Improved modified Hummers method	Few layer graphene	UV/VIS, XRD, FESEM	Electrochemical sensing of caffeine	SENTHIL KUMAR et al. (2017).
Coal tar pitch	nano-ZnO-template strategy coupled with in-situ KOH activation technique	3D graphene nano capsules	TEM, FESEM, XPS	Supercapacitor electrode	HE et al. (2017).
Anthracite coal	Graphitization of coal, removing the iron element with HCl, modified Hummers method combined with the in situ precipitation method	Graphene	XRD, Raman spectrum, SEM, TEM, HRTEM, XPS	Supercapacitors	GAO et al. (2014).

Source: Author´s own elaboration

Where: XRD - X-ray diffraction ; SEM – Scanning Electron Microscopy; FTIR - Fourier Transform Infrared Spectroscopy; XPS – X-ray photoelectron spectroscopy; TEM- Transmission Electron Microscopy; FESEM - Field Emission Scanning Electron Microscopy; AFM - The Atomic Force Microscope; HRTEM – High Resolution Transmission Electron Microscopy

Table 2.3 - Overview of coal as precursor of graphene and graphene oxide

(Conclusion)

Raw Material	Synthesis Method	Product	Characterizations	Applications	Reference
Lignite coal	Hummers method	Graphene Oxide	Raman spectrum		POWELL; BEALL, (2015).
Coal	Concentrated H_2SO4, oxidation by $NaNO_2$, stirred for 15.5 h, stirred for 6 h at 80 °C, dilution with HNO_3 and sedimentation by centrifugation at 10000 rpm	Graphene Oxide	AFM, DRX, Raman spectrum and XPS	Electronic Industry	WU et al. (2013).
non-coking coal	Concentrated H_2SO_4, oxide by $NaNO_2$, stirred for 15 h, stirred for 6 h at 80 °C, diluted by HNO_3 and centrifugation at 10000 rpm to 15 min	Graphene Oxide	FTIR, UV-Vis, SEM, DLS, XRD and TGA		SAHOO et al. (2022).
Semi-bituminous coal	Concentrated H_2SO_4 in presence of $NaNO_2$ in an ultra-sonication system at 80 °c for 24 h, followed by the addition of HNO_3	Graphene Oxide	Raman spectrum, XRD, XPS, FTIR, UV-vis, Zeta Potential	Material science and technology	DAS; KUNDU; CHAKRAVARTY (2022).
Bituminous coal	Modified Hummers method	Graphene Oxide	XRD, FTIR, UV/Vis, SEM		PURWANDARI et al. (2018).
Coal liquids	Hummer's method	Graphene oxide	TGA, AFM	Metallurgical coke industry	FERNÁNDEZ-GARCÍA et al. (2017).

Source: Author´s own elaboration

Where: XRD - X-ray diffraction; SEM – Scanning Electron Microscopy; FTIR - Fourier Transform Infrared Spectroscopy; XPS – X-ray photoelectron spectroscopy; TEM- Transmission Electron Microscopy; FESEM - Field Emission Scanning Electron Microscopy; AFM - The Atomic Force Microscope; TG - Thermogravimetric analysis.

2.2.2 Graphene oxide and geopolymer as adsorbents of pharmaceutical compounds

Many materials are currently used as adsorbents for the removal of constituents in water. These materials include silica, activated carbon, geopolymers, and graphene oxide (DE GISI et al., 2016). GO has shown better performance than graphene due to its porous structure and abundant oxygen-containing functional groups. These functional groups generate strong interactions with organic structures, such as antibiotics. Most of these pharmaceutical compounds have suitable interactions with graphene oxide via π-π stacking (ROSTAMIAN; BEHNEJAD, 2016). Similarly, geopolymers have attracted interest for adsorption problems due to their unusual 3D structure, including fixed-sized pores and pathways that allow the passage of certain pollutants (ARIFFIN et al., 2017).

Therefore, Table 2.4 presents a detailed study of the recent works in which graphene oxide and geopolymers have been used as adsorbents for pharmaceutical compounds.

Table 2.4 - Overview of graphene oxide and geopolymer as adsorbents of pharmaceutical compounds

Adsorbent	Adsorbate	Synthesis method	Maximum adsorption capacity (mg g^{-1})	Reference
Graphene Oxide Nanosheets	Tetracycline Doxycycline Ciprofloxacin Sulfamethoxazole	Purchased from US Research nanomaterials, Inc.	173.4 131 96.9 69.65	ROSTAMIAN; BEHNEJAD, (2016).
Graphene Oxide Nanosheets	Trimethoprim Isoniazid	Modified Hummer's method	204.08 13.89	ÇALIŞKAN SALIHI et al. (2021).
Single layer Graphene Oxide	Sulfamethoxazole Ciprofloxacin	Hummer method	379 240	CHEN; GAO; LI, (2015).
Graphene Oxide	Tetracycline	Modified Hummer's method	313	GAO et al. (2012).
Magnetic Graphene oxide sponge	Tetracycline	Modified Hummer's method for GO, and mixture with Fe_3O_4	473	YU et al. (2017).
Layered double hydroxide-graphene oxide-chitosan	Nalidixic	Modified Hummer's method	279.79	RADMEHR et al. (2021).

Table 4 – Overview of Graphene oxide and geopolymer as adsorbents of pharmaceutical compounds

(Conclusion)

Adsorbent	Adsorbate	Synthesis method	Maximum adsorption capacity (mg g^{-1})	Reference
Magnetite/Geopolymer	Tetracycline	Alkaline activation with addition of Fe_3O_4	20.45	AL-HUSSEINY; EBRAHIM (2022).
Metakaolin-based geopolymer microspheres	Tetracycline	Alkaline activation	645.7	WANG; ZHANG; GE (2022).

In Table 4, it possible to observe that the works of geopolymer for drug adsorption are scarce compared to that of graphene oxide. It can also be seen that the adsorption capacity of geopolymer is much higher than that of graphene oxide. This is due to the fact that geopolymer is a more porous material with a fixed size. Similarly, the works reported for graphene oxide all come from its traditional synthesis using the modified Hummers method. This is problematic because, as mentioned several times in this work, this synthesis leaves a lot of toxic residues. Therefore, it is not feasible to reproduce it on a large scale for wastewater treatment.

3 CHAPTER 3

This chapter deals with the study of the synthesis of graphene oxide from HCl-treated coal and coke by thermal exfoliation with sulfuric acid and oxidation with ozone.

3.1 SYNTHESIS OF MULTI-LAYER GRAPHENE OXIDE FROM HCL-TREATED COKE AND BRAZILIAN COALS BY SULFURIC ACID THERMAL EXFOLIATION AND OZONE OXIDATION

3.1.1 Introduction

Mineral coal has recently been proposed (LEE; MAHAJAN, 2021; LIU et al., 2022; PURWANDARI et al., 2023) for use as a low-cost alternative to graphite as a raw material for graphene production via chemical exfoliation. In addition to being low cost, coal is very abundant in several parts of the world. This has led to the development of competitive processes to convert this raw material into a key resource for the manufacture of new materials (VASIREDDY et al., 2011). Various grades of coal found in abundance are favorable sources for synthesis or for their transformation into nanomaterials such as graphite, graphene oxide, carbon fibers and carbon nano-particles (HOANG; HASSAN; GOMES, 2018; LI et al., 2022a).

Graphene-based compounds such as graphene oxide and reduced graphene oxide have received great attention in recent years, and due to their excellent electrical, mechanical and thermal properties have been considered for use in polymer nanocomposites, energy storage, thin films, and degradation of organic pollutants, among other applications (SAHOO et al., 2022). Therefore, several methods for the production of graphene have been reported, such as electrochemical exfoliation (LIU et al., 2019; RUBÉN ALEJANDRO ORTIZ FRANCISCO, 2022; YU et al., 2015), arc dis-charge (WANG et al., 2010; WU et al., 2009), chemical vapor deposition (SAEED et al., 2020), and sonication (KAUR et al., 2022). The process most used to date is the individual exfoliation of the graphite layers based on the Hummers method (MARCANO et al., 2010; PRIYADHARSHINI et al., 2023). Nevertheless, this procedure has several problems such as the use of concentrated acids that can present health risks and problems for the reuse of waste (POWELL; BEALL, 2015).

Graphene is not thermodynamically stable due to its melting temperature, which decreases as its thickness decreases. For this reason, a method has been found to switch from graphene to graphene oxide (GO) (AJALA et al., 2022). GO is composed of functional groups on its surface such as carboxylic acid, hydroxyl, and epoxy. It also has excellent adsorption capacity due to the aromatic hexagonal plane within its structure, which favors strong adhesion to different organic and inorganic molecules (CHAUDHURI; YUN, 2022). GO can be easily synthesized by chemical oxidation and exfoliation of graphite. It is also of vital importance to properly introduce reactive functional groups (carboxyl) to GO, since this improves the catalytic and adsorption properties. Likewise, the inclusion of oxygenated groups allows easy dispersion in water and organic solvents (AJALA et al., 2022).

In contrast to the syntheses that have been used and already mentioned here, a new method of synthesis with ozone has been found and it has been shown that ozone gives rise to atomic oxygen and hydroxyl radicals leading to the oxidation in this case of carbon, although the mechanism of this reaction is still not very clear (GROVEMAN et al., 2017). In Lesiak et al. (2014) GO was prepared through ozone oxidation, obtaining a lower amount of C sp^3 and oxygen groups, using a more economical, safe, effective and environmentally friendly method. Similarly, ozone oxidation and thermal treatment were used to modify the optical properties of GO (GROVEMAN et al., 2017; HASAN et al., 2017).

Nevertheless, the coal-based graphene properties depend on the coal rank, the structural evolution of the coal, degree of graphitization, and ash content (LI et al., 2022b). The coal impurities (mineral components) may destroy the integrity of the aromatic layer during graphitization, and the raw coal should be treated by HCl or purified before coal-based graphene preparation (LAN et al., 2019; LIU et al., 2020; NYATHI; CLIFFORD; SCHOBERT, 2013).

The maceral composition of the mineral coals also affects the coal-based graphene properties. Bituminous coal and anthracite are potentially useful for producing graphene, but there is no consensus about the formation mechanisms of coal-based graphene from macerals and the most suitable method for obtaining high yield and optimized properties for each GO application.

The main objective of this research was to prepare GO from Brazilian mineral coal and coke using a new route with chemical exfoliation and ozone oxidation. This synthesis is environmentally friendly because it lowers the amount of concentrated acid

used as well as the amount of wastes. FTIR, XRD ZP, PSD analyses proved the synthesis of GO, and TEM and RAMAN analyses showed the morphology of the synthesized material.

3.1.2 Materials and methods

Two different Brazilian bituminous coals were supplied by different companies, as designated in Table 3.1. Additionally, a mineral coke was used as raw material to prepare GO. Hydrochloric acid (HCl, PA, 37%, Wt.: 36.458 g mol^{-1}) was purchased from Exôdo Científica, São Paulo, Brazil and sulfuric acid (H2SO4, PA, 99.8%, Wt.: 98.079 g mol^{-1}) from Vetec, Rio de Janeiro, Brazil. Nitrogen under high pressure was purchased from White Martins, Brazil and ozone was generated *in situ* by an ozone generator (O3R, Brazil).

Table 3.1 - Sample names and nomenclature of coke and coal

Supplier	Sample	Nomenclature
Company B, Brazil	Mineral coke	Cq
Company B, Brazil	Bituminous coal	CB
Company S, Brazil	Bituminous coal	CS

The coal samples were treated by adding 500 mL of 20% hydrochloric acid (HCl) to 10 g of solid coal in a flask under magnetic stirring for 24 h. The suspension was then filtered in a vacuum system followed by extensive washing using deionized water until reaching neutral pH. This was followed by drying at 45 °C in an oven (MS Equipamentos) for 48 h.

Then, the chemical treatment was performed by adding 10 mL of sulfuric acid (H_2SO_4) to the solid, and they were left in contact for 24 h at room temperature. Thermal exfoliation was then performed in a tubular pyrolysis reactor placed in an oven (MS Equipamentos) at 950 °C for 30 min in a nitrogen atmosphere. The furnace was previously heated at a rate of 20 °C min^{-1}. For the oxidative treatment, the resulting powder was suspended in water and treated with ozone for 18 h using a flow rate of 1 L min^{-1}. Next, the aqueous suspension was sonicated (Unique, model USC-1650A) for 60 min at a frequency of 25 kHz. Finally, the GO was separated by vacuum filtration (glass membrane filter 0.55 µm and PVDF membrane 0.22 µm, Millipore, Brazil) and oven-dried at 45 °C overnight. This methodology was adapted from Moreira (2021).

Non-HCl treated samples were also submitted to chemical, thermal, oxidation and sonication treatments to examine the effect of the mineral content on the GO properties. The Figure 3.1 presents a schematic representation of the process applied for obtaining the GO.

Figure 3.1 - Schematic process for obtaining the GO.

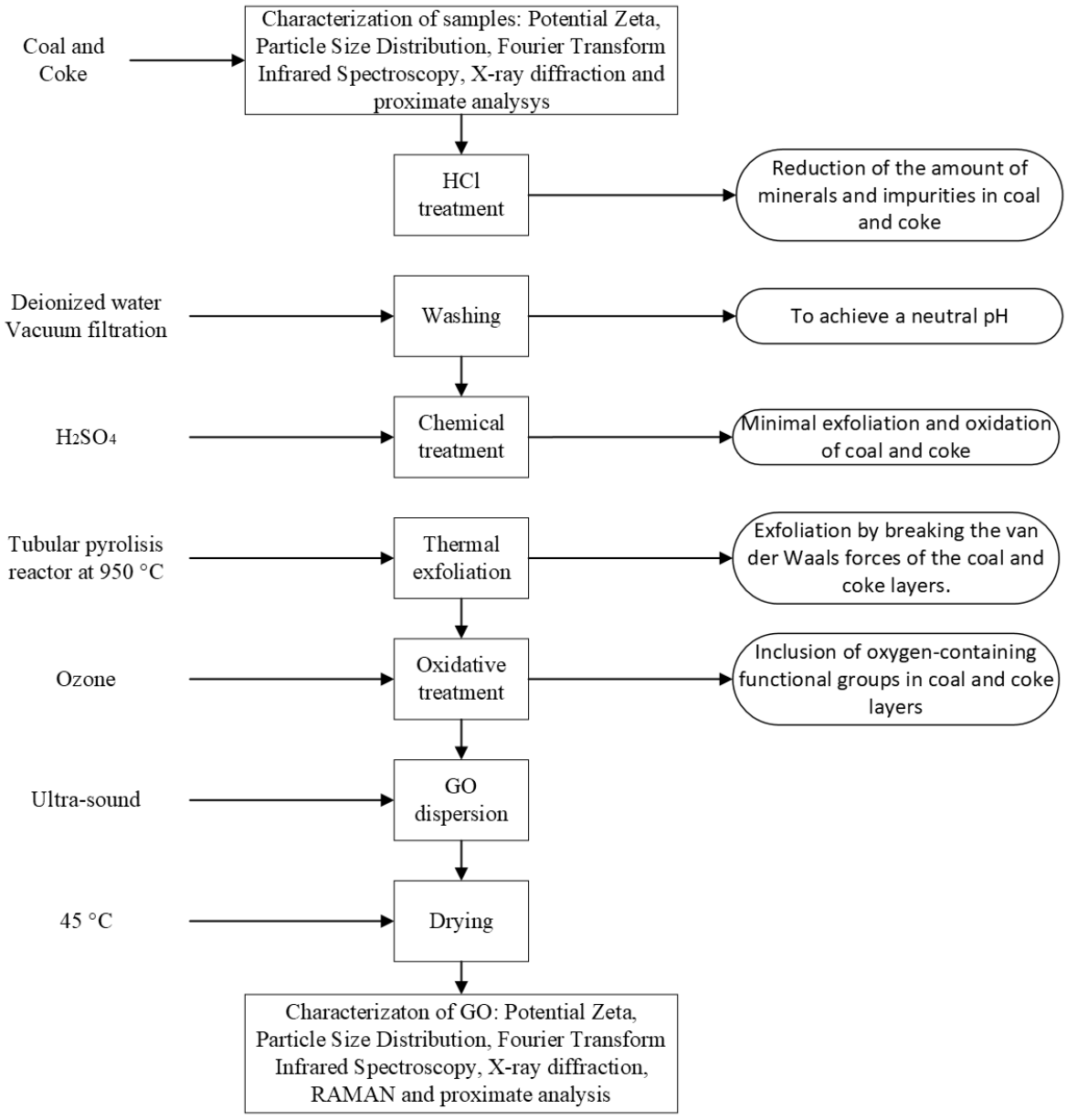

Table 3.2 shows the designation given to the synthesized materials according to the treatment applied, where XX can be Cq, CB or CS.

Table 3.2 - Nomenclature of the product samples according to the treatment applied.

Nomenclature*	Treatment
XX_HCl_OG	HCl treatment, thermal exfoliation followed by oxidation with ozone and ultra-sound
XX_OG	Thermal exfoliation followed by oxidation with ozone and ultra-sound

* Where XX can be Cq, CB or CS

The resulting GO was characterized by X-Ray Diffraction (XRD) on a Rigaku Miniflex 600 diffractometer operating with radiation CuKα (λ=0.1542 nm) and the Scherrer equation (Eq. 12) was used to determine the crystallite size, where λ is the wavelength, θ is the Bragg angle, L is the apparent particle size, β is the half peak width and K is the Scherrer constant (LUCÍA MARTÍNEZ GOYENECHE, 2018).

$$\beta = K\lambda/L\cos\theta \quad (12)$$

The X-ray generator was set at a voltage of 40 kV and current of 40 mA. The continuous scan mode was used in a 2θ between 10° and 90° with a step of 0.05° at a rate of 10° min^{-1}. The zeta potential of the sample was determined by Electrophoretic Light Scattering (ELS) at 173° on a Malvern MPT-2 equipment. The particle size distribution was determined by Dynamic Light Scattering (DLS) in the range of 0.3 nm to 10 μm. The FTIR spectra of GO was analyzed on a PerkinElmer Spectrum 100 equipment, using KBr pellets with a wavenumber range of 4000 to 40. The morphology of the resulting material was obtained on a JEM-2100 TEM microscope with a maximum accelerating voltage of 200 kV. The approximate analysis was done in the Shimadzu DTA-60 equipment and the analysis conditions can be seen in Table 3.3

Table 3.3 - Conditions applied for approximate analysis.

Temperature rate, °C/min	Holding temperature, °C	Retention time, min	Gas
10	35	20	Nitrogen
50	50	5	Nitrogen
50	110	5	Nitrogen
20	950	15	Nitrogen
-10	750	0	CO_2
1	750	40	CO_2

3.1.3 Results and discussion

3.1.3.1 Proximate analysis

For the production of GO it is important to analyze the initial quality of the materials used and the final quality of the products obtained. The main parameters are the percentages of moisture (U), fixed carbon (FC), volatile matter (VM), and ash (CZ). The moisture result is the basis for calculating the other parameters on a dry basis.

$$VM' = VM\frac{100}{100-U} \quad (13)$$

$$CZ' = CZ\frac{100}{100-U} \quad (14)$$

$$FC' = 100\% - MV - CZ \quad (15)$$

Table 3.4 shows the results obtained in the proximate analysis of the raw and treated samples.

Table 3.4 - Results of the proximate analysis of the raw and treated samples

Nomenclature	Fixed Carbon, wt% (db*)	Volatile Material, wt% (db)	Ash, wt% (db)
Cq	82.39	6.70	10.91
Cq_OG	77.49	9.00	13.51
Cq_HCl_OG	81.37	8.39	10.23
CB	52.32	33.18	14.50
CB_OG	58.31	23.60	18.09
CB_HCl_OG	63.45	17.89	18.66
CS	54.46	31.26	14.27
CS_OG	68.77	17.39	13.84
CS_HCl_OG	68.42	13.74	17.84

* db: dry basis

The percentage of fixed carbon is the portion of carbon that remains as a residue after the volatile matter has been removed from the material. It generally consists of only carbon but may contain trace amounts of hydrogen, oxygen, nitrogen and sulfur (SARKAR, 2015). Volatile matter is composed of components that burn easily in the presence of oxygen, including short and long chain hydrocarbons, aromatics and sulfur (BOTTLE; WHITE, 2023; MUTHU DINESH KUMAR; ANAND, 2019). Finally, ashes are produced during the combustion of the organic fraction (PATRA et al., 2012).

In this study, three materials were chemically treated, expecting to minimize interferences in the graphitic regions to avoid undesired reactions that could lead to the oxidation and exfoliation of coal and coke (LEE; MAHAJAN, 2021). Table 3.4 is very important as it helps to understand the nature of the raw material. Cq, being a high temperature pretreated material, has a lower percentage of volatile material than CB and CS. While bituminous coals, being of the same species, have a similar percentage of volatile material. In the same way, CB and CS have a lower percentage of fixed carbon and their percentage of ash is higher than that of Cq.

Table 3.4 shows how the percentage of volatile matter was reduced in the coals CB and CS, with a reduction of 15.29% and 17.52%, respectively. On the other hand, there was a small increase in the VM content for coke, which was expected since coke is a material that has been previously treated at a high temperature.

The chemical treatment was expected to eliminate that percentage of ash that can interfere in the subsequent steps of the process. In this case, what was expected was a decrease in the percentage, but Table 3.4 shows that for Cq it decreases low proportion (0.68%) but for CB and CS it increases so the demineralization process was not effective. This increase is due to the decrease in volatile material lost from the synthesized samples due to heat treatment and the coals were only treated with HCl, which will only eliminate some minerals from the coal, but this acid is not capable of eliminating other minerals or compounds such as SiO_2 (DAS; KUNDU; CHAKRAVARTY, 2022; MANOJ; KUNJOMANA, 2014).

3.1.3.2 FTIR Analysis

The FTIR spectra of the different GO synthesized (Figure 3.2) show the presence of the absorption bands at 1032 cm^{-1}, 1053 cm^{-1} and 1426 cm^{-1}, which are attributed to C-O stretching vibrations (MANORATNE; ROSA; KOTTEGODA, 2017; RATTANA et al., 2012; SUREKHA et al., 2020). The 1032 cm^{-1} peak is found to be not so intense in the Cq_OG, while good intensity is seen for the Cq_HCl_OG and CS_OG materials. The 1053 cm^{-1} peak is only seen in the CB_OG, CB_HCl_OG and CS_OG materials, although in the latter material its intensity is low. Meanwhile, the 1426 cm^{-1} peak is only found in the CS_OG material with medium intensity. The peak at 1529 cm^{-1} is related to C=C stretching (SHARMA et al., 2017; SUREKHA et al., 2020) and is found with a low intensity in Cq_HCl_OG, CB_OG and CB_HCl_OG. A characteristic peak of commercial GO, the peak at 1600 cm^{-1}, is attributed to the O-H vibrations of water (MANORATNE; ROSA; KOTTEGODA, 2017) and can be found in materials made from CS coal. Likewise, in the materials originating from coke, two high intensity peaks were clear at 2039 cm^{-1} and 2155 cm^{-1}, which are related to the C=C=C stretching of a material derived from coal. Similarly, in the CS_OG, two peaks were clear at 2835 cm^{-1} and 2919 cm^{-1}, corresponding to the hydrogen bonded OH groups of the COOH groups and the O-H stretching (MANORATNE; ROSA; KOTTEGODA, 2017). In the materials made from CB and CS coals, a large amplitude peak was observed at 3428 cm^{-1} with strong intensity, and which corresponds to the stretching vibrations of the OH groups of water (SHAHRIARY; ATHAWALE, 2014; SHARMA et al., 2017). Finally, in the sample CS_OG, there were more oxygenated groups because the oxidation with ozone was more effective than in the other GO syntheses. Similarly,

it could be noted that the materials made from coke were the poorest in oxygenated groups, although they still presented peaks characteristic of untreated coal.

Figure 3.2 - FTIR spectrum of the treated samples Cq_OG, Cq_HCl_OG, CB_OG, CB_HCl_OG, CS_OG and Cq_HCl_OG

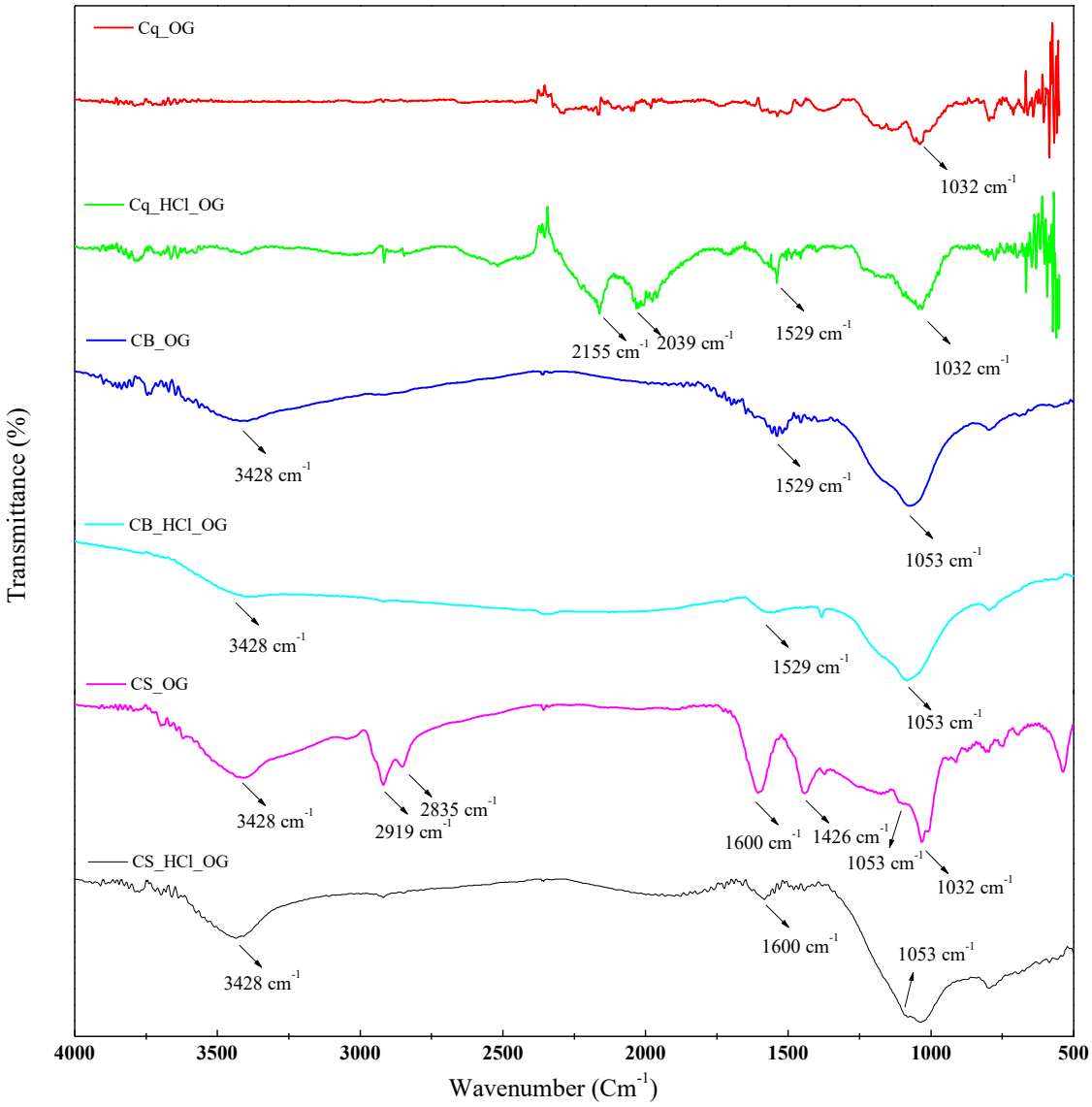

3.1.3.3 Zeta potential analysis

The zeta potential of the treated samples (Table 3.5) was measured in aqueous solution at neutral pH to determine the stability of the synthesized GOs (KUMAR MAHATO et al., 2022), which is dependent on the stabilization of the electrostatic charge

Table 3.5 - Results for zeta potential for the aqueous dispersions obtained from raw and treated samples.

Nomenclature	Zeta potential, mV
Cq	-26.4
Cq_OG	-21.3
Cq_HCl_OG	-17.8
CB	-13.8
CB_OG	-14.1
CB_HCl_OG	-17.5
CS	-14.2
CS_OG	-25.36
CS_HCl_OG	-21.2

The results obtained for all the GO synthesized had negative values, which may be due to the ionization of the carboxylic acid group, and the appearance of negatively charged functional groups (DAS; KUNDU; CHAKRAVARTY, 2022; HAN; MAO; LIU, 2022). Likewise, a high negative value would indicate a high physical stability. Therefore, the carbon-based materials obtained in this study achieved a zeta potential more negative than its initial value, indicating the improvement in the electrical activity and the inhibition of aggregates due to electrostatic repulsion (KUMAR MAHATO et al., 2022). However, the materials synthesized from coke did not improve their stability, achieving a less negative zeta potential value than the initial coke value.

3.1.3.4 Particle size distribution

Particle size distribution has been reported as a simple and fast method of graphene characterization (AMARO-GAHETE et al., 2019). Figure 3.3 shows the particle size distributions of all the carbon-based materials with a Gaussian approximation. For the CS_OG material, an average of 3800 nm was obtained, the largest particle size achieved. The second largest particle size has an average of

1500 nm and is from the Cq_OG, while for the rest of the synthesized materials a particle size between 200 nm and 800 nm can be seen.

Figure 3.3 - Results of the DTP analysis for the treated samples Cq_OG, Cq_HCl_OG, CB_OG, CB_HCl_OG, CS_OG and Cq_HCl_OG

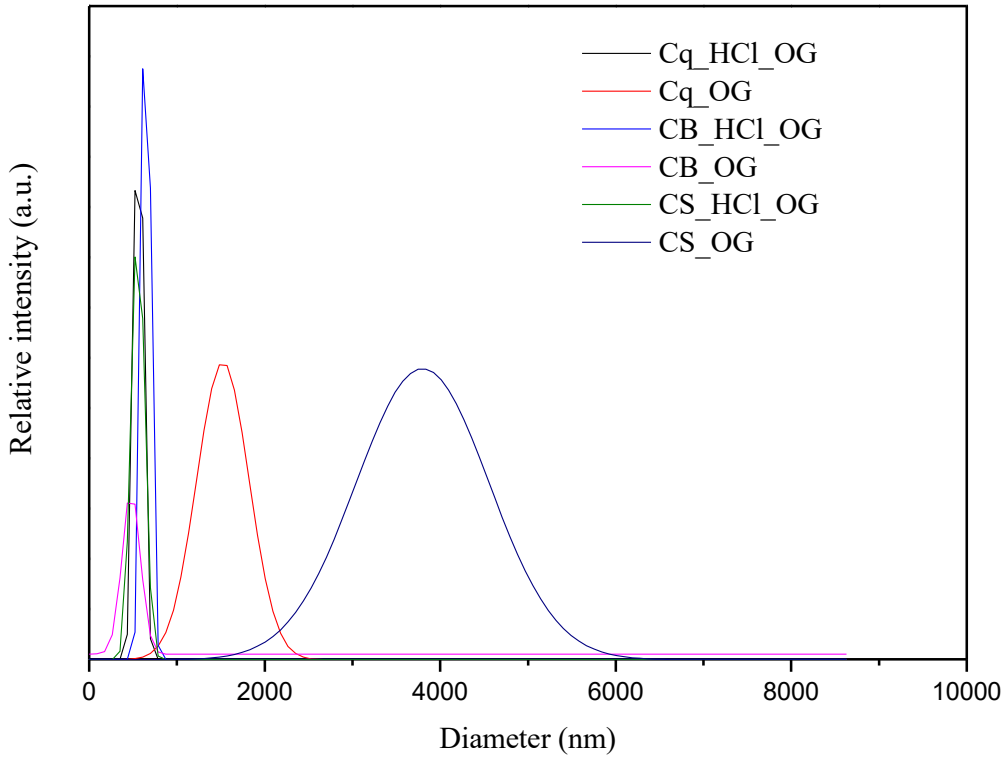

The initial particle sizes of Cq, CB and CS were 1403 nm, 1306 nm and 3236 nm respectively. In fact, the particle size of the graphene obtained according to previous studies is related to the size of the coke or coal used (HUSKIĆ et al., 2018). This can be seen in the results of this study. In the materials obtained from Cq_OG and CS_OG treatments, the size remained the same or very similar to the initial size. On the other hand, for the Cq_HCl_OG, CB_HCl_OG and CB_OG treatments, a reduction in size of 42%, 38% and 35% respectively, was achieved. Likewise, the material that reduced in size the most was CS_OG, dropping by 78.3%, while it was initially the largest. Similarly, smaller particles may be due to the breakage of the larger carbon particles during the synthesis, increasing the hydrophilic property of graphene (HU et al., 2013; HUSKIĆ et al., 2018).

3.1.3.5 TEM analysis

The morphology of the synthesized GO was studied by TEM images presented in Figure 3.4.

Figure 3.4 - TEM of the samples (a) Cq_HCl_OG, (b) Cq_OG, (c) CB_HCl_OG, (d) CB_OG, (e) CS_HCl_OG and (f) CS_OG

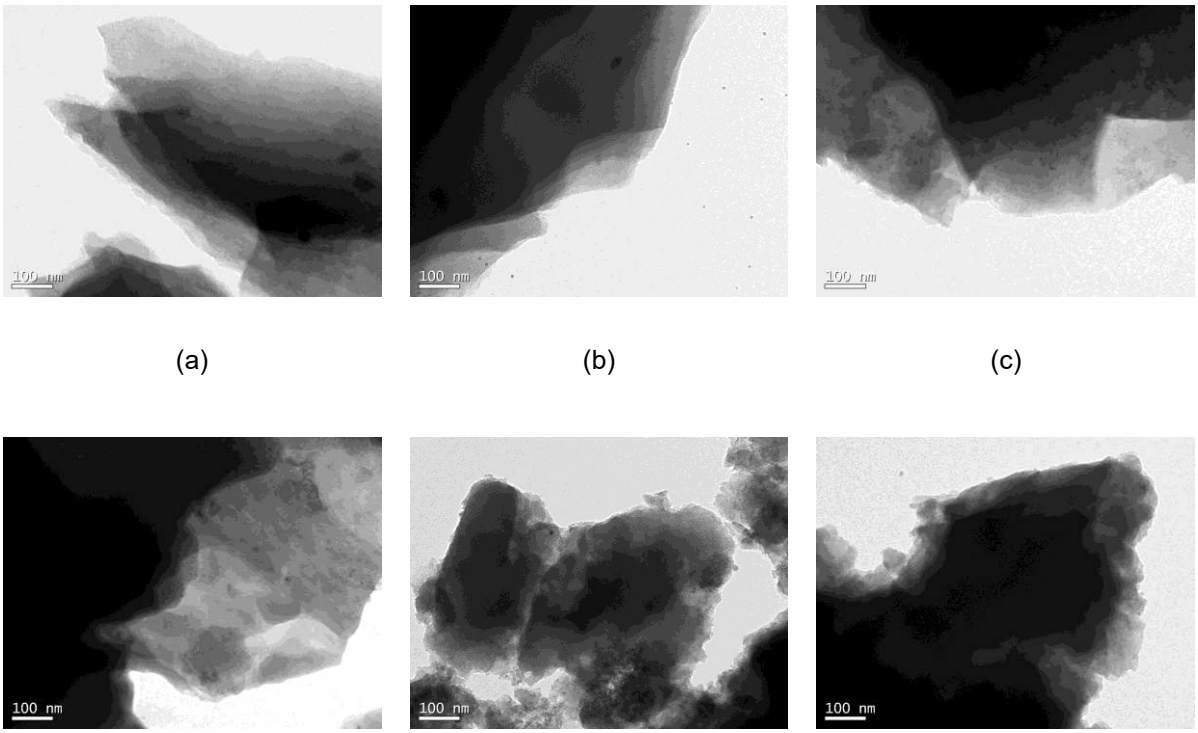

(a) (b) (c)

(d) (e) (f)

The morphology of the six GOs produced were similar, and are formed by lamellae with different transparencies, which reveal the nature of the material (FENG et al., 2013). In fact, the darker portions correspond to where there is a greater stacking of layers of GO (multilayer), while the most transparent parts are formed by one or two layers (STOBINSKI et al., 2014). This can occur when the chemical exfoliation with H_2SO_4 is not complete, but only takes place at the edges of the GO layers. On the contrary, in the process of oxidation with ozone, it was expected that the functional groups with oxygen and hydrogen were formed only at the edges of the layers, which was evident in the results obtained in the FTIR (Fig 1). In the same way, the presence of darker parts in the TEM images may be due to the low stability of solid GO, which causes its layers to stick together again after some time. It may also be due to

contaminants adsorbing on the surface at room temperature, which makes direct observation of the GO morphology difficult (DAVE et al., 2016).

3.1.3.6 XRD analysis

The results obtained by X-Ray Diffraction are presented in Figure 3.5. The graphs show the initial and after treatment conditions for each sample. For the three raw materials, Cq, CB and CS, the peak at 26.5° can be seen, which is characteristic of bituminous coal and confirms the presence of quartz. On the other hand, the CS presents hematite derived from the reaction between the sulfur of the pyrite and the calcite of the coal (MOHAMAD et al., 2013).

Figure 3.5 - XRD results obtained for the raw and treated samples (a) Cq, Cq_OG, Cq_HCl_OG, (b) CB, CB_OG, CB_HCl_OG, (c) CS, CS_OG and CS_HCl_OG.

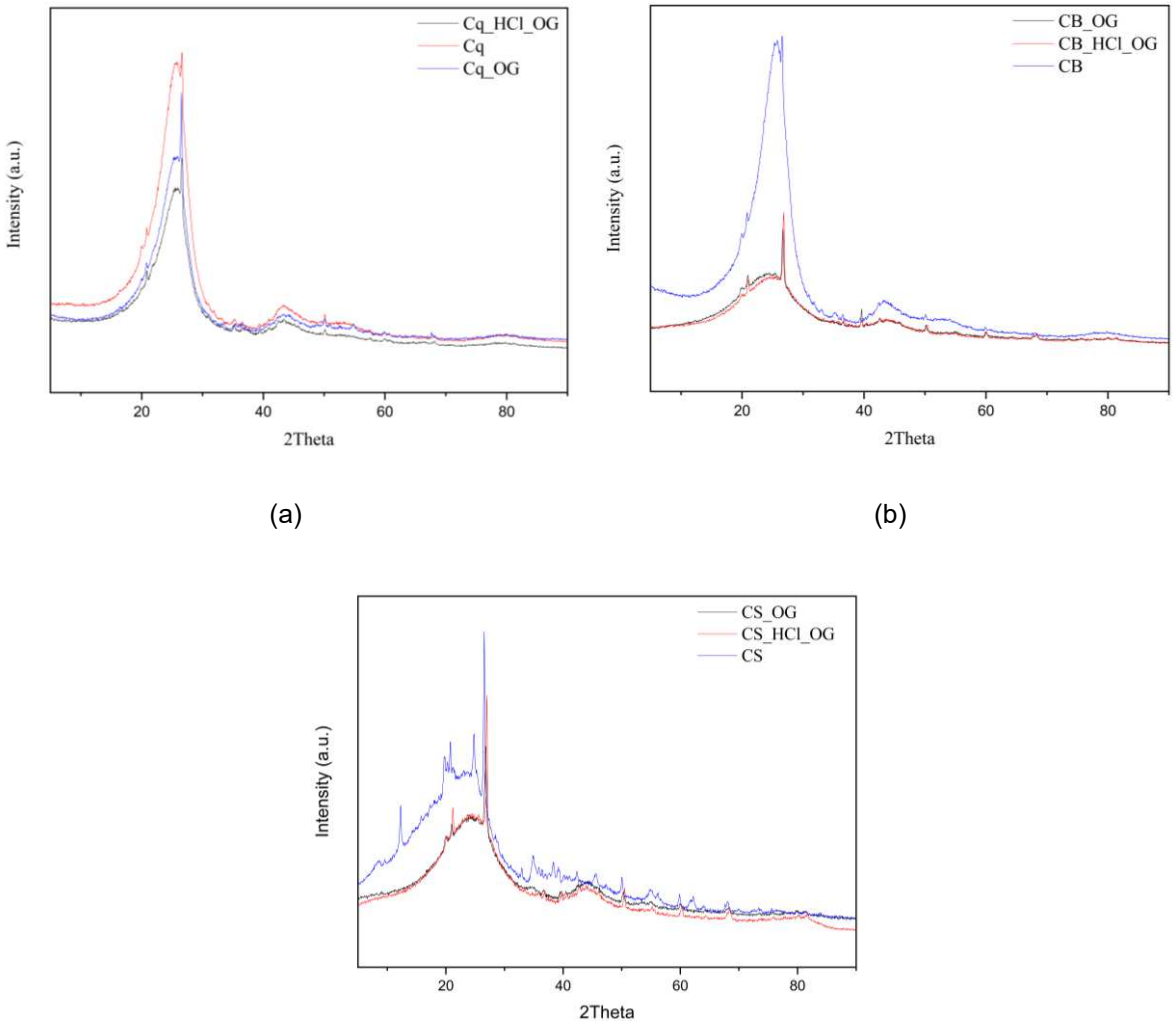

The peak at 26.5 was present in all the GOs produced, which means that GO may be mixed with quartz. This peak was lower after the treatments performed in this work, which is characteristic of the formation of GO from carbon exfoliation. Likewise, the incomplete reduction of these peaks indicates that the demineralization was not effective with HCl. One aspect to emphasize is that the crystal size, shown in Table 3.6 and calculated with the Scherrer equation (Eq. 12), decreased after the treatments performed, confirming the expected behavior in the transformation of carbon to GO (GUPTA et al., 2017; HAZIM et al., 2023; SAXENA et al., 2011; SUREKHA et al., 2020). The non-demineralization of carbon can also be seen in Table 3.6, where the carbon-based materials crystal size were 22.3 nm and 20.2 nm for CB_HCl_OG and CS_HCl_OG, respectively, while the average value expected for a completely demineralized material is 2.354 nm.

Table 3.6 - Crystal size of the raw and treated samples Cq, Cq_OG, Cq_HCl_OG, CB, CB_OG, CB_HCl_OG, CS, CS_OG and Cq_HCl_OG

Nomenclature	**Crystal size, nm**
Cq	3.1
Cq_OG	2.6
Cq_HCl_OG	0.8
CB	25.3
CB_OG	20.9
CB_HCl_OG	22.3
CS	24.2
CS_OG	22.8
CS_HCl_OG	20.2

3.1.3.7 RAMAN analysis

The RAMAN spectra obtained for each GO synthesized are shown in Figure 3.6. A D-band can be seen all the GO at 1376 cm^{-1}, a G-band at 1596 cm^{-1}, which corresponds to the order dispersion of the E_{2g} mode, and a 2D-band at 2893 cm^{-1}, which is the overtone of the D-band and is helpful for determining the structural

parameters of the c-axis orientations (KRISHNAMOORTHY et al., 2013). Meanwhile, in the materials synthesized from coke, a D band can be seen with lower intensity than in those produced by coal, which may be due to a defective formation and the presence of hetero-atoms in the plane grain boundaries. Similarly, the intensity of the 2D band was minimal due to the breaking of the stacking of the coal and coke layers by oxidation with sulfuric acid (KRISHNAMOORTHY et al., 2013).

Figure 3.6 - RAMAN spectra obtained for the treated samples Cq_OG, Cq_HCl_OG, CB_OG, CB_HCl_OG, CS_OG and CS_HCl_OG

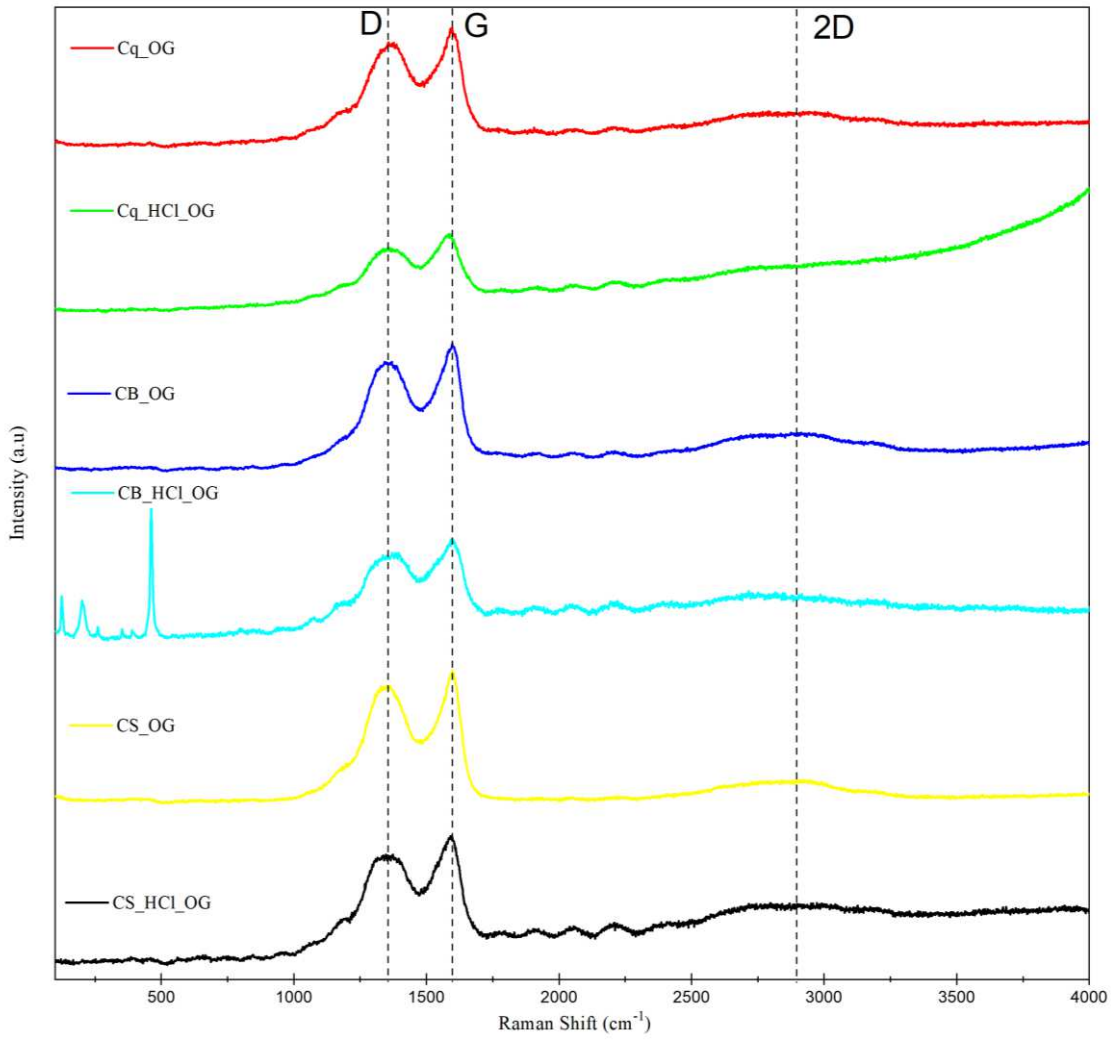

These bands observed for the treated samples are in agreement with the characteristics of other GO reported in the literature (DAVE et al., 2016; DÍEZ-BETRIU et al., 2013; MEHTA et al., 2017; XU et al., 2022) given that they presented several heat-treated GO films and obtained a D band at 1340 cm^{-1} and a G band at 1580 cm^{-1}. The characterization of the GO synthesized through the methods reported in this

study has shown a G band towards a higher wavenumber, which means that the GO synthesized had a higher oxidation level. Moreover, the results for the crystallite size (La) of each material can be seen in Table 3.7 and the Tuinstra Koenig ratio (Eq. 16) was used for this calculation. The I_D/I_G ratio was also reported, this ratio is used to verify whether the material was modified during the synthesis performed. In (AMARO-GAHETE et al., 2019), an I_D/I_G ratio for coal of 0.10 was reported, and for the materials obtained from Cq, CS and CB, values were obtained between 0.8 and 0.9, which means that this ratio increased, confirming the exfoliation of coal and coke, although between the synthesized materials there was no significant difference (FENG et al., 2013). The crystallite size of the synthesized materials was calculated according to Equation 16.

$$La(nm) = \frac{(2.4x10-10)(\lambda)^4}{I_D/I_G} \quad (16)$$

Table 3.7 - I_D/I_G ratio values and crystallite size (La) estimated by RAMAN spectroscopy for the GO samples obtained.

Nomenclature	I_D/I_G	La, nm
Cq_OG	0.854	22
Cq_HCl_OG	0.900	21
CB_OG	0.876	22
CB_HCl_OG	0.899	21
CS_OG	0.897	21
CS_HCl_OG	0.887	21

All materials presented similar crystallite size (La), and the results agree with XRD results. From the I_D/I_G ratio, it possible conclude that multilayered materials were synthesized by the thermal exfoliation followed by oxidation with ozone and ultra-sound.

3.1.4 Conclusions

In this study, multilayer GO was synthesized from coke and coal as base materials. Ozone oxidation was proved to be efficient for the production of oxidized materials. The sample CS_OG was the most oxidized of the synthesized materials and

this is proven by the amount of oxygenated groups seen in the FTIR spectra and by the decrease in crystal size of 78.3%. The GO obtained was characterized by FTIR, zeta potential, TEM, XRD and RAMAN. The XRD pattern showed a peak at 26 with a lower intensity after the treatments performed. The TEM images revealed that the exfoliation of the coal and coke layers was better at the edges of these materials. The methodology proposed in this paper presents a new method for fast, and environmentally friendly synthesis from coal and coke. Finally, it is recommended that future studies conduct demineralization with HF and HCl to reduce the initial percentage of ash, obtain a better quality GO.

3.1.5 References

AJALA, O. J. et al. A critical review on graphene oxide nanostructured material: Properties, Synthesis, characterization and application in water and wastewater treatment. Environmental Nano-technology, Monitoring & Management, v. 18, p. 100673, dez. 2022.

AMARO-GAHETE, J. et al. A Comparative Study of Particle Size Distribution of Graphene Nanosheets Synthesized by an Ultrasound-Assisted Method. Nanomaterials, v. 9, n. 2, p. 152, 26 jan. 2019.

BOTTLE, J.; WHITE, A. R. J. Coal analysis. Em: The Coal Handbook. [s.l.] Elsevier, 2023. p. 133–161.

CHAUDHURI, H.; YUN, Y.-S. Synthesis and environmental applications of graphene oxide/layered double hydroxides and graphene oxide/MXenes: A critical review. Separation and Purification Technology, v. 297, p. 121518, set. 2022.

DAS, B.; KUNDU, R.; CHAKRAVARTY, S. Preparation and characterization of graphene oxide from coal. Materials Chemistry and Physics, v. 290, p. 126597, out. 2022.

DAVE, S. H. et al. Chemistry and Structure of Graphene Oxide via Direct Imaging. ACS Nano, v. 10, n. 8, p. 7515–7522, 23 ago. 2016.

DÍEZ-BETRIU, X. et al. Raman spectroscopy for the study of reduction mechanisms and optimization of conductivity in graphene oxide thin films. Journal of Materials Chemistry C, v. 1, n. 41, p. 6905, 2013.

FENG, H. et al. Correction: Corrigendum: A low-temperature method to produce highly reduced graphene oxide. Nature Communications, v. 4, n. 1, p. 1927, 8 jul. 2013.

GROVEMAN, S. et al. The role of ozone in the formation and structural evolution of graphene oxide obtained from nanographite. Carbon, v. 122, p. 411–421, out. 2017.

GUPTA, V. et al. Higher oxidation level in graphene oxide. Optik, v. 143, p. 115–124, ago. 2017.

HAN, F.; MAO, J.; LIU, S. Preparation of reduced graphene oxide-carbon nanotubes membranes for conductive heating membrane distillation treatment of humic acid. Separation and Purification Technology, v. 302, p. 122181, dec. 2022.

HASAN, M. T. et al. Modifying optical properties of reduced/graphene oxide with controlled ozone and thermal treatment in aqueous suspensions. Nanotechnology, v. 28, n. 6, p. 065705, 10 feb. 2017.

HAZIM, S. et al. Graphene oxide-gastrointestinal drugs for no side effect: Ultrasound synthesis and characterization. Materials Today: Proceedings, p. S2214785322076374, jan. 2023.

HOANG, V. C.; HASSAN, M.; GOMES, V. G. Coal derived carbon nanomaterials – Recent advances in synthesis and applications. Applied Materials Today, v. 12, p. 342–358, set. 2018.

HU, X. et al. Effects of particle size and pH value on the hydrophilicity of graphene oxide. Applied Surface Science, v. 273, p. 118–121, may 2013.

HUSKIĆ, M. et al. One-step surface modification of graphene oxide and influence of its particle size on the properties of graphene oxide/epoxy resin nanocomposites. European Polymer Journal, v. 101, p. 211–217, abr. 2018.

KAUR, A. et al. Temperature as a key parameter for graphene sono-exfoliation in water. Ultrasonics Sonochemistry, v. 90, p. 106187, nov. 2022.

KRISHNAMOORTHY, K. et al. The chemical and structural analysis of graphene oxide with different degrees of oxidation. Carbon, v. 53, p. 38–49, mar. 2013.

KUMAR MAHATO, P. et al. Evaluation of crystal size present in graphene oxide quantum dots using optical and Raman spectroscopy. Materials Today: Proceedings, p. S221478532206905X, nov. 2022.

LAN, C. et al. Effects of Minerals in Anthracite on the Formation of Coal-Based Graphene. ChemistrySelect, v. 4, n. 19, p. 5937–5944, 24 maio 2019.

LEE, S.-Y.; MAHAJAN, R. L. A facile method for coal to graphene oxide and its application to a bio-sensor. Carbon, v. 181, p. 408–420, ago. 2021.

LESIAK, B. et al. Preparation of graphene oxide and characterisation using electron spectroscopy. Journal of Electron Spectroscopy and Related Phenomena, v. 193, p. 92–99, mar. 2014.

LI, H. et al. Synthesis, modification strategies and applications of coal-based carbon materials. Fuel Processing Technology, v. 230, p. 107203, jun. 2022a.

LI, R. et al. Effects of Coal Rank and Macerals on the Structure Characteristics of Coal-Based Graphene Materials from Anthracite in Qinshui Coalfield. Minerals, v. 12, n. 5, p. 588, 6 may 2022b.

LIU, F. et al. Synthesis of graphene materials by electrochemical exfoliation: Recent progress and future potential. Carbon Energy, v. 1, n. 2, p. 173–199, dec. 2019.

LIU, G. et al. Coal-based graphene as a promoter of TiO2 catalytic activity for the photocatalytic degradation of organic dyes. New Carbon Materials, v. 37, n. 6, p. 1172–1180, dec. 2022.

LIU, L. et al. Pyrolysis behavior and product distribution of exinite submacerals. Journal of Analytical and Applied Pyrolysis, v. 152, p. 104957, nov. 2020.

LUCÍA MARTÍNEZ GOYENECHE. DETERMINACIÓN DEL TAMAÑO DE PARTÍCULA ME-DIANTE DIFRACCIÓN DE RAYOS X. Universidad de Cantabria, , set. 2018. Disponível em: <https://repositorio.unican.es/xmlui/bitstream/handle/10902/15651/Martinez%20Goyeneche%20Lucia.pdf?sequence=1>. Access in: 28 mar. 2023

MANOJ, B.; KUNJOMANA, A. G. Systematic investigations of graphene layers in sub-bituminous coal. Russian Journal of Applied Chemistry, v. 87, n. 11, p. 1726–1733, nov. 2014.

MANORATNE, C. H.; ROSA, S. R. D.; KOTTEGODA, I. R. M. XRD-HTA, UV Visible, FTIR and SEM Interpretation of Reduced Graphene Oxide Synthesized from High Purity Vein Graphite. Material Science Research India, v. 14, n. 1, p. 19–30, 28 jun. 2017.

MARCANO, D. C. et al. Improved Synthesis of Graphene Oxide. ACS Nano, v. 4, n. 8, p. 4806–4814, 24 ago. 2010.

MEHTA, J. S. et al. How Reliable Are Raman Spectroscopy Measurements of Graphene Oxide? The Journal of Physical Chemistry C, v. 121, n. 30, p. 16584–16591, 3 ago. 2017.

MOHAMAD, N. F. et al. Characteristics of bituminous coal, sub-bituminous coal and bottom ash from a coal-fired power plant. 2013 IEEE Business Engineering

and Industrial Applications Colloquium (BEIAC). Anais...in: 2013 IEEE BUSINESS ENGINEERING AND INDUSTRIAL APPLICA-TIONS COLLOQUIUM (BEIAC). Langkawi, Malaysia: IEEE, abr. 2013. Disponível em: <http://ieeexplore.ieee.org/document/6560193/>. Access in: 15 mar. 2023

MUTHU DINESH KUMAR, R.; ANAND, R. Production of biofuel from biomass downdraft gasification and its applications. Em: Advanced Biofuels. [s.l.] Elsevier, 2019. p. 129–151.

NYATHI, M. S.; CLIFFORD, C. B.; SCHOBERT, H. H. Characterization of graphitic materials pre-pared from different rank Pennsylvania anthracites. Fuel, v. 114, p. 244–250, dez. 2013.

PATRA, K. C. et al. Elemental analysis of coal and coal ASH by PIXE technique. Applied Radiation and Isotopes, v. 70, n. 4, p. 612–616, abr. 2012.

POWELL, C.; BEALL, G. W. Graphene oxide and graphene from low grade coal: Synthesis, characterization and applications. Current Opinion in Colloid & Interface Science, v. 20, n. 5–6, p. 362–366, out. 2015.

PRIYADHARSHINI, K. et al. Green synthesis and application of graphene oxide extracted from Punica granatum. Materials Today: Proceedings, p. S2214785323001360, fev. 2023.

PURWANDARI, V. et al. The role of biocatalysts in the synthesis of graphene nanosheets from sub-bituminous coal. Materials Science for Energy Technologies, v. 6, p. 282–289, 2023.

RATTANA et al. Preparation and characterization of graphene oxide nanosheets. Procedia Engineering, v. 32, p. 759–764, 2012.

RUBÉN ALEJANDRO ORTIZ FRANCISCO. Síntesis y caracterización morfológica y electroquímica de puntos cuánticos de grafeno. , ago. 2022. Disponível em: <http://bibdigital.epn.edu.ec/handle/15000/22886>. Acesso em: 15 mar. 2023

SAEED, M. et al. Chemical Vapour Deposition of Graphene—Synthesis, Characterisation, and Ap-plications: A Review. Molecules, v. 25, n. 17, p. 3856, 25 ago. 2020.

SAHOO, P. et al. Synthesis and characterization of graphene oxide and graphene from coal. Mate-rials Today: Proceedings, v. 56, p. 2421–2427, 2022.

SARKAR, D. K. Fuels and Combustion. Em: Thermal Power Plant. [s.l.] Elsevier, 2015. p. 91–137.

SAXENA, S. et al. Investigation of structural and electronic properties of graphene oxide. Applied Physics Letters, v. 99, n. 1, p. 013104, 4 jul. 2011.

SHAHRIARY, L.; ATHAWALE, A. A. Graphene Oxide Synthesized by using Modified Hummers Approach. BRCORP, v. 02, n. 01, p. 58–63, feb. 2014.

SHARMA, N. et al. Synthesis and Characterization of Graphene Oxide (GO) and Reduced Graphene Oxide (rGO) for Gas Sensing Application. Macromolecular Symposia, v. 376, n. 1, p. 1700006, dec. 2017.

STOBINSKI, L. et al. Graphene oxide and reduced graphene oxide studied by the XRD, TEM and electron spectroscopy methods. Journal of Electron Spectroscopy and Related Phenomena, v. 195, p. 145–154, ago. 2014.

SUREKHA, G. et al. FTIR, Raman and XRD analysis of graphene oxide films prepared by modified Hummers method. Journal of Physics: Conference Series, v. 1495, n. 1, p. 012012, 1 mar. 2020.

VASIREDDY, S. et al. Clean liquid fuels from direct coal liquefaction: chemistry, catalysis, techno-logical status and challenges. Energy Environ. Sci., v. 4, n. 2, p. 311–345, 2011.

WANG, Z. et al. Low-cost and large-scale synthesis of graphene nanosheets by arc discharge in air. Nanotechnology, v. 21, n. 17, p. 175602, 30 abr. 2010.

WU, Z.-S. et al. Synthesis of Graphene Sheets with High Electrical Conductivity and Good Thermal Stability by Hydrogen Arc Discharge Exfoliation. ACS Nano, v. 3, n. 2, p. 411–417, 24 fev. 2009.

XU, Q. et al. Green reduction of graphene oxide using Bacillus sphaericus. Journal of Colloid and Interface Science, v. 605, p. 881–887, jan. 2022.

YU, P. et al. Electrochemical exfoliation of graphite and production of functional graphene. Current Opinion in Colloid & Interface Science, v. 20, n. 5–6, p. 329–338, out. 2015.

4 CHAPTER 4

This chapter describes the synthesis and characterization of carbon-based adsorbent materials used in a Ciprofloxacin adsorption analysis. The evaluation encompasses adsorption kinetics, kinetic modelling, and molecular modelling using the Density Functional Theory (DFT). The adsorption experimentation occurred at the LEA/LEPA laboratory located at the State University of Campinas (UNICAMP), under an INCT MIDAS exchange program. The materials' synthesis took place at the LEMA laboratory of the Federal University of Santa Catarina.

4.1 ADSORPTION OF CIPROFLOXACIN ON GRAPHENE OXIDE-BASED ADSORBENTS: SYNTHESIS, CHARACTERIZATION AND DFT CALCULATIONS

4.1.1 Introduction

The increase in the use of antibiotics in recent years is due to their great utility in the treatment of human infectious diseases, in livestock, and aquaculture (DUTTA; MALA, 2020). These drugs have high selectivity against bacteria and no side effects on human cells and tissues (AHMED et al., 2015). Antibiotics are sometimes not fully metabolized, resulting in their disposal into ecosystems such as natural waters through excretion in feces and urine of humans and animals (FU et al., 2017). Municipal wastewater treatment plants also proved to be ineffective in removing this type of contaminant, since they are found in low concentrations in water (BHAGAT et al., 2020). Therefore, antimicrobial residues were found in raw and treated wastewater, hospital effluents, and surface water. The accumulation of these residues in high concentrations leads to antibiotic resistance in microbial communities and disruption of food chains (DOS SANTOS et al., 2021).

Antibiotics can be classified according to their chemical structure and mechanism of action. Amongst them it can be found quinolones, which have a basic structure of 4-quinolones, and the antibiotic Ciprofloxacin (CIP) is one of the most used pharmaceuticals in the world (ALI, 2010; CONLEY et al., 2018). As a consequence of its high consumption, CIP is one of the most common antibiotics found in aquatic environments and its low bio-degradability favors the growth of bacteria resistant to this type of medicine (SPAOLONZI et al., 2022). Thus, it is essential to develop

treatment techniques to eliminate or control it in aqueous media. For this purpose, several techniques such as membrane separation (CHIN; AHMAD; LOW, 2023), ozonation (FRANCOEUR et al., 2023), photocatalytic degradation (ABDULLAH et al., 2023) and adsorption (WU et al., 2013) have been used. The latter has been shown to be efficient (ZHOU et al., 2012), low cost and easy to design (AHMED et al., 2015), and it has been proposed as the Best Available Technology (BAT) to remove micropollutants from water (SHAHID et al., 2021).

Carbon-based adsorbents (activated carbon, carbon nanotubes, graphene, graphene oxide, for example) have proven to be useful for micropollutants removal from water. Nevertheless, enhanced adsorption capacity could be assessed by modification on the surface properties of those materials (SINGH et al., 2023; SONTAKKE; TIWARI; PURKAIT, 2023). The oxidation of graphene to graphene oxide (GO) has been proposed to produce adsorbents with higher adsorptive properties (AJALA et al., 2022). GO is a material with a single atomic layer structure with sp^2 hybridization and is known for its potential for environmental remediation applications due to its large XY plane (CHEN; GAO; LI, 2015; WU et al., 2013). It has been demonstrated that the interactions between GO surface and contaminants are given by electrostatic attraction, hydrogen bonding, and π-π stacking (CHEN; GAO; LI, 2015). However, GO particles are usually very small for applications in large scale, justifying the preparation of composites with geopolymers and others adsorbents (GONÇALVES et al., 2014)

Geopolymers are three-dimensional amorphous materials and are synthesized by alkali activation of aluminum silicate (FREIRE et al., 2020). These material can be produced by alkali-activation of metakaolin, fly ash and or others wastes containing silica and/or aluminum. In recent years, several advantages of these materials as adsorbents have been reported due to their low cost, high adsorption capacity and chemical stability (DELLA ROCCA et al., 2021). Likewise, the adsorption capacity of these materials on antibiotic contaminants has yet to be evaluated, as the reported information is limited (SANGUANPAK et al., 2022). Graphene-geopolymer composites have recently been used to improve the microstructure and flexural strength of geopolymer composites. It also contributes to the reduction of porosity due to the strong bond between the graphene and the geopolymer matrix (HUANG; SUN, 2021).

In this study, GOs were prepared from mineral coal or coke, and incorporated to produce a composite with a phosphate waste-based geopolymer. The synthesized materials were very well characterized by Zeta Potential analysis, Particle Size Distribution, RAMAN spectra, and FEG/EDS, FTIR and TGA analyses. The materials obtained were used for the adsorption of Ciprofloxacin. To analyze the characteristics of the adsorption process, a kinetic study was performed and quantum chemical descriptors such as electronic chemical potential (μ), total chemical hardness (η) and total electrophilicity index (ω) of CIP were determined through molecular modeling applying the Density Functional Theory (DFT).

4.1.2 Materials and Methods

4.1.2.1 Materials

Samples of bituminous coal (CR) and mineral coke (Cq) were supplied by a Brazilian company from the Santa Catarina State, Brazil. Hydrofluoric acid (HF, PA, 48%, Vetec) and sulfuric acid (H2SO4, PA, 99.8%, Wt.: 98.079 g mol^{-1}, Vetec) were obtained from Vetec, Rio de Janeiro/Brazil. The kaolin clay was purchased from Caulisa LTDA (Campina Grande/Brazil). Phosphate – mining tailings waste – was acquired from a mine located in Goiás/Brazil. Sodium silicate was purchased from Quimidrol (Brazil). Sodium hydroxide (NaOH, 97%) in micro pearls was acquired from NEON (Brazil). Nitrogen under high pressure was purchased from White Martins (Brazil) and ozone was generated in situ by an ozone generator (O3R, Brazil). High purity pharmaceutical Ciprofloxacin (>99%) was donated by EMS Pharmaceutical (Brazil).

4.1.2.2 Graphene oxide synthesis

Before GO synthesis, samples of CR or Cq were demineralized using HF by adding 100 mL of this acid to 5 g of material under magnetic stirring for 24 h. The resulting suspension was washed with deionized water by vacuum filtering (PVDF membrane 0.22 μm, Millipore, Brazil) until the pH became neutral. After that, the demineralized samples (D_CR and D_Cq) were added to 10 mL of H_2SO_4, and the

solid materials were left in contact with sulfuric acid for 24 h at room temperature. Thermal exfoliation of the solids was performed in a in horizontal tube furnace (Universal Dist) at 950 °C for 30 min in a nitrogen atmosphere flowing at a rate of 20 °C min^{-1}. The thermal exfoliation was followed by ozone oxidation in aqueous suspension (solid concentration of 0.015 g mL^{-1}) for 18 h at an ozone flow rate of 1 L min^{-1}. The resulting solution was then transferred to an ultrasonic cleaner (Hielscher, UP400St) (Figure 4.1) to be sonicated for 10 min at a percentage amplitude of 60% and a temperature of 45 °C controlled by a cooling unit (Marconi, MA083). Finally, vacuum filtration was used to filter the obtained solids (OG_D_CR and OG_D_Cq). The effect of the presence of mineral matter from the bituminous coal or coke on the adsorbent characteristics was investigated by the synthesis of non-demineralized graphene oxide-based adsorbents.

Figure 4.1 - Schematic process of the sonicator

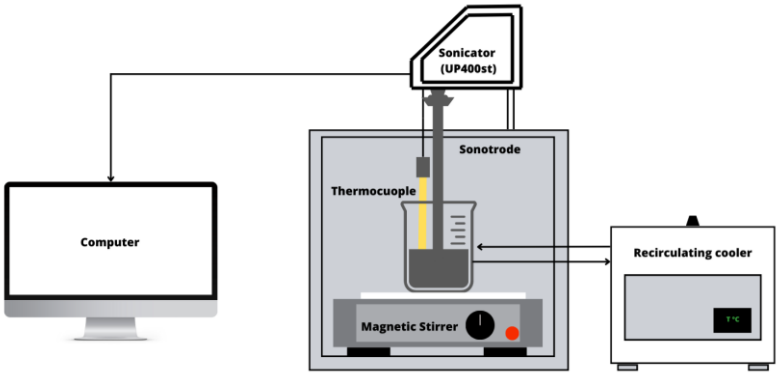

4.1.2.3 Geopolymer synthesis

For the synthesis of the geopolymer with graphene oxide (G_OG_CR) the procedure performed in (FREIRE et al., 2020) was used. Briefly, metakaolin was obtained by calcination of kaolin in a muffle furnace (F2-DM) at 900 °C for 60 min at a rate of 5 °C min^{-1}. Up to 900 °C with a 60 min hold. Then, by magnetic stirring at 500 rpm for 10 min, metakaolin and phosphate residues were homogenized. The alkaline activator was obtained by mixing NaOH and sodium silicate with magnetic stirring at 500 rpm for 10 min. Likewise, the solid mate-rials were mixed with the alkaline activator by magnetic stirring at 2000 rpm for 20 min. The paste obtained was mixed with a 1% solution of OGCR by magnetic stirring for 2 minutes. Finally, the

G_OG_C were molded into a cylinder and placed in an oven (MS equipment) for 48 h at 65 °C. The G_OG_C samples were demolded and immersed in water at room temperature for 28 days and crushed for use in adsorption tests. Table 4.1 shows the mass percentages of precursor materials previously studied in Freire et al. (2020) and also applied in this study.

Table 4.1 - Formulation of G_OG_G (%w/w)

Nomenclature	Metakaolin	Phosphate Waste	NaOH	Sodium Silicate	OGCR
G_OG_G	35.0	19.0	11.0	13.0	22.0

4.1.2.4 Characterization of adsorbents

The geopolymer and GO obtained were characterized by proximate analysis and thermogravimetric analysis on a Shimadzu DTA-60 and the analysis conditions were given in the Supplementary Material (Table 4.6). Fourier Transform Infrared Spectroscopy (FTIR) spectrum was performed on a PerkinElmer Spectrum 100 using KBr pellets with a wavenumber range of 4000 cm^{-1} to 40 cm^{-1}. X-ray diffraction (XRD) was also performed on a Rigaku Miniflex 600 diffractometer using CuKα radiation (λ=0.1542 nm). The continuous scanning mode was used at a 2θ between 10° and 90° with a step of 0.05° at a speed of 10° min^{-1}. The X-ray generator was set to a voltage of 40 kV and a current of 40 mA. The Zeta Potential of the samples was determined by Electrophoretic Light Scattering (ELS) at 173° on a Malvern MPT-2 equipment. The Particle Size Distribution was determined by Dynamic Light Scattering (DLS) in the range of 0.3 nm to 10 μm on a Malvern MPT-2 equipment.

Morphological analysis of the obtained samples was performed using a TermoFisher Scientific High Resolution Scanning Electron Microscope with an X-ray Energy Dispersive Detector (FEG/EDS) at a voltage of 20 kV and a current of 32 pA. Sample preparation for FEG was performed on an EMITECH Sputter Coater model K450. For RAMAN, a NRS 5100-JASCO Raman spectrometer microscope was used, the excitation for the measurements was performed by Nd:YAG lasers with a wavelength of 532 nm, power of 1.8 mW.

4.1.2.5 Affinity test

This procedure was performed following the methodology proposed in SPAOLONZI et al., 2022). In summary, five different solutions were prepared, each containing CIP (at a concentration of 0.1 mmol L^{-1}) as adsorbate and a different adsorbent (OG_D_Cq, OGCq, OG_D_CR, OGCR and G_OG_C). Each solution was agitated on a rotary shaker (Lab Companion SE-600R) at 25 °C and 200 rpm for 24 h. The solutions were then filtered through a 0.22 µm hydrophilic PVDF syringe filter. The residual concentration of solutions was determined by UV-Vis spectra (Shimadzu UVmini-1240) at λ = 276 nm. Equations 17 and 18 were used to calculate the percentage of removal and the adsorption capacity q_e (mmol g^{-1}), respectively.

$$\%R = \left(C_0 - C_f/C_0\right) * 100 \quad (17)$$

$$q_e = (V/m)(C_0 - C_f) \quad (18)$$

Where C_0 is the initial concentration of the solutions (mmol L^{-1}), C_f is the final concentration (mmol L^{-1}), m is the mass of the adsorbent (g), and V is the volume of the solution (L).

4.1.2.6 Kinetic study

Three different concentrations of CIP solution (C_0 = 0.05 mmol L^{-1}, 0.1 mmol L^{-1} and 0.2 mmol L^{-1}) were analyzed with G_OG_C as adsorbent. The procedure was based on that performed in Spaolonzi et al. (2022), where each flask contained 60 mL of CIP solution and 0.09 g (1.5 g L^{-1}) of adsorbent. The solutions were magnetically stirred (CMAG HS7 IKA) for 250 min at room temperature. Aliquots were collected at predetermined times and filtered with a syringe filter (hydrophilic PVDF 0.22 µm). A UV-Vis spectrum at a wavelength of 276 nm was used to measure the residual concentration of the contaminant. Adsorption capacity was calculated using Equation 17.

Pseudo-first order (PFO) (S. LAGERGREN, 1898), pseudo-second order (PSO) (HO; MCKAY, 1999) and Intra-Particle Diffusion (IPD) (WEBER; MORRIS, 1963) kinetic models were adjusted to the experimental data. The equations for each model were given below:

$$q_t = q_e(1 - e^{-k_1 t}) \quad \text{PFO} \quad (19)$$

$$q_t = (k_2 q_e^2 t)/\,(1 + k_2 q_e t) \quad \text{PSO} \quad (20)$$

$$q_t = k_i t^{1/2} + c \quad \text{IPD} \quad (21)$$

Where q_e is the amount of drug adsorbed at equilibrium, qt is the amount of drug adsorbed at any time t, k_1 (min^{-1}) is the velocity constant, k_2 (min^{-1}) is the second rate constant and ki represent PFO (min^{-1}), PSO (g $mmol^{-1}$ min^{-1}) and IPD (mmol g^{-1} min^{-1}).

To compare the kinetic models, the parameters of R^2 (Equation 22) and Akaike Information Criterion (AICc) (Equation 23) were used to compare and identify the model that best fits the experimentally obtained data. The best model is the one with the lowest AICc value and the highest R^2 (EWIS et al., 2022; OLIVEIRA et al., 2023).

$$R^2 = \frac{\sum_{i=1}^{N}\left(Y_i - \hat{Y}_i\right)^2}{\sum_{i=1}^{N}(Y_i - \bar{Y}_i)^2} \quad (22)$$

$$AICc = N.ln\left(\sum_{i=1}^{N}\left(\frac{\left(Y_i - \hat{Y}_i\right)^2}{N}\right)\right) + \left(\frac{2p(p+1}{N-p-1}\right) \quad (23)$$

Where *N*: number of experimental observations; *Y* is the mean value of the experimental results; $\hat{Y}$ is the experimental value; *p*: number of parameters and $\hat{Y}_i$ is the estimated value.

4.1.2.7 Molecular modeling

Molecular modeling was used for the CIP antibiotic to investigate chemical interactions and reactivity during the adsorption process. This uses theoretical models capable of representing and incorporating chemical structures that establish relationships with the physical and chemical properties of molecules (ANTONELLI et al., 2021; DE ANDRADE et al., 2020). The Marvin Sketch software was used to design the molecular structure of CIP and the Avogadro software was used for its three-dimensional (3D) structure design.

For the calculation of the highest occupied molecular orbital energy (HOMO, E_H), the lowest unoccupied molecular orbital energy (LUMO, E_L), the energy gap (ΔH_H-

$_L$) (Equation 24), the electronic chemical potential (μ) (Equation 25), the overall chemical hardness (η) (Equation 26) and the total electrophilicity index (ω) (Equation 27), it was necessary to subject the structures obtained to a Density Functional Theory (DFT) calculation using the Gaussian 09 software. For this, the Becke, 3-parameter, Lee-Yang-Parr (B3LYP) theory was used, and the 6-31G(d) and 6-31G(d, p) variations of the base set 6.31G were evaluated (DE SOUZA et al., 2018).

$$\Delta \mathrm{H} - \mathrm{L} = E_H - E_L \quad (24)$$
$$\mu = -(E_H - E_L)/2 \quad (25)$$
$$\eta = (-E_H + E_L)/2 \quad (26)$$
$$\omega = \mu^2/2\eta \quad (27)$$

4.1.3 Results and discussion

4.1.3.1 Characterization of adsorbents

4.1.3.1.1 Proximate analysis

The proximate analysis consisted of heating the previously dried samples under different temperature and time conditions to determine the volatile matter, fixed carbon and ash contents. Volatile matter was determined by heating the coal up to 950 °C in an N_2 atmosphere. To obtain the amount of ash, the residue from the previous process was burned at 750 °C with synthetic air and the fixed carbon was determined by the difference between 100 and the sum of the percentage of volatile material and ash on a dry basis (ASIM et al., 2022; PISUPATI; KRISHNAMOORTHY, 2017). Figure 4.2 shows the percentages obtained for synthesized GO and geopolymer and the respective raw materials.

Figure 4.2 - Results of proximate analysis of raw and synthetized materials.

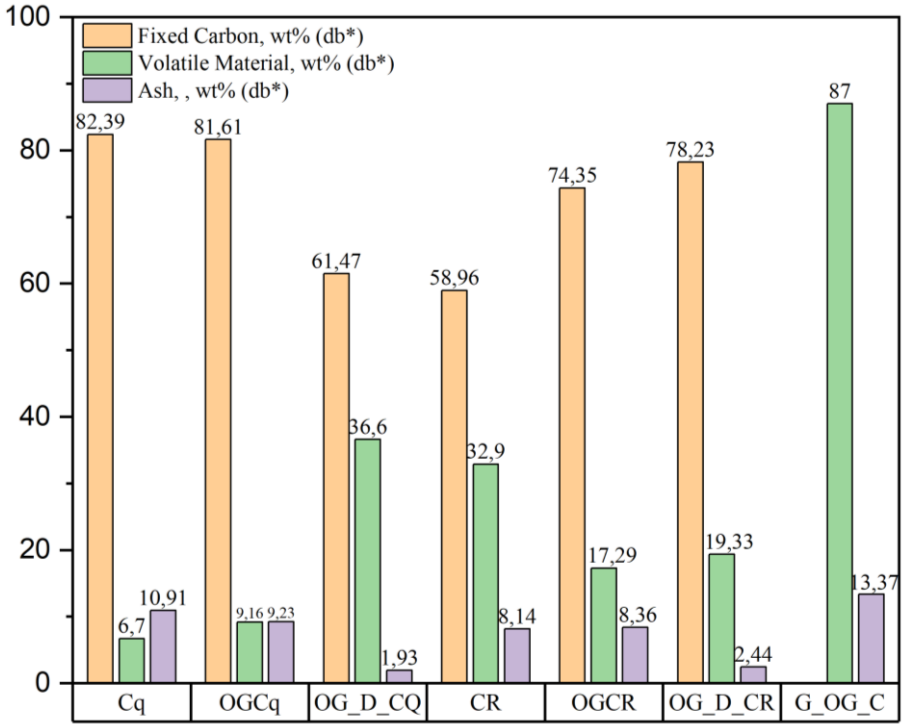

Bituminous coals contain a significant amount of ash or mineral matter (DAS; KUNDU; CHAKRAVARTY, 2022). The main component of this mineral matter is silica and it was evident in Figure 4.2 that the chemical treatment with H_2SO_4 was not enough to eliminate it. Without the demineralization process, a 15% ash reduction was achieved for OGCq, and for OGCR the ash percentage was not reduced at all. On the contrary, for the demineralized materials OG_D_CQ and OG_D_CR a reduction of 82.3% and 70.1%, respectively, was achieved, indicating that the coal mineral matter was efficiently eliminated.

4.1.3.1.2 Thermogravimetric analysis

The TGA allowed the evaluation of the thermal stability of the synthesized GO and the geopolymer.

Figure 4.3 - Mass loss curves for the GOs and the geopolymer

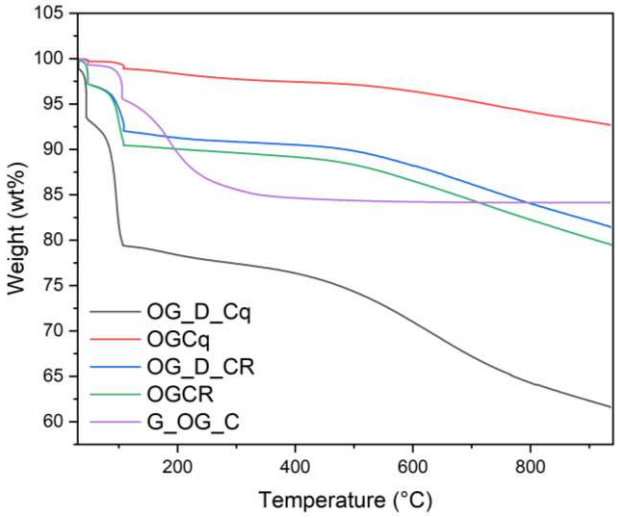

Figure 4.3 shows the mass loss curves corresponding to the synthesized materials. It can be observed that GOs presented three steps in its mass loss profile. The first step was below 100 °C and represents the volatilization or elimination of water. The second mass loss occurred between 100 °C and 150 °C and can be related to the loss of oxygen functional groups, and between 150 °C and 900 °C there was a mass loss due to the oxidative process of Farivar et al. (2021); Peng et al. (2017); Wang; Li, (2018). OG_D_Cq obtained a mass loss of 10% before 100 °C, 12% between 100 °C and 150 °C and 17% up to 900 °C, being the GO that lost the most mass during the three steps. OG_D_CR and OGCR obtained similar mass losses, losing 5% in the dewatering phase, 10% in the pyrolysis phase, for the intermediate phase OG_D_CR and OGCR lost 6% and 8%, respectively. OGCq was the material with the lowest mass loss, losing less than 1% in the first two phases and 7% in the last phase.

For G_OG_C, a gradual mass loss of 10% was observed between 150 °C and 350 °C, where there was an increase in reactivity for alkaline activation. This mass loss may be at-tributed to the faujasite decomposition (ELICHE-QUESADA et al., 2021; ETTOUMI et al., 2021).

4.1.3.1.3 Zeta Potential

The stability and surface charge of the synthesized materials were evaluated using the Zeta Potential analysis at natural pH (6.5). Table 4.2 shows the results obtained for Cq, CR, GO and geopolymer.

Table 4.2 - Zeta Potential values for GOs, geopolymer and raw material

Nomenclature	Zeta potential, mV
Cq	-26.4
CR	-18.4
OG_D_Cq	-40.9
OG_D_CR	-32.9
OGCq	-43.6
OGCR	-0.3
G_OC_C	-31.8

When the ZP is ± 30 mV, it is considered stable, as it represents mutual repulsion to ensure its stability (KANTI; MAIYA, 2022). From the obtained results, OG_D_Cq, OGCq, OG_D_CR and G_OG_C improved their stability by presenting a more negative value than Cq and CR. The OGCR, on the other hand, presented a value very close to zero, indicating that it is a material that easily coagulates or flocculates. These obtained values are in agreement with (LI et al., 2014; UMEJURU; PRABAKARAN; PILLAY, 2021; ZHAO et al., 2015), which studied the ZP at different pH values for GO and obtained a value at pH 7 that was between -40 mV and -30 mV.

4.1.3.1.4 Distribution Particle Size

The results of the particle size and polydispersity index (PDI) determination were shown in Table 4.3.

Table 4.3 - Particle size distribution of the raw and treated samples

Nomenclature	Average particle size, nm	PDI
Cq	1400.3	0.437
CR	1654.3	0.973
OG_D_Cq	1087	0.823
OG_D_CR	1037.7	0.598
OGCq	894.8	0.661
OGCR	3780.3	0.428
G_OC_C	1153	0.459

The PDI, or heterogeneity index, is used to represent the degree of non-uniformity of a particle size distribution. PDI values greater than 0.7 indicate a very broad particle size distribution and the DLS technique is probably not the best for this

analysis. PDI values between 0.05 and 0.7 are adequate according to the algorithms used in particle size distribution (DANAEI et al., 2018). The size of the synthesized GO is directly related to the initial size of the Cq and CR particles, where in general, the larger the particle size, the greater the reduction in the synthesized GO is expected (HUSKIĆ et al., 2018). In this case, CR, OG_D_Cq and OGCq have PDI greater or almost equal to 0.7, therefore these values are not comparable with the others obtained. Thus, a particle agglomeration was obtained and this technique is not suitable for its characterization. The synthesized geopolymer had an average particle size of 1153 nm.

4.1.3.1.5 X-ray Diffraction (XRD)

The X-ray Diffraction patterns of the synthesized and raw materials were shown in Figure 4.4.

Figure 4.4 - XRD patterns for raw coal and raw coke, GO with and without demineralization and geopolymer Cq (a), CR (b) and G_OG_C (c)

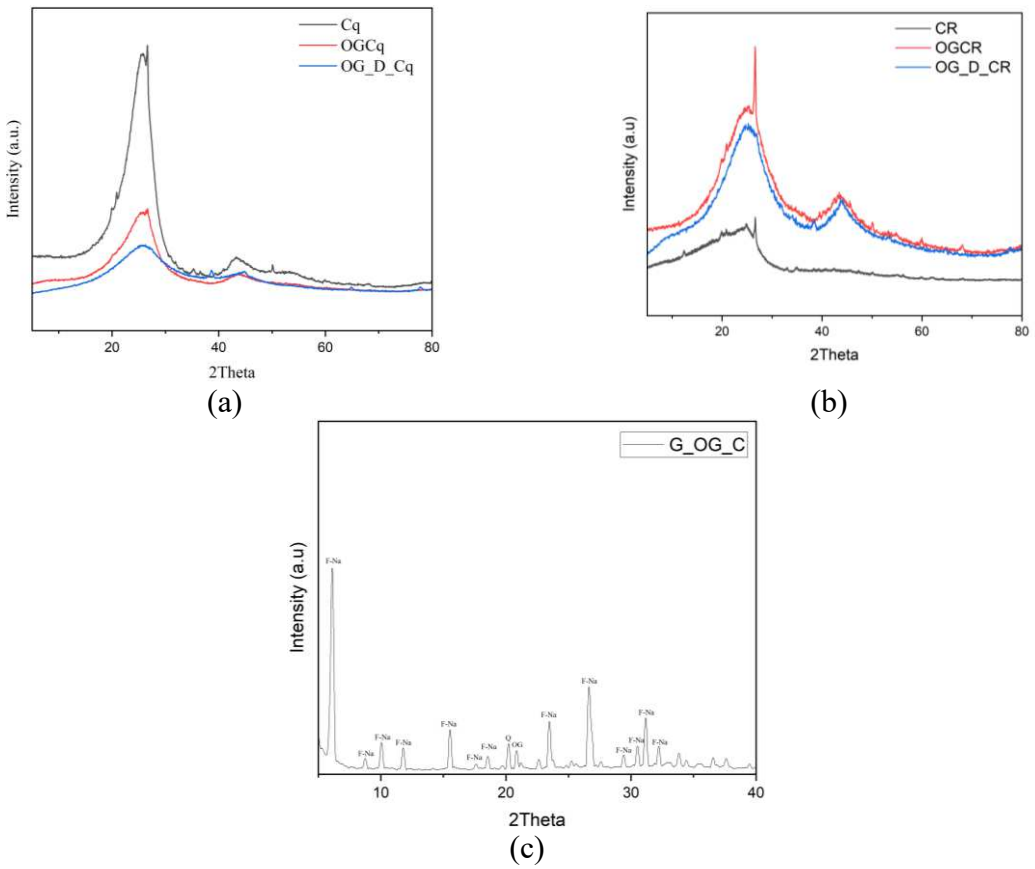

For Cq and CR, two peaks can be seen at 26° (002) and another one on the left at 24°. This is a normal XRD spectrum for carbonaceous materials. Peak 002 is associated with aromatic crystallites formed by polycondensation. The 24° peak represents branched crystallites as-sociated with the aromatic core of polycondensation and it is also a characteristic peak of amorphous structures (JIANG et al., 2021). Likewise, for Cq and CR, a peak at 19° related to kaolinite (ICSD-0291488) and a peak at 21° associated with quartz (ICSD-0861560) (Arsyad et al. 2021) were noted. For GO synthesized from Cq, a pattern could be observed where the characteristic peak 001 was transformed into a broad peak with low intensity. This indicates the exfoliation of graphite layers to graphene oxide layers (SAHOO et al., 2022). While for OG_D_CR it was evident that peak 001 decreases its intensity, but for OGCR it remains the same. Similarly, the synthesized GOs showed a low intensity peak at 42°, indicating the formation of GO, despite the addition of oxygen functional groups by ozonation, the graphitic carbon phase was still noticeable (JOHRA; LEE; JUNG, 2014; LEE; MAHAJAN, 2021). The results obtained were in agreement with those of (LEE; MAHAJAN, 2021) where they synthesized GO from carbon. For G_OG_C, the formation of aluminum silicate (amorphous) was observed. After the hardening process, a zeolite phase (Faujasite-Na $Na_2Al_2Si_3.3O_{10.6}$ $7H_2O$ ICSD-0120228), quartz (SiO_2 ICSD-010891961) and the peak contributed by the GO introduced into the geopolymer were obtained (FREIRE et al., 2020).

4.1.3.1.6 Fourier Transform Infrared Spectroscopy (FTIR)

Figure 4.5 shows the FTIR spectra of the synthesized materials.

Figure 4.5 - FTIR spectra for all synthetized materials

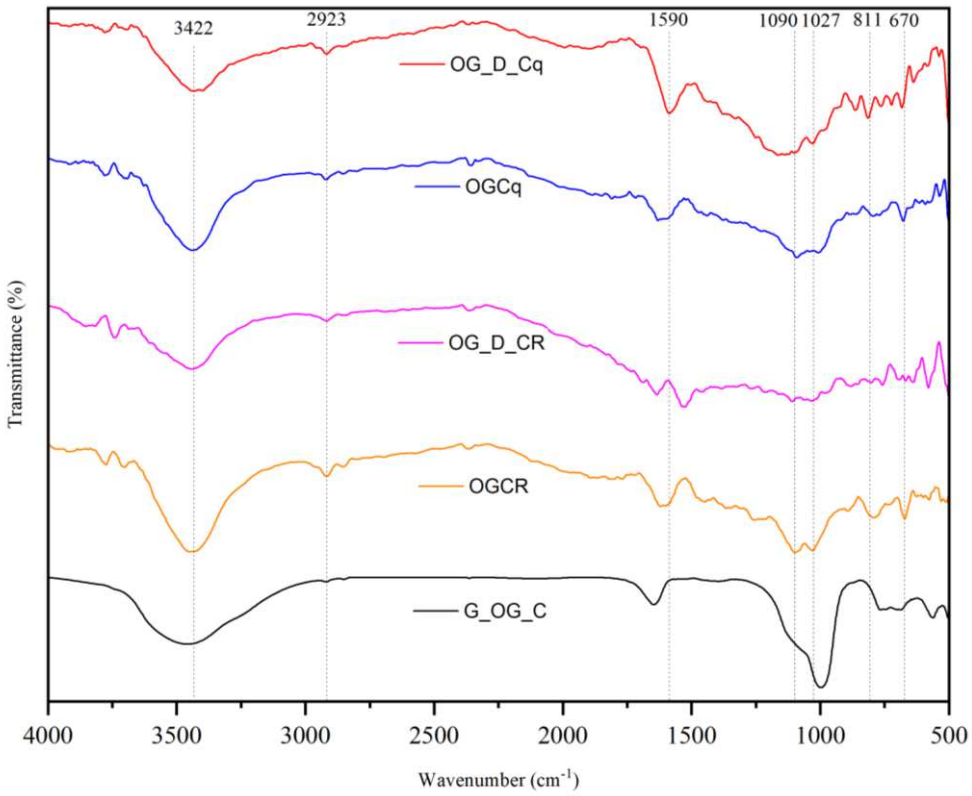

For GO, it does not depend on the synthesis method, as it is characterized by some strong and medium bands (MERMOUX; CHABRE; ROUSSEAU, 1991). The FTIR spectrum shows, for all synthesized GOs, an intermediate band at 3422 cm^{-1} assigned to the O-H stretching, indicating the presence of hydroxyl groups and the graphitization of the sp^3 carbon by the oxidative process (DAS; KUNDU; CHAKRAVARTY, 2022; LEE; MAHAJAN, 2021 In the range of 2923 - 2800 cm^{-1}, a peak with the appearance of a very weak band was found, which is related to the asymmetric stretching of -CH_2- and -CH_3- bonds. This suggests a change from the initial sample towards the GO obtained (DAS; KUNDU; CHAKRAVARTY, 2022). In the range of 1550 - 1600 cm^{-1} were the peaks related to the C=C stretching of the unoxidized graphite material (OSSONON; BÉLANGER, 2017). C-O stretching and C-O bending peaks were found at 1090 cm^{-1} and 1027 cm^{-1}, respectively (SAHOO et al., 2022). Peaks with bands between 900 cm^{-1} and 600 cm^{-1} are due to C-H stretching (SUREKHA et al., 2020). G_OG_C presented three characteristic peaks. The first one at 3450 cm-1 was related to Si-OH and Si-OH-Al stretching. The second peak at 1500 cm^{-1} indicates the vibrations of the OH group. And the last one was found at

1000 cm^{-1}, which is characteristic of a geopolymer peak, corresponding to Si-O-Si or Si-O-Al stretching. Finally, the absence of any peak be-tween 1550 cm^{-1} and 1200 cm^{-1} reveals the absence of carbonate formation (FIGUEIREDO et al., 2021; KLJAJEVIĆ et al., 2017; KRÓL; MINKIEWICZ; MOZGAWA, 2016).

4.1.3.1.7 Fields Emission Gun – Scanning Electron Microscopy (FEG)

To analyze the morphology of the synthesized GO and the geopolymer, the Field Emission Gun was used with magnifications of 500x and 5000x. The FEG images of GO can be found in the Supplementary Material (Figure 4.12), showing varying particle sizes and some particle agglomerations, which are consistent with the results obtained in the particle size determination. Likewise, an irregular morphology could be seen on the surface of the GOs, which is expected when dealing with a synthesis with sub-bituminous carbon.

Figure 4.6 - FEG images for GO synthetized as OGCq (a) and OGCR (b) at 500 x magnification.

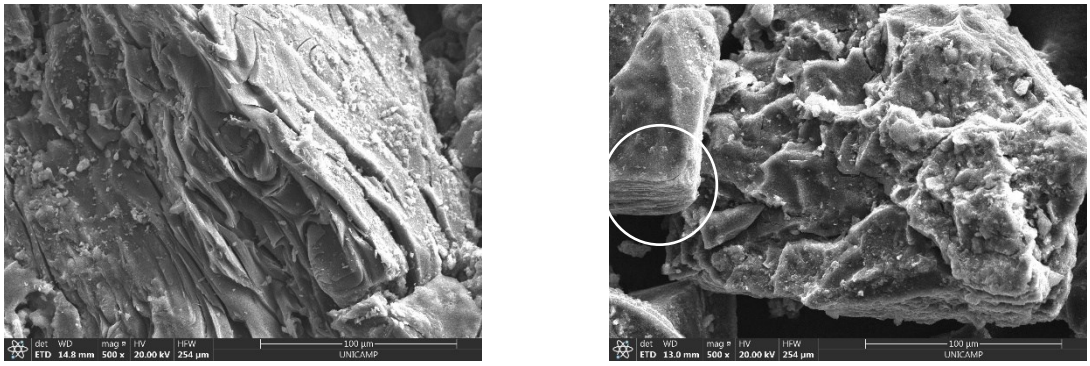

(a) (b)

Similarly, in some synthesized GOs such as OGCq and OGCR (Figure 4.6 a and b), a tendency towards the formation of layers on their surface could be detected, indicating a carbon graphitization process. In the case of OGCq, it was possible to measure layers with an average size of 14.61 µm, which are irregular materials. For both cases, multilayers could be observed, which is in agreement with the results of RAMAN spectroscopy. By means of the I_D/I_G ratio, it was verified that for all synthesized materials, multilayered GO was obtained. For G_OG_C, an uniformity in the particles obtained, as well as a more regular surface could be demonstrated.

4.1.3.1.8 RAMAN spectra for synthesized samples

RAMAN spectroscopy has been applied to study the sp^2 to sp^3 hybridization of carbon atoms by examining the order of crystallinity in carbon materials (KRAUSS et al., 2010; KUDIN et al., 2008; WANG et al., 2011). It would also be useful for identifying the number of layers of the synthesized GO (KRAUSS et al., 2010; WANG et al., 2011).

Figure 4.7 - RAMAN spectra for synthesized samples

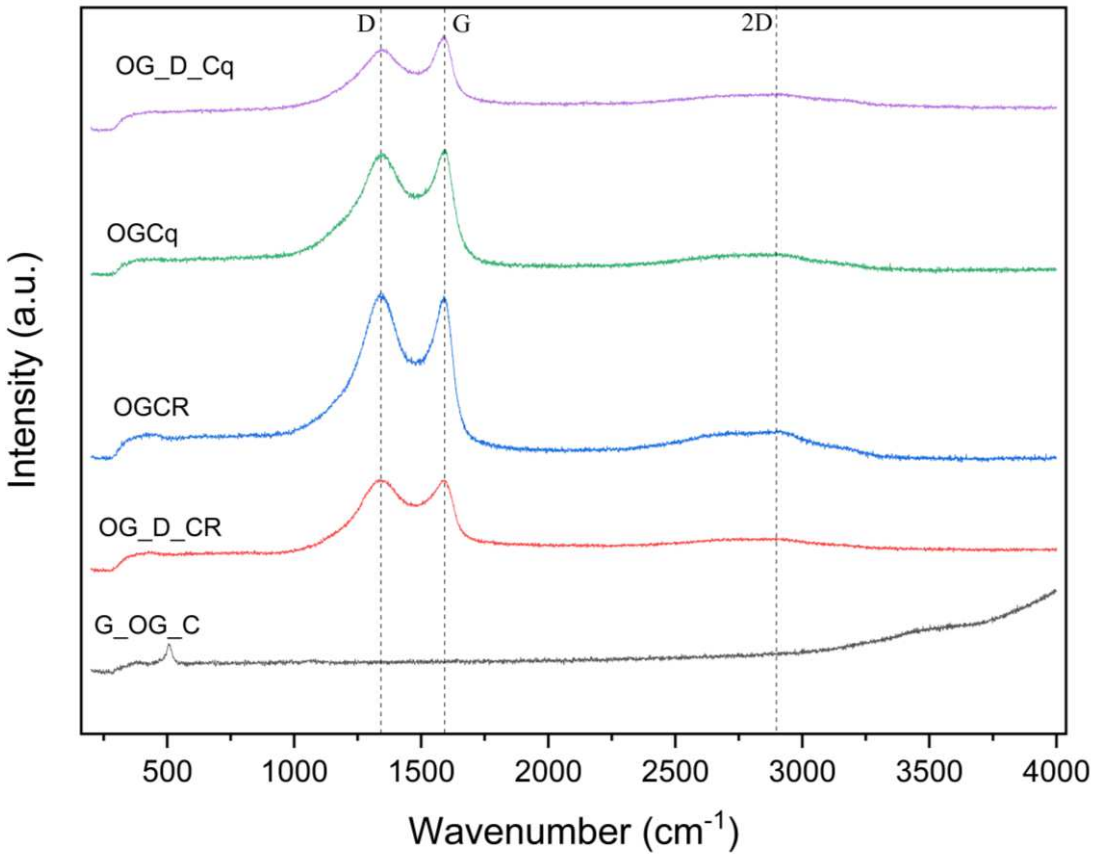

Figure 4.7 shows the RAMAN spectra obtained for the synthesized samples. All synthesized GO RAMAN spectra showed D and G peaks at 1350 cm^{-1} and 1585 cm^{-1}, respectively, and a 2D band at 2900 cm^{-1}. These bands are related to the C-C stretching vibrations of the sp^2 domain, and the 2D band is related to the second-order two-phonon process. As shown in the obtained spectra, the 2D band has a low and broad intensity due to structural defects in the carbon ring (DAS; KUNDU; CHAKRAVARTY, 2022). These RAMAN spectra were in good agreement with reports

in the literature (CLARAMUNT et al., 2015; LÓPEZ-DÍAZ et al., 2017; MINITHA; RAJENDRAKUMAR, 2013).

The crystallite size was investigated using Equation 28 and the results were presented in Table 4.7. It was evident that the integral area for the synthesized GOs was very close to 1.00. This indicates that the crystallite sizes of the obtained GOs are very close with values ranging from 19.2 to 19.82. Likewise, this value close to 1.00 indicates a final GO with multilayer, which is consistent with what was found in XRD and FEG analyses (KURNIASARI et al., 2017; MALARD et al., 2009).

$$La(nm) = \frac{(2.4x10 - 10)(\lambda)^4}{I_D/I_G} \quad (28)$$

Where I_D/I_G is the integral area under D and G peaks, respectively.

4.1.3.2 Affinity test

All synthesized materials were evaluated for CIP adsorption in aqueous media. Figure 4.8 shows the results obtained for the removal percentage and adsorption capacity of each material.

Figure 4.8 - Removal percentage and adsorption capacity of Ciprofloxacin adsorption

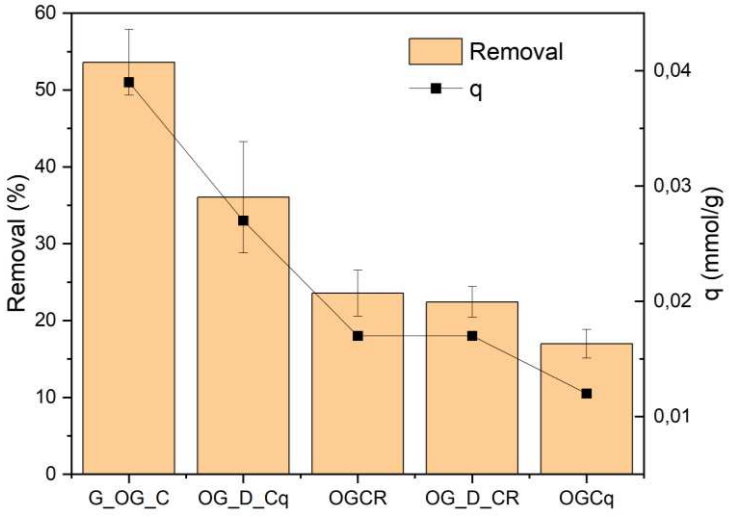

Through Figure 4.8, it can be seen that the material with the highest removal was G_OG_C, with values close to 55%. In addition, the GO from coke with

demineralization (OG_D_Cq) obtained a removal percentage close to 40%. The other materials, on the other hand, obtained a percentage below 25%, not proving to be efficient for the removal of CIP. Comparing the results obtained in this work with the literature, it was found that GO fibers with a dosage as in (WU et al., 2013), and it was achieved a removal percentage of 45%, similar to that achieved with OG_D_Cq and lower than that of G_OG_C. The above reflects the results obtained in the characterization part. The geopolymer is a more organized and porous material while the graphene oxide is a material that by its nature has low adsorption capacities for pharmaceuticals. Therefore, the inclusion of graphene oxide in the geopolymer makes it a more promising material, with a higher adsorption capacity and better physical properties. In the TEM images, it can be seen how this combination has more porous and much more organized structures. Finally, the geopolymer gives the graphene oxide some compounds necessary for interactions with contaminants.

4.1.3.3 Kinetic study

The kinetic studies were performed with G_OG_C as it was the material that achieved the highest removal in the affinity tests. Three concentrations were evaluated and through the results obtained it was possible to observe that the adsorption capacity increased with the increase in the initial concentration of CIP, going from 0.0332 mmol g^{-1} (C_0 = 0.05 mmol L^{-1}) to 0.0733 mmol g^{-1} (C_0 = 0.2 mmol L^{-1}). This behavior was expected, as higher concentrations generate a greater driving force in mass transfer. This may indicate that active sites are still available on the surface of the material, being occupied by increasing the initial concentration until reaching saturation.

Figure 4.9 - Kinetic curves for CIP adsorption at initial concentrations of 0.05 mmol L^{-1}, 0.1 mmol L^{-1} and 0.2 mmol L^{-1}

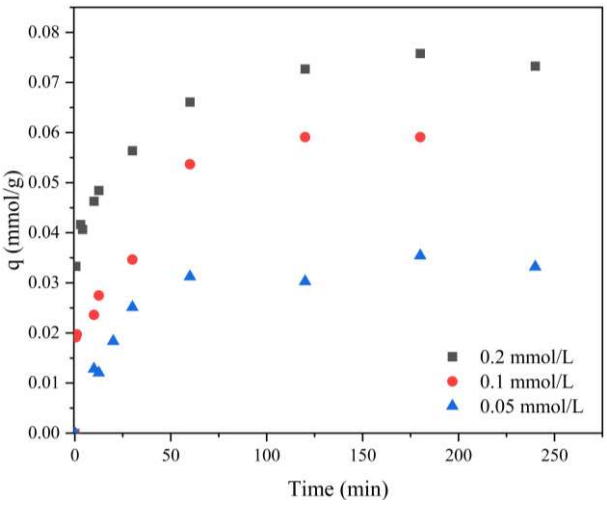

In Figure 4.9, it is possible to observe that the curves for all concentrations were very similar, reaching equilibrium in approximately 100 min for the concentration of 0.05 mmol L^{-1} and 120 min for the concentrations of 0.1 mmol L^{-1} and 0.2 mmol L^{-1}. Comparing the results obtained with Avci; İnci; Baylan, (2020), where it was studied the adsorption of CIP on multiwalled carbon nanotubes, the authors showed that the equilibrium time was close to 200 min with a q_e of 0.01 mmol g^{-1}. Similarly, Carabineiro et al. (2011) studied the adsorption of CIP on carbon nanotubes and obtained an equilibrium time of 40 h. This shows that the adsorption of CIP with a geopolymer synthesized with GO in its composition was faster than with other carbonaceous materials.

The PFO, PSO and IPD models were fitted to the data (Figure 4.14, Supplementary material). These three models were able to satisfactorily describe the CIP kinetics in G_OG_C, as show in Table 4.4.

Table 4.4 - Parameters of pseudo-first order, pseudo-second order and intraparticle diffusion kinetic models

Models	Parameters	C_0 (mmol L^{-1})		
		0.05	**0.1**	**0.2**
Experimental	q_e (mmol g^{-1})	0.0332	0.0591	0.0733
PFO	q_{pred} (mmol g^{-1})	0.0332	0.0569	0.0644
	k_1 (min^{-1})	0.0426	0.2163	0.2799
	R^2 (-)	0.9811	0.8897	0.6883
	AICc (-)	-104.76	-62.34	-87.28
PSO	q_{pred} (mmol g^{-1})	0.0377	0.0583	0.0681
	k_2 (g $mmol^{-1}$ min^{-1})	0.0514	0.3245	0.4642
	R^2(-)	0.9699	0.9257	0.8179
	AICc (-)	-57.90	-61.24	-69.52
IPD	c (mmol g^{-1})	0.0205	0.0174	0.0332
	k_i (mmol g^{-1} min^{-1})	0.0011	0.0047	0.0042
	R^2(-)	0.6741	0.9995	0.9937
	AICc (-)	-71.56	-68.86	-83.21

At lower concentration, the pseudo-first order model showed the best fit with higher R^2 and more negative AICc values. This may indicate that the adsorption process occurs faster in its initial part and when it reaches equilibrium the process becomes slower (LEE et al., 2011). On the other hand, the PSO model was the most suitable for concentrations of 0.1 mmol L^{-1} and 0.2 mmol L^{-1}. This shows that for concentrations above 0.1 mmol L^{-1}, the adsorption process takes place by chemisorption and the adsorption capacity of G_OG_C is related to the number of active regions (AVCI; İNCI; BAYLAN, 2020). In addition, it is possible to evaluate that physisorption and chemisorption occur at the same time in the adsorption process of the antibiotic ciprofloxacin onto G_OG_C.

In the case of the intraparticle diffusion model, it is possible to observe that the process occurs in three stages (Figure 4.13, Supplementary Material), namely external diffusion, internal diffusion, and equilibrium. In the first stage, the adsorbate diffuses to the outer surface of the adsorbent, in the second stage, the contaminate leaves the outer surface and is carried into the intraparticle region of the adsorbent, and finally, material saturation occurs, and the system enters equilibrium, as few active sites remain and the concentration of the contaminant is very low (SUN et al., 2016). From Table 4, it is possible to observe that model PSO fitted well to the initial concentrations of 0.1 mmol L-1 and 0.2 mmol L-1. This may indicate that at these concentrations intraparticle diffusion may be the limiting step of the process, however, for the lowest concentration, internal diffusion may have some influence, but is not the limiting step of adsorption.

4.1.3.4 Molecular modeling

To analyze the CIP adsorption behavior of the materials synthesized, theoretical calculations based on Density Functional Theory (DFT) were performed to obtain the electronic and molecular properties. For the above, two calculation bases, 6-31G(d) and 6-31G(d, p), were used to optimize the molecules using the B3LYP method. The 6-31G(d) basis showed a more stable structure. Table 4.8 shows the connection lengths for the CIP molecule.

Figure 4.10 - HOMO (a) and LUMO (b) orbitals (purple: positive, pink: negative), and the electrostatic potential surface (c) for the CIP molecule at the 6-31G(d) basis set

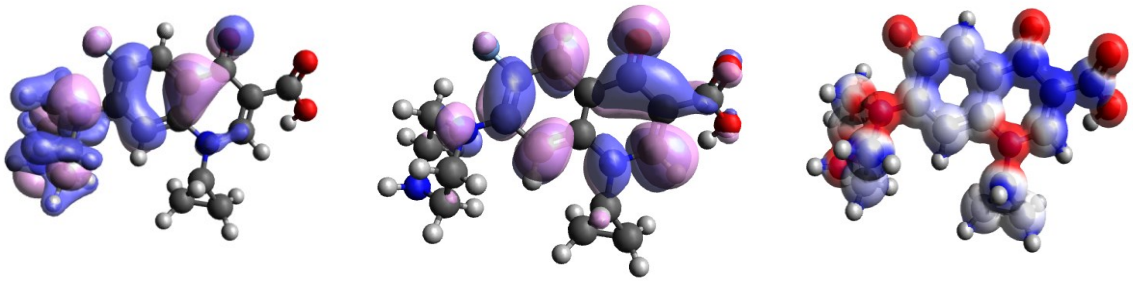

(a) (b) (c)

Figure 4.10 shows the 3D representations of the highest occupied molecular orbital (HOMO, E_H), lowest unoccupied molecular orbital (LUMO, E_L) and electrostatic potential of the CIP molecule. The E_H energy shows the ability of the CIP to donate electrons, while the EL relates the ability of the antibiotic to accept electrons (HSISSOU et al., 2019). The orbital HOMO is not located close to the oxygen ligands and is concentrated on 1-piperazine, while the orbital LUMO is located on the oxygen ligands and minimally on the cyclopropylamine of the CIP molecule. The values of these energies were given in Table 4.5

Table 4.5 - Calculated parameters of CIP

6-31G(d) basis	
LUMO (E_L)	-1.395 eV
HOMO (E_H)	-5.524 eV
GAP (ΔH_{H-L})	-4.18 eV
Electronic Chemical Potential (μ)	3.44 eV
Overall chemical Hardness (η)	2.09 eV
General Electrophilicity Index (ω)	2.83 eV

The values are in agreement with work reported in the literature (GUTIÉRREZ-SÁNCHEZ et al., 2023; KHALIL et al., 2020; UDDIN et al., 2022; YADAV et al., 2023). Comparing the values obtained with other antibiotics such as Cinoxacin, Levofloxacin and Ofloxacin, it is evident that the E_H energy of CIP is greater than the antibiotics mentioned above, while for the E_L energy it is lower. This indicates that the CIP has an electron-accepting layered molecule.

For the electrostatic potential (Figure 4.10c), it was represented by a blue color for a low electron density, while the red color denotes a high electron density (HSISSOU et al., 2019). In this case, the CIP molecule shows strong density in oxygen, nitrogen, and fluorine atoms while low density is found in carbon atoms. As for the hardness and electrophilicity of CIP, it can be considered as a material with strong nucleophiles (MBAH et al., 2022).

Thus, these results agree with those obtained in Affinity test. As CIP is a stable molecule with a high density of oxygen and nitrogen atoms, and the synthesized GO are not very uniform materials and are multilayers, the removal percentage is low. On the other hand, the geopolymer, a more uniform material, achieved a removal rate above 50%.

4.1.3.5 Elucidation of possible adsorption mechanisms

The mechanisms that can occur in the CIP adsorption system were shown in Figure 4.11. CIP is a zwitterionic compound whose predominant species at pH <6.1is cationic. While at pH>8.7 it is in anionic form with a deprotonated carboxylic acid group (ANTONELLI et al., 2020). Therefore, if the CIP is positively charged, the Al and Si atoms of the adsorbate will interact with oxygen, whereas if it is negatively charged, the interaction will be with the N of 1-piperazine. On the other hand, the O, C, H atoms can have a covalent interaction with the F, H, O atoms of the CIP (YANG et al., 2022).

Figure 4.11 - Possible CIP adsorption mechanism on G_OG_C

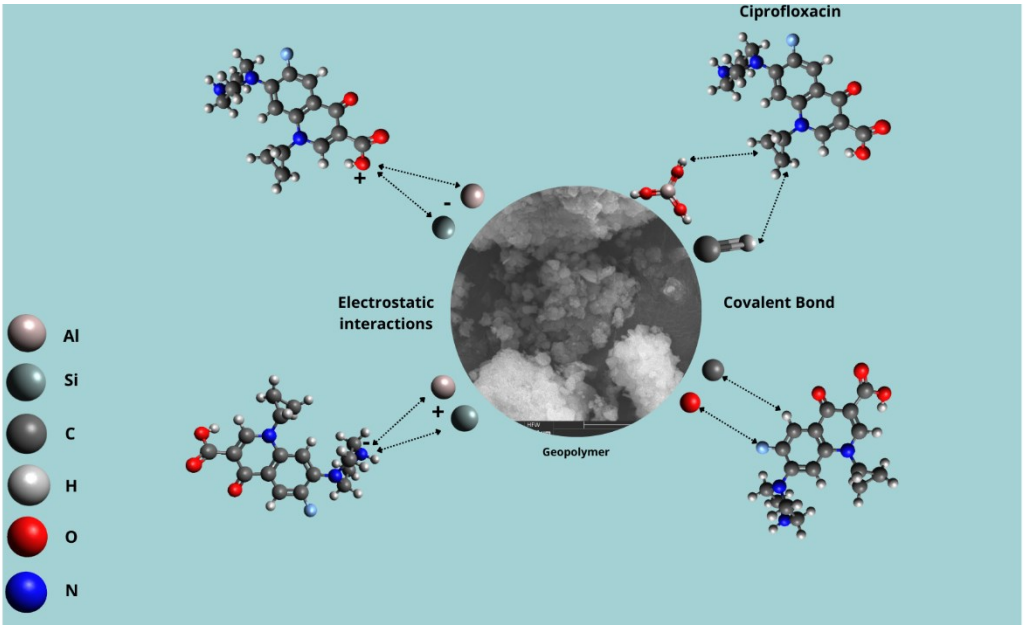

Another type of interaction that can occur is π-π due to GO in the geopolymer. The above will depend on the pH of the CIP, when it has a pH<6.1, the positive charge will do a π extraction from the aromatic ring of the CIP and will interact with the π donor structures of graphene oxide (CHEN; GAO; LI, 2015; LI; ZHANG, 2010). Similarly, a hydrogen bonding interaction can occur between the oxygen groups of GO with the carbon atoms of the aromatic rings of CIP (OLIVEIRA et al., 2023). Finally, as shown in section 3.3, other possible mechanisms are chemisorption and physisorption

4.1.4 Conclusions

In this work, graphene oxides with and without demineralization and GO-impregnated geopolymer were used as adsorbent materials for the Ciprofloxacin antibiotic removal in aqueous media. The characterization of the materials revealed the incorporation of OH groups in the graphene oxide layers by FTIR and Si-O-Si bonds in the geopolymer. Likewise, the FEG/EDS and RAMAN spectra showed the transformation of carbon and coke into a multilayered and amorphous material, while the geopolymer showed uniformity in its particles. The Zeta Potential showed that the synthesized materials exhibited better stability in water than their raw material. XRD revealed carbon and coke exfoliation for the GOs, while for the geopolymer it showed a composition with silica-alumina and faujasite. G_OG_C showed the best removal

(~55%) of CIP, while G_OG_Cq was the second-best adsorbent with ~40% removal. The kinetics took 120 min to reach equilibrium, which is lower than those reported in the literature. The kinetic models applied were fitted to the data obtained, in this case the PFO was the best fit for the lowest concentration, while PSO was the best fit for the highest concentrations. This indicates that at lower concentrations, chemisorption influences the process, but at higher concentrations, it is physisorption that ends up influencing. CIP molecular modeling helped to corroborate the results obtained, showing that the antibiotic is a stable molecule with a high density of oxygen and nitrogen atoms. This helped to clarify that the possible reaction mechanisms are electrostatic interactions and covalent bonds. Finally, the results found in this study indicate that the synthesis of multilayer GOs from coke and coal was achieved. Furthermore, GO can be added in the composition of a geopolymer and these synthesized materials are promising for the removal of pharmaceutical contaminants in aqueous media. For future studies, it is recommended to increase the graphene oxide composition in the geopolymer and evaluate its importance through kinetic and equilibrium studies in the adsorption of more antibiotics.

4.1.5 References

ABDULLAH, M. et al. Removal of ceftriaxone sodium antibiotic from pharmaceutical wastewater using an activated carbon based TiO2 composite: Adsorption and photocatalytic degradation evaluation. Chemosphere, v. 317, p. 137834, mar. 2023.

AHMED, M. B. et al. Adsorptive removal of antibiotics from water and wastewater: Progress and challenges. Science of The Total Environment, v. 532, p. 112–126, nov. 2015.

AJALA, O. J. et al. A critical review on graphene oxide nanostructured material: Properties, Synthesis, characterization and application in water and wastewater treatment. Environmental Nano-technology, Monitoring & Management, v. 18, p. 100673, dec. 2022.

ALI, S. Q. Resistance Pattern of Ciprofloxacin Against Different Pathogens. Oman Medical Journal, oct. 2010.

ANTONELLI, R. et al. Adsorption of ciprofloxacin onto thermally modified bentonite clay: Experimental design, characterization, and adsorbent regeneration. Journal of Environmental Chemical Engineering, v. 8, n. 6, p. 104553, dec. 2020.

ANTONELLI, R. et al. Fixed-Bed Adsorption of Ciprofloxacin onto Bentonite Clay: Characterization, Mathematical Modeling, and DFT-Based Calculations. Industrial & Engineering Chemistry Re-search, v. 60, n. 10, p. 4030–4040, 17 mar. 2021.

ARSYAD, W. S. et al. Synthesize of rGO from coal (sub-bituminous) as a counter-electrode on dye-sensitized solar cells. Journal of Physics: Conference Series, v. 1951, n. 1, p. 012005, 1 jun. 2021.

ASIM, M. et al. Synthesis and Characterization of Reduced Graphene Oxide from Indigenous Coal: A Non-Burning Solution. International Journal of Membrane Science and Technology, v. 9, n. 1, p. 1–12, 22 jan. 2022.

AVCI, A.; İNCI, İ.; BAYLAN, N. Adsorption of ciprofloxacin hydrochloride on multiwall carbon nanotube. Journal of Molecular Structure, v. 1206, p. 127711, apr. 2020.

BHAGAT, C. et al. Proclivities for prevalence and treatment of antibiotics in the ambient water: a review. npj Clean Water, v. 3, n. 1, p. 42, 16 oct. 2020.

CARABINEIRO, S. A. C. et al. Adsorption of ciprofloxacin on surface-modified carbon materials. Water Research, v. 45, n. 15, p. 4583–4591, oct. 2011.

CHEN, H.; GAO, B.; LI, H. Removal of sulfamethoxazole and ciprofloxacin from aqueous solutions by graphene oxide. Journal of Hazardous Materials, v. 282, p. 201–207, jan. 2015.

CHIN, J. Y.; AHMAD, A. L.; LOW, S. C. Evolution of photocatalytic membrane for antibiotics degradation: Perspectives and insights for sustainable environmental remediation. Journal of Water Process Engineering, v. 51, p. 103342, feb. 2023.

CLARAMUNT, S. et al. The Importance of Interbands on the Interpretation of the Raman Spectrum of Graphene Oxide. The Journal of Physical Chemistry C, v. 119, n. 18, p. 10123–10129, 7 may 2015.

CONLEY, Z. C. et al. Wicked: The untold story of ciprofloxacin. PLOS Pathogens, v. 14, n. 3, p. e1006805, 1 mar. 2018.

DANAEI, M. et al. Impact of Particle Size and Polydispersity Index on the Clinical Applications of Lipidic Nanocarrier Systems. Pharmaceutics, v. 10, n. 2, p. 57, 18 may 2018.

DAS, B.; KUNDU, R.; CHAKRAVARTY, S. Preparation and characterization of graphene oxide from coal. Materials Chemistry and Physics, v. 290, p. 126597, out. 2022.

DE ANDRADE, J. R. et al. Comparative adsorption of diclofenac sodium and losartan potassium in organophilic clay-packed fixed-bed: X-ray photoelectron spectroscopy characterization, experimental tests and theoretical study on DFT-based chemical descriptors. Journal of Molecular Liquids, v. 312, p. 113427, aug. 2020.

DE SOUZA, T. N. V. et al. Adsorption of basic dyes onto activated carbon: Experimental and theoretical investigation of chemical reactivity of basic dyes using DFT-based descriptors. Applied Sur-face Science, v. 448, p. 662–670, aug. 2018.

DELLA ROCCA, D. G. et al. Adding value to aluminosilicate solid wastes to produce adsorbents, catalysts and filtration membranes for water and wastewater treatment. Journal of Materials Science, v. 56, n. 2, p. 1039–1063, jan. 2021.

DOS SANTOS, A. J. et al. Recent advances in electrochemical water technologies for the treatment of antibiotics: A short review. Current Opinion in Electrochemistry, v. 26, p. 100674, apr. 2021.

DUTTA, J.; MALA, A. A. Removal of antibiotic from the water environment by the adsorption technologies: a review. Water Science and Technology, p. wst2020335, 21 jul. 2020.

ELICHE-QUESADA, D. et al. Geopolymers made from metakaolin sources, partially replaced by Spanish clays and biomass bottom ash. Journal of Building Engineering, v. 40, p. 102761, aug. 2021.

ETTOUMI, M. et al. Characterization of phosphate processing sludge from Tunisian mining basin and its potential valorization in fired bricks making. Journal of Cleaner Production, v. 284, p. 124750, feb. 2021.

EWIS, D. et al. Enhanced Removal of Diesel Oil Using New Magnetic Bentonite-Based Adsorbents Combined with Different Carbon Sources. Water, Air, & Soil Pollution, v. 233, n. 6, p. 195, jun. 2022.

FARIVAR, F. et al. Thermogravimetric Analysis (TGA) of Graphene Materials: Effect of Particle Size of Graphene, Graphene Oxide and Graphite on Thermal Parameters. C, v. 7, n. 2, p. 41, 27 apr. 2021.

FIGUEIREDO, R. A. M. et al. Mechanical and chemical analysis of one-part geopolymers synthe-sised with iron ore tailings from Brazil. Journal of Materials Research and Technology, v. 14, p. 2650–2657, sep. 2021.

FRANCOEUR, M. et al. Removal of antibiotics by adsorption and catalytic ozonation using magnetic activated carbons prepared from Sargassum sp. Journal of Water Process Engineering, v. 53, p. 103602, jul. 2023.

FREIRE, A. L. et al. Geopolymers produced with fly ash and rice husk ash applied to CO2 capture. Journal of Cleaner Production, v. 273, p. 122917, nov. 2020.

FU, H. et al. Activated carbon adsorption of quinolone antibiotics in water: Performance, mechanism, and modeling. Journal of Environmental Sciences, v. 56, p. 145–152, jun. 2017.

GONÇALVES, G. et al. Breakdown into nanoscale of graphene oxide: Confined hot spot atomic re-duction and fragmentation. Scientific Reports, v. 4, n. 1, p. 6735, 23 out. 2014.

GUTIÉRREZ-SÁNCHEZ, P. et al. Efficient removal of antibiotic ciprofloxacin by catalytic wet air oxidation using sewage sludge-based catalysts: Degradation mechanism by DFT studies. Journal of Environmental Chemical Engineering, v. 11, n. 2, p. 109344, apr. 2023.

HO, Y. S.; MCKAY, G. Pseudo-second order model for sorption processes. Process Biochemistry, v. 34, n. 5, p. 451–465, jul. 1999.

HSISSOU, R. et al. Experimental, DFT and molecular dynamics simulation on the inhibition pe-formance of the DGDCBA epoxy polymer against the corrosion of the E24 carbon steel in 1.0 M HCl solution. Journal of Molecular Structure, v. 1182, p. 340–351, apr. 2019.

HUANG, T.; SUN, Z. Advances in multifunctional graphene-geopolymer composites. Construction and Building Materials, v. 272, p. 121619, feb. 2021.

HUSKIĆ, M. et al. One-step surface modification of graphene oxide and influence of its particle size on the properties of graphene oxide/epoxy resin nanocomposites. European Polymer Journal, v. 101, p. 211–217, apr. 2018.

JIANG, J. et al. Molecular structure characterization of bituminous coal in Northern China via XRD, Raman and FTIR spectroscopy. Spectrochimica Acta Part A: Molecular and Biomolecular Spectroscopy, v. 255, p. 119724, jul. 2021.

JOHRA, F. T.; LEE, J.-W.; JUNG, W.-G. Facile and safe graphene preparation on solution based plat-form. Journal of Industrial and Engineering Chemistry, v. 20, n. 5, p. 2883–2887, sep. 2014.

KANTI, P. K.; MAIYA, M. P. Rheology and thermal conductivity of graphene oxide and coal fly ash hybrid nanofluids for various particle mixture ratios for heat

transfer applications: Experimental study. International Communications in Heat and Mass Transfer, v. 138, p. 106408, nov. 2022.

KHALIL, T. E. et al. Synthesis, characterization, antimicrobial activity, 3D-QSAR, DFT, and molecular docking of some ciprofloxacin derivatives and their copper(II) complexes. Applied Organo-metallic Chemistry, v. 34, n. 12, dec. 2020.

KLJAJEVIĆ, L. M. et al. Structural and chemical properties of thermally treated geopolymer samples. Ceramics International, v. 43, n. 9, p. 6700–6708, jun. 2017.

KRAUSS, B. et al. Raman Scattering at Pure Graphene Zigzag Edges. Nano Letters, v. 10, n. 11, p. 4544–4548, 10 nov. 2010.

KRÓL, M.; MINKIEWICZ, J.; MOZGAWA, W. IR spectroscopy studies of zeolites in geopolymeric materials derived from kaolinite. Journal of Molecular Structure, v. 1126, p. 200–206, dec. 2016.

KUDIN, K. N. et al. Raman Spectra of Graphite Oxide and Functionalized Graphene Sheets. Nano Letters, v. 8, n. 1, p. 36–41, 1 jan. 2008.

KURNIASARI et al. Defect and Magnetic Properties of Reduced Graphene Oxide Prepared from Old Coconut Shell. IOP Conference Series: Materials Science and Engineering, v. 196, p. 012021, may 2017.

LEE, C.-R. et al. Pseudo First-Order Adsorption Kinetics of N719 Dye on TiO 2 Surface. ACS Applied Materials & Interfaces, v. 3, n. 6, p. 1953–1957, 22 jun. 2011.

LEE, S.-Y.; MAHAJAN, R. L. A facile method for coal to graphene oxide and its application to a bio-sensor. Carbon, v. 181, p. 408–420, ago. 2021.

LI, B.; ZHANG, T. Biodegradation and Adsorption of Antibiotics in the Activated Sludge Process. Environmental Science & Technology, v. 44, n. 9, p. 3468–3473, 1 maio 2010.

LI, M. et al. The evolution of surface charge on graphene oxide during the reduction and its application in electroanalysis. Carbon, v. 66, p. 302–311, jan. 2014.

LÓPEZ-DÍAZ, D. et al. Evolution of the Raman Spectrum with the Chemical Composition of Graphene Oxide. The Journal of Physical Chemistry C, v. 121, n. 37, p. 20489–20497, 21 sep. 2017.

MALARD, L. M. et al. Raman spectroscopy in graphene. Physics Reports, v. 473, n. 5–6, p. 51–87, apr. 2009.

MBAH, M. B. et al. Unraveling the sequence of electron flow along the cyclocondensation reaction between ciprofloxacin and thiosemicarbazide

through the bonding evolution theory. Journal of Molecular Graphics and Modelling, v. 113, p. 108141, jun. 2022.

MERMOUX, M.; CHABRE, Y.; ROUSSEAU, A. FTIR and 13C NMR study of graphite oxide. Carbon, v. 29, n. 3, p. 469–474, 1991.

MINITHA, C. R.; RAJENDRAKUMAR, R. T. Synthesis and Characterization of Reduced Graphene Oxide. Advanced Materials Research, v. 678, p. 56–60, mar. 2013.

OLIVEIRA, M. G. et al. Adsorption kinetics of ciprofloxacin and ofloxacin by green-modified carbon nanotubes. Environmental Research, v. 233, p. 116503, sep. 2023.

OSSONON, B. D.; BÉLANGER, D. Synthesis and characterization of sulfophenyl-functionalized reduced graphene oxide sheets. RSC Advances, v. 7, n. 44, p. 27224–27234, 2017.

PENG, W. et al. Effect of oxidation degree of graphene oxide on the electrochemical performance of CoAl-layered double hydroxide/graphene composites. Applied Materials Today, v. 7, p. 201–211, jun. 2017.

PISUPATI, S. V.; KRISHNAMOORTHY, V. Utilization of coal in IGCC systems. Em: Integrated Gasification Combined Cycle (IGCC) Technologies. [s.l.] Elsevier, 2017. p. 83–120.

S. LAGERGREN. Zur theorie der Sogenannten adsorción gelöster stoffe, kungliga svenska veten-skapsakademiens. n. 24, p. 1–39, 1898.

SAHOO, P. et al. Synthesis and characterization of graphene oxide and graphene from coal. Mate-rials Today: Proceedings, v. 56, p. 2421–2427, 2022.

SANGUANPAK, S. et al. TiO2-immobilized porous geopolymer composite membrane for removal of antibiotics in hospital wastewater. Chemosphere, v. 307, p. 135760, nov. 2022.

SHAHID, M. K. et al. Current advances in treatment technologies for removal of emerging contaminants from water – A critical review. Coordination Chemistry Reviews, v. 442, p. 213993, sep. 2021.

SINGH, J. et al. Role of green chemistry in synthesis and modification of graphene oxide and its application: A review study. Chemical Physics Impact, v. 6, p. 100185, jun. 2023.

SONTAKKE, A. D.; TIWARI, S.; PURKAIT, M. K. A comprehensive review on graphene oxide-based nanocarriers: Synthesis, functionalization and biomedical applications. FlatChem, v. 38, p. 100484, mar. 2023.

SPAOLONZI, M. P. et al. Green-functionalized carbon nanotubes as adsorbents for the removal of emerging contaminants from aqueous media. Journal of Cleaner Production, v. 373, p. 133961, nov. 2022.

SUN, Y. et al. Characterization and ciprofloxacin adsorption properties of activated carbons pre-pared from biomass wastes by H3PO4 activation. Bioresource Technology, v. 217, p. 239–244, oct. 2016.

SUREKHA, G. et al. FTIR, Raman and XRD analysis of graphene oxide films prepared by modified Hummers method. Journal of Physics: Conference Series, v. 1495, n. 1, p. 012012, 1 mar. 2020.

UDDIN, M. A. et al. UV-Visible spectroscopic and DFT studies of the binding of ciprofloxacin hydrochloride antibiotic drug with metal ions at numerous temperatures. Korean Journal of Chemical Engineering, v. 39, n. 3, p. 664–673, mar. 2022.

UMEJURU, E. C.; PRABAKARAN, E.; PILLAY, K. Coal Fly Ash Decorated with Graphene Oxide–Tungsten Oxide Nanocomposite for Rapid Removal of Pb 2+ Ions and Reuse of Spent Adsorbent for Photocatalytic Degradation of Acetaminophen. ACS Omega, v. 6, n. 17, p. 11155–11172, 4 may 2021.

WANG, L. et al. Characteristics of Raman spectra for graphene oxide from ab initio simulations. The Journal of Chemical Physics, v. 135, n. 18, p. 184503, 14 nov. 2011.

WANG, Z.; LI, X. Synthesis of CoAl-layered double hydroxide/graphene oxide nanohybrid and its reinforcing effect in phenolic foams. High Performance Polymers, v. 30, n. 6, p. 688–698, aug. 2018.

WEBER, W. J.; MORRIS, J. C. Kinetics of Adsorption on Carbon from Solution. Journal of the Sani-tary Engineering Division, v. 89, n. 2, p. 31–59, apr. 1963.

WU, S. et al. Adsorption of ciprofloxacin onto biocomposite fibers of graphene oxide/calcium algi-nate. Chemical Engineering Journal, v. 230, p. 389–395, aug. 2013.

YADAV, A. et al. Unravelling the Potential of Silicon Carbide for Water Treatment: Insights on the Interactions of Fluoroquinolone Antibiotics. Silicon, v. 15, n. 5, p. 2251–2262, apr. 2023.

YANG, Y. et al. Efficient with low-cost removal and adsorption mechanisms of norfloxacin, ciprofloxacin and ofloxacin on modified thermal kaolin: experimental and theoretical studies. Journal of Hazardous Materials, v. 430, p. 128500, may 2022.

ZHAO, J. et al. Fabricating graphene oxide-based ultrathin hybrid membrane for pervaporation dehydration via layer-by-layer self-assembly driven by multiple interactions. Journal of Membrane Science, v. 487, p. 162–172, aug. 2015.

ZHOU, Q. et al. Efficient removal of tetracycline by reusable magnetic microspheres with a high surface area. Chemical Engineering Journal, v. 210, p. 350–356, nov. 2012.

4.2 SUPPLEMENTARY MATERIAL

Table 4.6 - Conditions applied for approximate analysis.

Temperature rate, °C/min	Holding temperature, °C	Retention time, min	Gas
10	35	20	Nitrogen
50	50	5	Nitrogen
50	110	5	Nitrogen
20	950	15	Nitrogen
-10	750	0	CO_2
1	750	40	CO_2

Table 4.7 - Crystallite size of synthesized samples

Nomenclature	I_D/I_G	La, nm
OG_D_C	1.00	19.2
OGC	1.00	19.1
OG_D_Cq	0.97	19.8
OGCq	0.99	19.4

Figure 4.12 - FEG images for (a,b) OG_D_Cq, (c) OGCq, (d) OGCR, (e,f) OG_D_CR and, (g,h) G_OG_C at 500x and 5 000x magnification

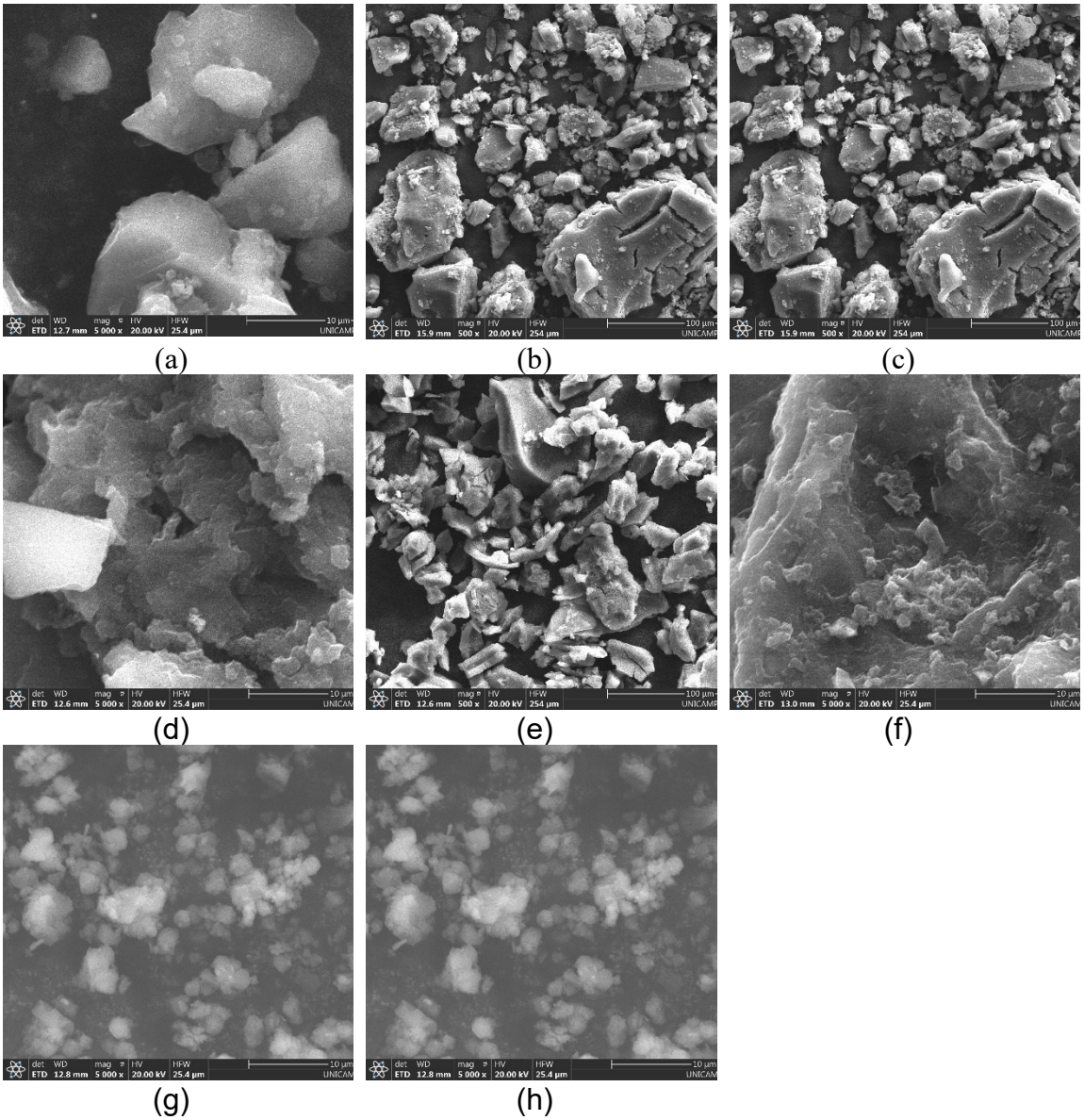

Figure 4.13 - Fittings of kinetic curves by PFO, PSO and IPD models for (a) 0.05 mmol L^{-1}, (b) 0.1 mmol L^{-1} and (c) 0.2 mmol L^{-1}

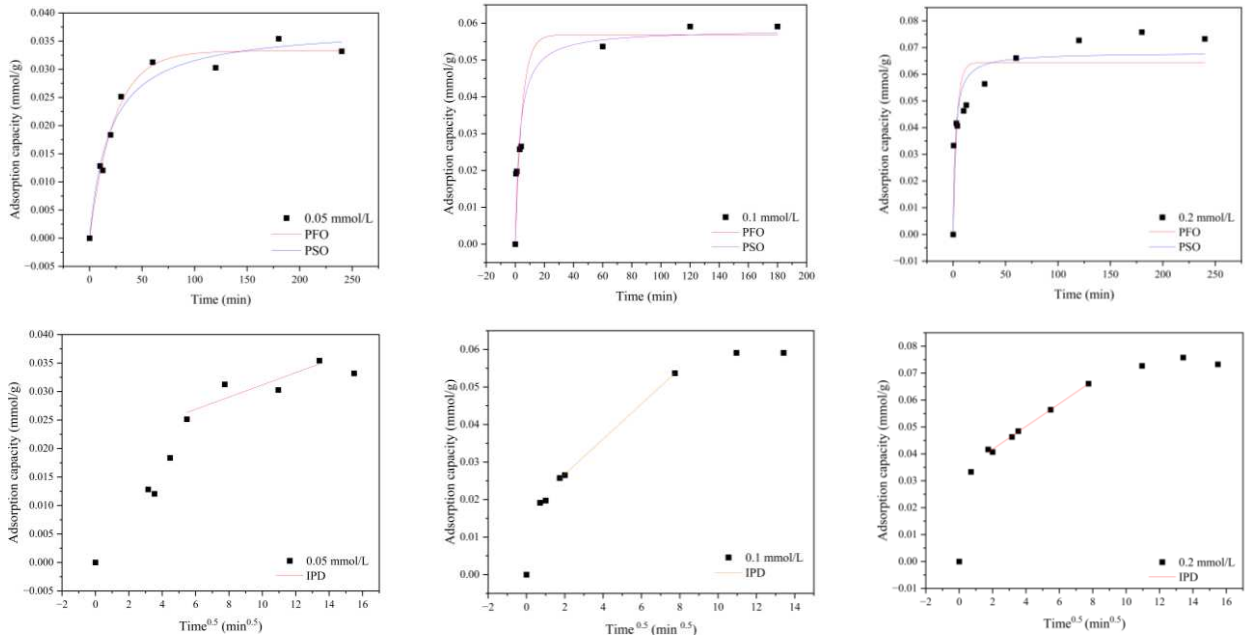

(a) (b) (c)

Table 4.8 - Connection lengths for the CIP molecule at the 6-31G(d) basis set

Bond type	Length (Å)	Bond type	Length (Å)
O-C	1.37482	C-C	1.42195
O-H	0.970978	N-C	1.46313
C-O	1.20224	N-C	1.47292
C-C	1.49592	C-C	1.5405
C-C	1.3661	C-H	1.10087
C-C	1.47093	C-H	1.09371
C-N	1.36721	C-N	1.4663
C-H	1.0846	C-H	1.09671
N-C	1.44766	C-H	1.09845
N-C	1.40748	N-C	1.46699
C-C	1.50683	N-H	1.02053
C-C	1.51033	C-C	1.53976
C-H	1.08943	C-H	1.09657
C-C	1.50579	C-H	1.0987
C-H	1.08574	C-H	1.10025
C-H	1.08569	C-H	1.08839
C-H	1.08641	C-F	1.35642
C-H	1.08576	C-C	1.37039
C-C	1.40536	C-C	1.40482
C-C	1.40964	C-H	1.08465
C-C	1.4044	C-C	1.47929
C-H	1.0796	C-O	1.22895
C-N	1.39266		

5 CHAPTER 5

5.1 CONCLUSIONS

In this work, multilayered graphene oxides were successfully synthesized by four different routes, the main methods being coal and coke demineralization, thermal exfoliation, and ozone oxidation. Characterizations such as FTIR showed the incorporation of oxygenated groups on the surface of the materials. The GOs also showed a significant improvement in stability. On the other hand, FEG/EDS showed the transformation of carbon and coke into a layered structure. This may indicate that in order to synthesize graphene oxide from coal and coke, it is necessary to first pass through a graphitic form before the final material. This would contradict much of the existing literature and would lead to a new scenario for the production of GO from an abundant and low-cost material, valorizing the Santa Catarina coal.

A graphene oxide-geopolymer composite was successfully synthesized. It showed a removal capacity of about 55% for ciprofloxacin. This capacity is higher than that obtained with GO. The kinetic equilibrium was reached in about 120 minutes. Compared with the literature, this time is similar to those reported in different works, although this one obtained a better removal capacity. Therefore, this polymeric composite with graphene oxide in its composition proved to be a promising material for the adsorption of antibiotics in aqueous media. The kinetic models showed what was expected, the higher the concentration, has the higher the adsorption capacity of the adsorbate. In this case, the polymeric compound reached a maximum value of 0.0733 mmol g^{-1}. The kinetic models used were Pseudo-First order (PFO) and Pseudo-Second Order (PSO). It was shown that for the lowest concentration (0.05 mmol L^{-1}) the PFO model was the best fit, while for the highest concentrations the PSO model was the best fit.

Finally, it can be concluded that the novel synthesis of graphene oxide is a promising process for GO production. Similarly, the graphene oxide-geopolymer composite is a prospective material for drug adsorption processes. Therefore, its use and synthesis with other pollutants should be further investigated.

5.2 SUGGESTIONS FOR FUTURE WORK

- Perform a process of graphitization of coal and coke to obtain a material that is easier to exfoliate.
- Optimize the process of oxidation by ozone, by evaluating the time that the samples are left in the ozonation.
- Optimize the oxidation process by heat treatment, by evaluating different times at a temperature of 950 °C.
- Characterize the GOs by Atomic Force Microscopy (AFM) to observe the lateral size of the graphene oxide layers.
- Preparation of a graphene oxide-geopolymer composite with higher GO concentration. Evaluate its adsorption capacity on ciprofloxacin and other antibiotics.
- Evaluate the graphene oxide-geopolymer composite in other applications such as cement and CO2 adsorption.
- Study of equilibrium, reuse and application in fixed bed dynamic system.

REFERENCES

ABDELKADER, A. M. et al. How to get between the sheets: a review of recent works on the electrochemical exfoliation of graphene materials from bulk graphite. **Nanoscale**, v. 7, n. 16, p. 6944–6956, 2015.

ADETAYO, A.; RUNSEWE, D. Synthesis and Fabrication of Graphene and Graphene Oxide: A Review. **Open Journal of Composite Materials**, v. 09, n. 02, p. 207–229, 2019.

AI, Y. et al. Insights into the adsorption mechanism and dynamic behavior of tetracycline antibiotics on reduced graphene oxide (RGO) and graphene oxide (GO) materials. **Environmental Science: Nano**, v. 6, n. 11, p. 3336–3348, 2019.

AL-HUSSEINY, R. A.; EBRAHIM, S. E. Synthesis of nano-magnetite and magnetite/synthetic geopolymer nano-porous composite for application as a novel adsorbent. **Environmental Nanotechnology, Monitoring & Management**, v. 18, p. 100700, dez. 2022.

ALI, I.; GUPTA, V. K. Advances in water treatment by adsorption technology. **Nature Protocols**, v. 1, n. 6, p. 2661–2667, dez. 2006.

AN, J.-E.; JEON, G. W.; JEONG, Y. G. Preparation and properties of polypropylene nanocomposites reinforced with exfoliated graphene. **Fibers and Polymers**, v. 13, n. 4, p. 507–514, abr. 2012.

ANM. **Anuário Mineral Brasileiro**. Agencia Nacional de Mineração, , 2018.

ARIFFIN, N. et al. **Geopolymer as an adsorbent of heavy metal: A review**. . Em: 3RD ELECTRONIC AND GREEN MATERIALS INTERNATIONAL CONFERENCE 2017 (EGM 2017). Krabi, Thailand: 2017. Disponível em: <https://pubs.aip.org/aip/acp/article/886571>. Acesso em: 20 ago. 2023

ASHOK KUMAR, S. S. et al. A review on graphene and its derivatives as the forerunner of the two-dimensional material family for the future. **Journal of Materials Science**, v. 57, n. 26, p. 12236–12278, jul. 2022.

ASHRAF, M. J.; IDREES, M.; AKBAR, A. Performance of silica fume slurry treated recycled aggregate concrete reinforced with carbon fibers. **Journal of Building Engineering**, v. 66, p. 105892, maio 2023.

AWASTHI, S. et al. Formation of single and multi-walled carbon nanotubes and graphene from Indian bituminous coal. **Fuel**, v. 147, p. 35–42, maio 2015.

BARROSO-BUJANS, F. et al. Permanent adsorption of organic solvents in graphite oxide and its effect on the thermal exfoliation. **Carbon**, v. 48, n. 4, p. 1079–1087, abr. 2010.

BELLUNO, C. B. L. **Produção de carvão**. Disponível em: <https://salvaro.cbelluno.com.br/index.php?url=producao-de-carvao>. Acesso em: 16 ago. 2023.

BERRY, V. Impermeability of graphene and its applications. **Carbon**, v. 62, p. 1–10, out. 2013.

BHAGAT, C. et al. Proclivities for prevalence and treatment of antibiotics in the ambient water: a review. **npj Clean Water**, v. 3, n. 1, p. 42, 16 out. 2020.

BHARECH, S.; KUMAR, R. A Review on the Properties and Applications of Graphene. **A Review on the Properties and Applications of Graphene**, p. 70–73, 2015.

BI, J. et al. On the Road to the Frontiers of Lithium-Ion Batteries: A Review and Outlook of Graphene Anodes. **Advanced Materials**, v. 35, n. 16, p. 2210734, abr. 2023.

BRITANNICA. **Coal mining - Extraction, Processing, Pollution | Britannica**. Disponível em: <https://www.britannica.com/technology/coal-mining/Coal-deposits>. Acesso em: 14 ago. 2023.

BRODIE, B. C. XIII. On the atomic weight of graphite. **Philosophical Transactions of the Royal Society of London**, v. 149, p. 249–259, 31 dez. 1859.

CAI, M. et al. Methods of graphite exfoliation. **Journal of Materials Chemistry**, v. 22, n. 48, p. 24992, 2012.

ÇALIŞKAN SALIHI, E. et al. Graphene oxide as a new generation adsorbent for the removal of antibiotics from waters. **Separation Science and Technology**, v. 56, n. 3, p. 453–461, 11 fev. 2021.

CAO, K. L. A. et al. Recent Advances in the Fabrication and Functionalization of Nanostructured Carbon Spheres for Energy Storage Applications. **KONA Powder and Particle Journal**, v. 40, n. 0, p. 197–218, 10 jan. 2023.

CASTRO NETO, A. H. et al. The electronic properties of graphene. **Reviews of Modern Physics**, v. 81, n. 1, p. 109–162, 14 jan. 2009.

CHEN, H.; GAO, B.; LI, H. Removal of sulfamethoxazole and ciprofloxacin from aqueous solutions by graphene oxide. **Journal of Hazardous Materials**, v. 282, p. 201–207, jan. 2015.

CHEN, J. et al. Water-enhanced oxidation of graphite to graphene oxide with controlled species of oxygenated groups. **Chemical Science**, v. 7, n. 3, p. 1874–1881, 2016.

CHEN, J. et al. Fabrication of macroporous magnetic carbon fibers via the cooperative etching-electrospinning technology toward ultra-light microwave absorption. **Carbon**, v. 208, p. 82–91, maio 2023.

CHEN, J.; DUAN, M.; CHEN, G. Continuous mechanical exfoliation of graphene sheets via three-roll mill. **Journal of Materials Chemistry**, v. 22, n. 37, p. 19625, 2012.

CIESIELSKI, A.; SAMORÌ, P. Graphene via sonication assisted liquid-phase exfoliation. **Chem. Soc. Rev.**, v. 43, n. 1, p. 381–398, 2014.

COLEMAN, J. N. Liquid-Phase Exfoliation of Nanotubes and Graphene. **Advanced Functional Materials**, v. 19, n. 23, p. 3680–3695, 9 dez. 2009.

CONG, P.; CHENG, Y. Advances in geopolymer materials: A comprehensive review. **Journal of Traffic and Transportation Engineering (English Edition)**, v. 8, n. 3, p. 283–314, jun. 2021.

COWAN, W. N. et al. The nexus of electricity consumption, economic growth and CO2 emissions in the BRICS countries. **Energy Policy**, v. 66, p. 359–368, mar. 2014.

CUERDA-CORREA, E. M.; ALEXANDRE-FRANCO, M. F.; FERNÁNDEZ-GONZÁLEZ, C. Advanced Oxidation Processes for the Removal of Antibiotics from Water. An Overview. **Water**, v. 12, n. 1, p. 102, 27 dez. 2019.

DĄBROWSKI, A. Adsorption — from theory to practice. **Advances in Colloid and Interface Science**, v. 93, n. 1–3, p. 135–224, out. 2001.

DAS, B.; KUNDU, R.; CHAKRAVARTY, S. Preparation and characterization of graphene oxide from coal. **Materials Chemistry and Physics**, v. 290, p. 126597, out. 2022.

DAVIDOVITS, J. **Geopolymer chemistry and sustainable development**. . Em: GEOPOLYMER GREEN CHEMISTRY AND SUSTAINABLE DEVELOPMENT SOLUTIONS. Saint-Quentin, France: 2005.

DE GISI, S. et al. Characteristics and adsorption capacities of low-cost sorbents for wastewater treatment: A review. **Sustainable Materials and Technologies**, v. 9, p. 10–40, set. 2016.

DEHGHANI, Z.; OSTOVARI, F.; SHARIFI, S. A comparison of the crystal structure and optical properties of reduced graphene oxide and aminated graphene nanosheets for optoelectronic device applications. **Optik**, v. 274, p. 170551, mar. 2023.

DIMIEV, A. et al. Pristine Graphite Oxide. **Journal of the American Chemical Society**, v. 134, n. 5, p. 2815–2822, 8 fev. 2012.

DOS SANTOS, F. N. et al. The occurrence of pristine and functionalized fullerenes as constituents of airborne aerosols. **Scientific Reports**, v. 13, n. 1, p. 4248, 14 mar. 2023.

DUTTA, J.; MALA, A. A. Removal of antibiotic from the water environment by the adsorption technologies: a review. **Water Science and Technology**, p. wst2020335, 21 jul. 2020.

EI. **Statistical Review of World Energy**. Disponível em: <https://www.energyinst.org/statistical-review>. Acesso em: 14 ago. 2023.

EIA. **How much coal is left**. Disponível em: <https://www.eia.gov/energyexplained/coal/how-much-coal-is-left.php>. Acesso em: 14 ago. 2023.

EIGLER, S. et al. Sulfur Species in Graphene Oxide. **Chemistry - A European Journal**, v. 19, n. 29, p. 9490–9496, 15 jul. 2013.

EL-SHAFEY, E.-S. I.; AL-LAWATI, H.; AL-SUMRI, A. S. Ciprofloxacin adsorption from aqueous solution onto chemically prepared carbon from date palm leaflets. **Journal of Environmental Sciences**, v. 24, n. 9, p. 1579–1586, set. 2012.

FARJADIAN, F. et al. Recent Developments in Graphene and Graphene Oxide: Properties, Synthesis, and Modifications: A Review. **ChemistrySelect**, v. 5, n. 33, p. 10200–10219, 7 set. 2020.

FATIMA PERALTA MUNIZ MOREIRA, R. **Síntese do óxido de grafeno/grafite e grafeno utilizando tratamento com UV/ozônio, Relatório restrito.** , nov. 2021.

FAUST, S. D.; OSMAN, M. A. **Adsorption Processes for Water Treatment**. [s.l.] Elsevier, 2013.

FERNÁNDEZ-GARCÍA, L. et al. Peculiarities of the production of graphene oxides with controlled properties from industrial coal liquids. **Fuel**, v. 203, p. 253–260, set. 2017.

FRANCOEUR, M. et al. Removal of antibiotics by adsorption and catalytic ozonation using magnetic activated carbons prepared from Sargassum sp. **Journal of Water Process Engineering**, v. 53, p. 103602, jul. 2023.

FREIRE, A. L. et al. Geopolymers produced with fly ash and rice husk ash applied to CO2 capture. **Journal of Cleaner Production**, v. 273, p. 122917, nov. 2020.

FREIRE, A. L. **Synthesis, Characterization and Application of Geopolymers based on Phosphate Mining Tailings in Carbon Capture Sequestration**. Brazil: UNIVERSIDADE FEDERAL DO RIO GRANDE DO SUL, 2022.

FU, H. et al. Activated carbon adsorption of quinolone antibiotics in water: Performance, mechanism, and modeling. **Journal of Environmental Sciences**, v. 56, p. 145–152, jun. 2017.

GAO, F. et al. A green strategy for the synthesis of graphene supported Mn 3 O 4 nanocomposites from graphitized coal and their supercapacitor application. **Carbon**, v. 80, p. 640–650, dez. 2014.

GAO, Y. et al. Adsorption and removal of tetracycline antibiotics from aqueous solution by graphene oxide. **Journal of Colloid and Interface Science**, v. 368, n. 1, p. 540–546, fev. 2012.

GASNER, L. L.; DENLOYE, A. O.; REGAN, T. M. MICROWAVE AND CONVENTIONAL PYROLYSIS OF A BITUMINOUS COAL. **Chemical Engineering Communications**, v. 48, n. 4–6, p. 349–354, nov. 1986.

GILL, S. S. et al. Remediation of environmental toxicants using carbonaceous materials: opportunity and challenges. **Environmental Science and Pollution Research**, v. 30, n. 27, p. 69727–69750, 9 maio 2023.

GONÇALVES, G. et al. Breakdown into nanoscale of graphene oxide: Confined hot spot atomic reduction and fragmentation. **Scientific Reports**, v. 4, n. 1, p. 6735, 23 out. 2014.

GREEN, D. W.; PERRY, R. H. **Perry's Chemical Engineers' Handbook**. [s.l: s.n.].

GROVEMAN, S. et al. The role of ozone in the formation and structural evolution of graphene oxide obtained from nanographite. **Carbon**, v. 122, p. 411–421, out. 2017.

GUO, X.; SHI, H.; WEI, X. Pore properties, inner chemical environment, and microstructure of nano-modified CFA-WBP (class C fly ash-waste brick powder) based geopolymers. **Cement and Concrete Composites**, v. 79, p. 53–61, maio 2017.

GUO, Y. et al. Electrical Assembly and Reduction of Graphene Oxide in a Single Solution Step for Use in Flexible Sensors. **Advanced Materials**, v. 23, n. 40, p. 4626–4630, 25 out. 2011.

HAAR, S. et al. Enhancing the Liquid-Phase Exfoliation of Graphene in Organic Solvents upon Addition of n-Octylbenzene. **Scientific Reports**, v. 5, n. 1, p. 16684, 17 nov. 2015.

HE, X. et al. Direct synthesis of 3D hollow porous graphene balls from coal tar pitch for high performance supercapacitors. **J. Mater. Chem. A**, v. 2, n. 46, p. 19633–19640, 2014.

HE, X. et al. ZnO template strategy for the synthesis of 3D interconnected graphene nanocapsules from coal tar pitch as supercapacitor electrode materials. **Journal of Power Sources**, v. 340, p. 183–191, fev. 2017.

HERNÁNDEZ ROSAS, J. J. et al. First principles calculations of the electronic and chemical properties of graphene, graphane, and graphene oxide. **Journal of Molecular Modeling**, v. 17, n. 5, p. 1133–1139, maio 2011.

HO, Y. S.; MCKAY, G. Pseudo-second order model for sorption processes. **Process Biochemistry**, v. 34, n. 5, p. 451–465, jul. 1999.

HOIGNÉ, J.; BADER, H. Rate constants of reactions of ozone with organic and inorganic compounds in water—II. **Water Research**, v. 17, n. 2, p. 185–194, jan. 1983.

HU, Y. H.; WANG, H.; HU, B. Thinnest Two-Dimensional Nanomaterial-Graphene for Solar Energy. **ChemSusChem**, v. 3, n. 7, p. 782–796, 11 jun. 2010.

HUANG, T.; SUN, Z. Advances in multifunctional graphene-geopolymer composites. **Construction and Building Materials**, v. 272, p. 121619, fev. 2021.

HUANG, X. et al. Coupled Cu(II)-EDTA degradation and Cu(II) removal from acidic wastewater by ozonation: Performance, products and pathways. **Chemical Engineering Journal**, v. 299, p. 23–29, set. 2016.

HUANG, X.-M. et al. Physical properties and device applications of graphene oxide. **Frontiers of Physics**, v. 15, n. 3, p. 33301, jun. 2020.

IEA. **Renewables 2019 – Analysis**. Disponível em: <https://www.iea.org/reports/renewables-2019>. Acesso em: 17 ago. 2023.

IGWEGBE, C. A. et al. Adsorption of ciprofloxacin from water: A comprehensive review. **Journal of Industrial and Engineering Chemistry**, v. 93, p. 57–77, jan. 2021.

IKRAM, R.; JAN, B. M.; AHMAD, W. Advances in synthesis of graphene derivatives using industrial wastes precursors; prospects and challenges. **Journal of Materials Research and Technology**, v. 9, n. 6, p. 15924–15951, nov. 2020.

JI, D. et al. Smartphone-based square wave voltammetry system with screen-printed graphene electrodes for norepinephrine detection. **Smart Materials in Medicine**, v. 1, p. 1–9, 2020.

JIŘÍČKOVÁ, A. et al. Synthesis and Applications of Graphene Oxide. **Materials**, v. 15, n. 3, p. 920, 25 jan. 2022.

JORJANI, E.; CHAPI, H. G.; KHORAMI, M. T. Ultra clean coal production by microwave irradiation pretreatment and sequential leaching with HF followed by HNO3. **Fuel Processing Technology**, v. 92, n. 10, p. 1898–1904, out. 2011.

JOSHI, S. et al. Graphene derivatives: Properties and potential food applications. **Journal of Industrial and Engineering Chemistry**, v. 123, p. 1–18, jul. 2023.

JOY, A. et al. A novel combination of graphene oxide/palladium integrated polycaprolactone nanocomposite for biomedical applications. **Diamond and Related Materials**, v. 136, p. 110033, jun. 2023.

KALKREUTH, W. et al. Depositional setting, petrology and chemistry of Permian coals from the Paraná Basin: 2. South Santa Catarina Coalfield, Brazil. **International Journal of Coal Geology**, v. 84, n. 3–4, p. 213–236, dez. 2010.

KANG, J. H. et al. Hidden Second Oxidation Step of Hummers Method. **Chemistry of Materials**, v. 28, n. 3, p. 756–764, 9 fev. 2016.

KARA, İ.; YILMAZER, D.; AKAR, S. T. Metakaolin based geopolymer as an effective adsorbent for adsorption of zinc(II) and nickel(II) ions from aqueous solutions. **Applied Clay Science**, v. 139, p. 54–63, abr. 2017.

KASHIF, M. et al. Effect of potassium permanganate on morphological, structural and electro-optical properties of graphene oxide thin films. **Arabian Journal of Chemistry**, v. 14, n. 2, p. 102953, fev. 2021.

KHAN, Z. U. et al. A review of graphene oxide, graphene buckypaper, and polymer/graphene composites: Properties and fabrication techniques. **Journal of Plastic Film & Sheeting**, v. 32, n. 4, p. 336–379, out. 2016.

KHOEI, A. R.; KHORRAMI, M. S. Mechanical properties of graphene oxide: A molecular dynamics study. **Fullerenes, Nanotubes and Carbon Nanostructures**, v. 24, n. 9, p. 594–603, set. 2016.

KIM, C. et al. Arc discharge synthesis of graphene with enhanced boron doping concentration for electrochemical applications. **Applied Surface Science**, v. 637, p. 157825, nov. 2023.

KIM, H. et al. Scalable Functionalized Graphene Nano-platelets as Tunable Cathodes for High-performance Lithium Rechargeable Batteries. **Scientific Reports**, v. 3, n. 1, p. 1506, 21 mar. 2013.

KIM, S. et al. Room-temperature metastability of multilayer graphene oxide films. **Nature Materials**, v. 11, n. 6, p. 544–549, jun. 2012.

KOMNITSAS, K.; ZAHARAKI, D. Geopolymerisation: A review and prospects for the minerals industry. **Minerals Engineering**, v. 20, n. 14, p. 1261–1277, nov. 2007.

KUNDU, N.; SADHUKHAN, D.; SARKAR, S. Fluorescent carbon nano-materials from coal-based precursors: unveiling structure–function relationship between coal and nano-materials. **Carbon Letters**, v. 32, n. 3, p. 671–702, maio 2022.

KYMAKIS, E. et al. Flexible Organic Photovoltaic Cells with In Situ Nonthermal Photoreduction of Spin-Coated Graphene Oxide Electrodes. **Advanced Functional Materials**, v. 23, n. 21, p. 2742–2749, 6 jun. 2013.

LAN, J. et al. Progress on fabrication and application of activated carbon sphere in recent decade. **Journal of Industrial and Engineering Chemistry**, v. 120, p. 47–72, abr. 2023.

LEE, G.-H. et al. High-Strength Chemical-Vapor–Deposited Graphene and Grain Boundaries. **Science**, v. 340, n. 6136, p. 1073–1076, 31 maio 2013.

LEE, X. J. et al. Review on graphene and its derivatives: Synthesis methods and potential industrial implementation. **Journal of the Taiwan Institute of Chemical Engineers**, v. 98, p. 163–180, maio 2019.

LI, H. et al. Synthesis, modification strategies and applications of coal-based carbon materials. **Fuel Processing Technology**, v. 230, p. 107203, jun. 2022.

LIU, F.; XUE, D. Electrochemical energy storage applications of “pristine” graphene produced by non-oxidative routes. **Science China Technological Sciences**, v. 58, n. 11, p. 1841–1850, nov. 2015.

LIU, P. et al. Electrospinning of hierarchical carbon fibers with multi-dimensional magnetic configurations toward prominent microwave absorption. **Carbon**, v. 202, p. 244–253, jan. 2023a.

LIU, T. et al. Pore Perforation of Graphene Coupled with In Situ Growth of Co_3Se_4 for High-Performance Na-Ion Battery. **Advanced Materials**, v. 35, n. 13, p. 2207752, mar. 2023b.

LIU, W. et al. Construction of ultra-sensitive surface-enhanced Raman scattering substrates based on 3D graphene oxide aerogels. **Carbon**, v. 202, p. 389–397, jan. 2023c.

LOH, K. P. et al. Graphene oxide as a chemically tunable platform for optical applications. **Nature Chemistry**, v. 2, n. 12, p. 1015–1024, dez. 2010.

LUO, Z. et al. Dry coal beneficiation technique in the gas–solid fluidized bed: a review. **International Journal of Coal Preparation and Utilization**, v. 42, n. 4, p. 986–1014, 3 abr. 2022.

LUPINA, G. et al. Residual Metallic Contamination of Transferred Chemical Vapor Deposited Graphene. **ACS Nano**, v. 9, n. 5, p. 4776–4785, 26 maio 2015.

LUUKKONEN, T. et al. Optimization of the metakaolin geopolymer preparation for maximized ammonium adsorption capacity. **Journal of Materials Science**, v. 52, n. 16, p. 9363–9376, ago. 2017.

LYUBCHIK, S. et al. Comparison of the Thermodynamic Parameters Estimation for the Adsorption Process of the Metals from Liquid Phase on Activated Carbons. Em: MORENO PIRAJN, J. C. (Ed.). **Thermodynamics - Interaction Studies - Solids, Liquids and Gases**. [s.l.] InTech, 2011.

MAGAZZINO, C.; MELE, M.; SCHNEIDER, N. A machine learning approach on the relationship among solar and wind energy production, coal consumption, GDP, and CO2 emissions. **Renewable Energy**, v. 167, p. 99–115, abr. 2021.

MANCHISI, J. et al. Ironmaking and Steelmaking Slags as Sustainable Adsorbents for Industrial Effluents and Wastewater Treatment: A Critical Review of Properties, Performance, Challenges and Opportunities. **Sustainability**, v. 12, n. 5, p. 2118, 9 mar. 2020.

MARINOIU, A. et al. Graphene-based Materials Used as the Catalyst Support for PEMFC Applications. **Materials Today: Proceedings**, v. 2, n. 6, p. 3797–3805, 2015.

MASSA, P. **Produção de carvão mineral no Brasil**. **Massa - Pesagem e Automação Industrial**, 8 jun. 2022. Disponível em: <https://massa.ind.br/producao-de-carvao-mineral-no-brasil/>. Acesso em: 16 ago. 2023

MASUDA, S. et al. Electrostatic Beneficiation of Coal Using a Cyclone-Tribocharger. **IEEE Transactions on Industry Applications**, v. IA-19, n. 5, p. 789–793, set. 1983.

MCALLISTER, M. J. et al. Single Sheet Functionalized Graphene by Oxidation and Thermal Expansion of Graphite. **Chemistry of Materials**, v. 19, n. 18, p. 4396–4404, 1 set. 2007.

MORCOMBE, C. R.; ZILM, K. W. Chemical shift referencing in MAS solid state NMR. **Journal of Magnetic Resonance**, v. 162, n. 2, p. 479–486, jun. 2003.

NABEEL, A.; KHAN, T. A.; SHARMA, D. K. Studies on the Production of Ultra-clean Coal by Alkali-acid Leaching of Low-grade Coals. **Energy Sources, Part A: Recovery, Utilization, and Environmental Effects**, v. 31, n. 7, p. 594–601, 10 mar. 2009.

NAIEF, M. F. et al. A review of the role of carbon nanotubes for cancer treatment based on photothermal and photodynamic therapy techniques. **Journal of Organometallic Chemistry**, v. 999, p. 122819, out. 2023.

NIKOLAY, S.; VICTOR, K. Synthesis and Characteristics of Graphene–Graphene Oxide Material Obtained by an Underwater Impulse Direct Current Discharge. **Plasma Chemistry and Plasma Processing**, v. 43, n. 5, p. 1077–1092, set. 2023.

OLLIK, K.; LIEDER, M. Review of the Application of Graphene-Based Coatings as Anticorrosion Layers. **Coatings**, v. 10, n. 9, p. 883, 14 set. 2020.

OXFORD, S. **Coal reserves**. Disponível em: <https://ourworldindata.org/grapher/coal-proved-reserves>. Acesso em: 16 ago. 2023.

ÖZER, M.; BASHA, O. M.; MORSI, B. Coal-Agglomeration Processes: A Review. **International Journal of Coal Preparation and Utilization**, v. 37, n. 3, p. 131–167, 4 maio 2017.

PAPAGEORGIOU, D. G.; KINLOCH, I. A.; YOUNG, R. J. Mechanical properties of graphene and graphene-based nanocomposites. **Progress in Materials Science**, v. 90, p. 75–127, out. 2017.

PARK, J. et al. Characteristics tuning of graphene-oxide-based-graphene to various end-uses. **Energy Storage Materials**, v. 14, p. 8–21, set. 2018.

PETRY, T. S.; PHILIPP, R. P.; GONZATTI, C. Geologia estrutural aplicada à mineração subterrânea de carvão em Araranguá (SC, Brasil). **Pesquisas em Geociências**, v. 45, n. 1, 12 nov. 2018.

PHENGSAART, T. et al. Conventional and recent advances in gravity separation technologies for coal cleaning: A systematic and critical review. **Heliyon**, v. 9, n. 2, p. e13083, fev. 2023.

POP, E.; VARSHNEY, V.; ROY, A. K. Thermal properties of graphene: Fundamentals and applications. **MRS Bulletin**, v. 37, n. 12, p. 1273–1281, dez. 2012.

POWELL, C.; BEALL, G. W. Graphene oxide and graphene from low grade coal: Synthesis, characterization and applications. **Current Opinion in Colloid & Interface Science**, v. 20, n. 5–6, p. 362–366, out. 2015.

PRAMANIK, A. et al. Anomalies at the Dirac Point in Graphene and Its Hole-Doped Compositions. **Physical Review Letters**, v. 128, n. 16, p. 166401, 18 abr. 2022.

PRIYA, D. S.; KENNEDY, L. J.; ANAND, G. T. Emerging trends in biomass-derived porous carbon materials for energy storage application: A critical review. **Materials Today Sustainability**, v. 21, p. 100320, mar. 2023.

PRUD'HOMME, E. et al. In situ inorganic foams prepared from various clays at low temperature. **Applied Clay Science**, v. 51, n. 1–2, p. 15–22, jan. 2011.

PURWANDARI, V. et al. **Synthesis of graphene oxide from the Sawahlunto-Sijunjung coal via modified hummers method**. . Em: THE 3RD INTERNATIONAL SEMINAR ON CHEMISTRY: GREEN CHEMISTRY AND ITS ROLE FOR SUSTAINABILITY. Surabaya, Indonesia: 2018. Disponível em: <https://pubs.aip.org/aip/acp/article/726403>. Acesso em: 20 ago. 2023

QALYOUBI, L.; AL-OTHMAN, A.; AL-ASHEH, S. Removal of ciprofloxacin antibiotic pollutants from wastewater using nano-composite adsorptive membranes. **Environmental Research**, v. 215, p. 114182, dez. 2022.

QIU, H. et al. Critical review in adsorption kinetic models. **Journal of Zhejiang University-SCIENCE A**, v. 10, n. 5, p. 716–724, maio 2009.

RADMEHR, S. et al. Adsorption of nalidixic acid antibiotic using a renewable adsorbent based on Graphene oxide from simulated wastewater. **Journal of Environmental Chemical Engineering**, v. 9, n. 5, p. 105975, out. 2021.

RAHMAN, M.; PUDASAINEE, D.; GUPTA, R. Review on chemical upgrading of coal: Production processes, potential applications and recent developments. **Fuel Processing Technology**, v. 158, p. 35–56, abr. 2017.

RAO, C. N. R.; SOOD, A. K. **Graphene: Synthesis, Properties, and Phenomena**. [s.l: s.n.].

RASHI. Exploring the methods of synthesis, functionalization, and characterization of graphene and graphene oxide for supercapacitor applications. **Ceramics International**, v. 49, n. 1, p. 40–47, jan. 2023.

REKHATE, C. V.; SRIVASTAVA, J. K. Recent advances in ozone-based advanced oxidation processes for treatment of wastewater- A review. **Chemical Engineering Journal Advances**, v. 3, p. 100031, nov. 2020.

RIO DESERTO. **Carbonífera Rio Deserto**. Disponível em: <https://www.brasilmineral.com.br/maiores/riodeserto>. Acesso em: 16 ago. 2023.

ROBERTS, M. M.; WISEMAN, T. Curved-space Dirac description of elastically deformed monolayer graphene is generally incorrect. **Physical Review B**, v. 105, n. 19, p. 195412, 6 maio 2022.

ROSTAMIAN, R.; BEHNEJAD, H. A comparative adsorption study of sulfamethoxazole onto graphene and graphene oxide nanosheets through equilibrium, kinetic and thermodynamic modeling. **Process Safety and Environmental Protection**, v. 102, p. 20–29, jul. 2016.

ROSTAMIAN, R.; BEHNEJAD, H. A comprehensive adsorption study and modeling of antibiotics as a pharmaceutical waste by graphene oxide nanosheets. **Ecotoxicology and Environmental Safety**, v. 147, p. 117–123, jan. 2018.

SAHOO, P. et al. Synthesis and characterization of graphene oxide and graphene from coal. **Materials Today: Proceedings**, v. 56, p. 2421–2427, 2022.

SAIKIA, B. J. et al. **Natural Fullerene C60 from the Iridium-Rich Cretaceous-Paleogene (K-Pg) Boundary Layers of the Um-Sohryngkew River Section, Meghalaya, India- Ftir, Micro Raman Spectroscopic and Transmission Electron Microscopic Investigations**. [s.l.] SSRN, 2023. Disponível em: <https://www.ssrn.com/abstract=4523351>. Acesso em: 17 ago. 2023.

SALMA, A. et al. Dependence of transformation product formation on pH during photolytic and photocatalytic degradation of ciprofloxacin. **Journal of Hazardous Materials**, v. 313, p. 49–59, ago. 2016.

SANGUANPAK, S. et al. TiO2-immobilized porous geopolymer composite membrane for removal of antibiotics in hospital wastewater. **Chemosphere**, v. 307, p. 135760, nov. 2022.

SCHNIEPP, H. C. et al. Functionalized Single Graphene Sheets Derived from Splitting Graphite Oxide. **The Journal of Physical Chemistry B**, v. 110, n. 17, p. 8535–8539, 1 maio 2006.

SCHWIERZ, F. Graphene transistors. **Nature Nanotechnology**, v. 5, n. 7, p. 487–496, jul. 2010.

SENTHIL KUMAR, E. et al. Facile synthesis of few layer graphene from bituminous coal and its application towards electrochemical sensing of caffeine. **Advanced Materials Letters**, v. 8, n. 3, p. 239–245, 1 mar. 2017.

SHAHID, M. K. et al. Current advances in treatment technologies for removal of emerging contaminants from water – A critical review. **Coordination Chemistry Reviews**, v. 442, p. 213993, set. 2021.

SHARMA, A.; MORISADA, Y.; FUJII, H. Bending induced mechanical exfoliation of graphene interlayers in a through thickness Al-GNP functionally graded composite fabricated via novel single-step FSP approach. **Carbon**, v. 186, p. 475–491, jan. 2022.

SHEAN, B. J.; CILLIERS, J. J. A review of froth flotation control. **International Journal of Mineral Processing**, v. 100, n. 3–4, p. 57–71, set. 2011.

SHEHU IMAM, S.; ADNAN, R.; MOHD KAUS, N. H. Photocatalytic degradation of ciprofloxacin in aqueous media: a short review. **Toxicological & Environmental Chemistry**, v. 100, n. 5–7, p. 518–539, 9 ago. 2018.

SHI, C.; JIMÉNEZ, A. F.; PALOMO, A. New cements for the 21st century: The pursuit of an alternative to Portland cement. **Cement and Concrete Research**, v. 41, n. 7, p. 750–763, jul. 2011.

SHOPPERT, A. et al. Complete Extraction of Amorphous Aluminosilicate from Coal Fly Ash by Alkali Leaching under Atmospheric Pressure. **Metals**, v. 10, n. 12, p. 1684, 16 dez. 2020.

SHOUMKOVA, A. S. Magnetic separation of coal fly ash from Bulgarian power plants. **Waste Management & Research: The Journal for a Sustainable Circular Economy**, v. 29, n. 10, p. 1078–1089, out. 2011.

SHU, J. et al. Atomic-Molecular Engineering Tailoring Graphene Microlaminates to Tune Multifunctional Antennas. **Advanced Functional Materials**, v. 33, n. 15, p. 2212379, abr. 2023.

SI, Y.; SAMULSKI, E. T. Synthesis of Water Soluble Graphene. **Nano Letters**, v. 8, n. 6, p. 1679–1682, 1 jun. 2008.

SIERRA, U. et al. Cokes of different origin as precursors of graphene oxide. **Fuel**, v. 166, p. 400–403, fev. 2016.

SINGH, J. et al. Role of green chemistry in synthesis and modification of graphene oxide and its application: A review study. **Chemical Physics Impact**, v. 6, p. 100185, jun. 2023.

SMITH, A. T. et al. Synthesis, properties, and applications of graphene oxide/reduced graphene oxide and their nanocomposites. **Nano Materials Science**, v. 1, n. 1, p. 31–47, mar. 2019.

SONG, Y. et al. Graphene Transfer: Paving the Road for Applications of Chemical Vapor Deposition Graphene. **Small**, v. 17, n. 48, p. 2007600, dez. 2021.

SONTAKKE, A. D.; TIWARI, S.; PURKAIT, M. K. A comprehensive review on graphene oxide-based nanocarriers: Synthesis, functionalization and biomedical applications. **FlatChem**, v. 38, p. 100484, mar. 2023.

SPAOLONZI, M. P. et al. Green-functionalized carbon nanotubes as adsorbents for the removal of emerging contaminants from aqueous media. **Journal of Cleaner Production**, v. 373, p. 133961, nov. 2022.

STATISTA. **Brazil: coal consumption**. Disponível em: <https://www.statista.com/statistics/1224000/brazil-coal-consumption/>. Acesso em: 29 out. 2023.

STATISTA. **Brazil: coal production 2021 | Statista**. Disponível em: <https://www.statista.com/statistics/1223917/coal-production-brazil/>. Acesso em: 29 out. 2023.

STEEL, K. M.; PATRICK, J. W. The production of ultra clean coal by chemical demineralisation. **Fuel**, v. 80, n. 14, p. 2019–2023, nov. 2001.

STOLLER, M. D. et al. Graphene-Based Ultracapacitors. **Nano Letters**, v. 8, n. 10, p. 3498–3502, 8 out. 2008.

SUK, J. W. et al. Mechanical Properties of Monolayer Graphene Oxide. **ACS Nano**, v. 4, n. 11, p. 6557–6564, 23 nov. 2010.

SUN, X. et al. Mechanism of Graphene Oxide as an Enzyme Inhibitor from Molecular Dynamics Simulations. **ACS Applied Materials & Interfaces**, v. 6, n. 10, p. 7153–7163, 28 maio 2014.

SURWADE, S. P. et al. Water desalination using nanoporous single-layer graphene. **Nature Nanotechnology**, v. 10, n. 5, p. 459–464, maio 2015.

TEIXEIRA B., C. C. **AVALIAÇÃO DA COMBUSTIBILIDADE DE CARVÃO BRASILEIRO PARA INJEÇÃO EM ALTOS-FORNOS EM SIMULADOR DE PCI E**

EM TERMOBALANÇA. Porto Alegre: UNIVERSIDADE FEDERAL DO RIO GRANDE DO SUL, 2018.

THIESSEN, R. **What is Coal?** [s.l: s.n.].

TODA, K.; FURUE, R.; HAYAMI, S. Recent progress in applications of graphene oxide for gas sensing: A review. **Analytica Chimica Acta**, v. 878, p. 43–53, jun. 2015.

UMAR, E. et al. 3D graphene-based material: Overview, perspective, advancement, energy storage, biomedical engineering and environmental applications a bibliometric analysis. **Journal of Environmental Chemical Engineering**, v. 11, n. 5, p. 110339, out. 2023.

UPME, U. DE P. M. E. **La cadena del Carbón**. Ministerio de Minas y Energía, , nov. 2005.

USGS, S. FOR A CHANGING WORLD. **What is coal? | U.S. Geological Survey**. Disponível em: <https://www.usgs.gov/faqs/what-coal>. Acesso em: 14 ago. 2023.

VERMA, M. L. et al. Synthesis and application of graphene-based sensors in biology: a review. **Environmental Chemistry Letters**, v. 20, n. 3, p. 2189–2212, jun. 2022.

VIJAPUR, S. H. et al. An investigation of growth mechanism of coal derived graphene films. **Materials Today Communications**, v. 11, p. 147–155, jun. 2017.

VIJAPUR, S. H.; WANG, D.; BOTTE, G. G. Raw Coal Derived Large Area and Transparent Graphene Films. **ECS Solid State Letters**, v. 2, n. 7, p. M45–M47, 9 maio 2013.

WANG, H. et al. Construction of Fe3O4@β-CD/g-C3N4 nanocomposite catalyst for degradation of PCBs in wastewater through photodegradation and heterogeneous Fenton oxidation. **Chemical Engineering Journal**, v. 429, p. 132445, fev. 2022.

WANG, J.; GUO, X. Adsorption kinetic models: Physical meanings, applications, and solving methods. **Journal of Hazardous Materials**, v. 390, p. 122156, maio 2020.

WANG, X.; ZHANG, Z.; GE, Y. Oleic Acid-Tailored Geopolymer Microspheres with Tunable Porous Structure for Enhanced Removal from Tetracycline in Saline Water. **Sustainability**, v. 14, n. 11, p. 6705, 30 maio 2022.

WEBER, W. J.; MORRIS, J. C. Kinetics of Adsorption on Carbon from Solution. **Journal of the Sanitary Engineering Division**, v. 89, n. 2, p. 31–59, abr. 1963.

WISE, R. Antimicrobial resistance: priorities for action. **Journal of Antimicrobial Chemotherapy**, v. 49, n. 4, p. 585–586, 1 abr. 2002.

WU, C.; YU, H.; ZHANG, H. Extraction of aluminum by pressure acid-leaching method from coal fly ash. **Transactions of Nonferrous Metals Society of China**, v. 22, n. 9, p. 2282–2288, set. 2012.

WU, Y. et al. Efficient and Large Scale Synthesis of Graphene from Coal and Its Film Electrical Properties Studies. **Journal of Nanoscience and Nanotechnology**, v. 13, n. 2, p. 929–932, 1 fev. 2013.

XU, H. et al. Facile preparation of graphene nanosheets by pyrolysis of coal-tar pitch with the presence of aluminum. **Journal of Analytical and Applied Pyrolysis**, v. 110, p. 481–485, nov. 2014.

YAN, B. et al. Pore engineering: Structure-capacitance correlations for biomass-derived porous carbon materials. **Materials & Design**, v. 229, p. 111904, maio 2023.

YAN, S. et al. In situ fabrication and characterization of graphene/geopolymer composites. **Ceramics International**, v. 41, n. 9, p. 11242–11250, nov. 2015.

YAO, X. et al. Geopolymerization process of alkali–metakaolinite characterized by isothermal calorimetry. **Thermochimica Acta**, v. 493, n. 1–2, p. 49–54, set. 2009.

YESUDHAS JAYAKUMARI, B.; NATTANMAI SWAMINATHAN, E.; PARTHEEBAN, P. A review on characteristics studies on carbon nanotubes-based cement concrete. **Construction and Building Materials**, v. 367, p. 130344, fev. 2023.

YILDIZ, G.; BOLTON-WARBERG, M.; AWAJA, F. Graphene and graphene oxide for bio-sensing: General properties and the effects of graphene ripples. **Acta Biomaterialia**, v. 131, p. 62–79, set. 2021.

YU, B. et al. Adsorption behaviors of tetracycline on magnetic graphene oxide sponge. **Materials Chemistry and Physics**, v. 198, p. 283–290, set. 2017.

YUAN, G. et al. Self-Assembly of Free-Standing LiMn2O4-Graphene Flexible Film for High-Performance Rechargeable Hybrid Aqueous Battery. **Materials**, v. 11, n. 7, p. 1056, 21 jun. 2018.

ZHANG, J.; BROADSTOCK, D. C. The Causality between Energy Consumption and Economic Growth for China in a Time-varying Framework. **The Energy Journal**, v. 37, n. 01, 1 set. 2016.

ZHANG, L. et al. Size-controlled synthesis of graphene oxide sheets on a large scale using chemical exfoliation. **Carbon**, v. 47, n. 14, p. 3365–3368, nov. 2009.

ZHANG, P. et al. Influence of carbon nanotube on properties of concrete: A review. **Construction and Building Materials**, v. 369, p. 130388, mar. 2023a.

ZHANG, Q. et al. Advanced review of graphene-based nanomaterials in drug delivery systems: Synthesis, modification, toxicity and application. **Materials Science and Engineering: C**, v. 77, p. 1363–1375, ago. 2017.

ZHANG, W. et al. Single atomic cerium sites anchored on nitrogen-doped hollow carbon spheres for highly selective electroreduction of nitric oxide to ammonia. **Journal of Colloid and Interface Science**, v. 638, p. 650–657, maio 2023b.

ZHANG, Y. et al. Mechanical exfoliation assisted with carbon nanospheres to prepare a few-layer graphene for flexible strain sensor. **Applied Surface Science**, v. 611, p. 155649, fev. 2023c.

ZHAO, J. et al. Efficient Preparation of Large-Area Graphene Oxide Sheets for Transparent Conductive Films. **ACS Nano**, v. 4, n. 9, p. 5245–5252, 28 set. 2010.

ZHAO, J. et al. Preparation of porous carbon materials from black liquor lignin and its utilization as CO2 adsorbents. **Journal of the Energy Institute**, v. 107, p. 101179, abr. 2023.

ZHENG, Q. et al. Graphene oxide-based transparent conductive films. **Progress in Materials Science**, v. 64, p. 200–247, jul. 2014.

ZHOU, Q. et al. Graphene Sheets from Graphitized Anthracite Coal: Preparation, Decoration, and Application. **Energy & Fuels**, v. 26, n. 8, p. 5186–5192, 16 ago. 2012.

ZHOU, W. et al. A comparative study of high- and low-Al 2 O 3 fly ash based-geopolymers: The role of mix proportion factors and curing temperature. **Materials & Design**, v. 95, p. 63–74, abr. 2016.

ZHU, Y. et al. Mass production and industrial applications of graphene materials. **National Science Review**, v. 5, n. 1, p. 90–101, 1 jan. 2018.